Study of Shoulder Flow Zone Formation in Thick Section FSW of 6061 Al Alloy Using Scroll Shoulder Tool

David Ping Yan

**A thesis submitted to Auckland University of Technology
in fulfilment of the requirements for the degree of
Master of Philosophy (MPhil)**

2008

School of Engineering

Primary Supervisor: Associate Professor Zhan W. Chen

Acknowledgments

Abstract

Friction stir welding (FSW) is a relatively new solid-state welding technology invented at The Welding Institute of UK in 1991. It is versatile and has been widely adopted to join various materials. There has been strong research activity on revealing the details of the material flow pattern in the nugget zone induced by the conventional shoulder tool. However, there is insufficient understanding on the aspects of the scroll shoulder tool design and the shoulder flow zone formation utilizing this type of tool.

The major objective of this study was to conduct experiments, analyse results and then reveal the shoulder flow zone forming mechanism for the scroll shoulder tool. The method used was to identify the flow pattern in the shoulder flow zone using a 'marker insert' technique, and then to suggest the forming mechanism of the shoulder flow zone based on the obtained flow pattern; although the 'marker insert' technique has never been used to study the shoulder flow zone flow pattern induced by the scroll shoulder tool.

Experiments were conducted to examine the thick sections 6061 aluminium 'marker insert' welds, which were welded using a scroll shoulder tool at a range of welding parameters. These were followed by quantifying the mass of the accumulated workpiece material within the scroll groove (pick up material-PUM), evaluating the effect of welding parameters on the shoulder flow zone formation, and documenting the shoulder flow zone flow pattern.

The major finding was that there is a simple banded structure which forms in a layer to layer manner in the bottom portion of the shoulder flow zone, but it disappears in the top portion of the shoulder flow zone. Accordingly, the forming mechanism of the shoulder flow zone for the scroll shoulder tool was suggested as follows. Firstly, the tool pin is plunged into the workpiece, the workpiece material is extruded by the pin and pushed up into the scroll groove forming the PUM. Secondly, after the tool shoulder is plunged into the workpiece to a certain depth, the scroll groove is fully filled up with the PUM. Finally, during the forward movement of the tool, the central portion of PUM is driven downward by the root portion of the pin and then detaches from the pin (tip portion) in a layer to layer manner. It has also found that the thickness of the shoulder flow zone varies with a thicker on the advancing side than on the retreating

side, and there is a positive linear relationship between the mass of PUM and the weld quality. This study has revealed for the first time the forming mechanism of the shoulder flow zone, and has improved the understanding of the shoulder flow zone formation using a scroll shoulder tool.

It is recommended that a 'shoulder-breaking' technique is developed to break the rotating shoulder suddenly and hence embed it into the workpiece during FSW, in which a real-time shoulder-workpiece couple could be produced for a better three-dimensional examination of the shoulder flow zone.

Table of Contents

List of Figures

List of Tables

Statement of Originality

"I hereby declare that this submission is my own work and that, to the best of my knowledge and belief it contains no material previously published or written by another person nor material which to a substantial extent has been accepted for the qualification of any other degree or diploma of a university or other institution of higher learning, except where due acknowledgement is made in the acknowledgements."

…………………………….(signed)

...…………………………….(date)

1   Introduction

1.1   Welding Principle / Conventional Fusion Welding Techniques

Welding is a fabrication process that joins materials, usually metals or thermoplastics, by causing coalescence. 'The majority of welding processes rely on heat more than on pressure to accomplish joining by creating atomic bonding across the joint interface' [1]. There are two types of welding: fusion and non-fusion welding. During fusion welding, sufficient heat causes melting, and significant melting is necessary for welding to take place. In non-fusion welding, heat is only enough to soften the material in the solid state to facilitate plastic deformation or speed up the material solid phase diffusion [1].

Welding technology advanced quickly during the early 20th century, several modern welding techniques were developed, including gas metal arc welding, submerged arc welding and electroslag welding. Figure 1-1 schematically illustrates basic gas metal arc welding (GMAW), which is a conventional fusion welding technique that has been commercially used for welding aluminium (Al) since the 1950's [2]. The process uses an electric arc generated between the filler wire and the workpiece to initiate local heating that melts both the filler wire and base metal to form a weld. The shielding gas is utilized to protect the molten Al from reacting with nitrogen, oxygen or hydrogen in the atmosphere.
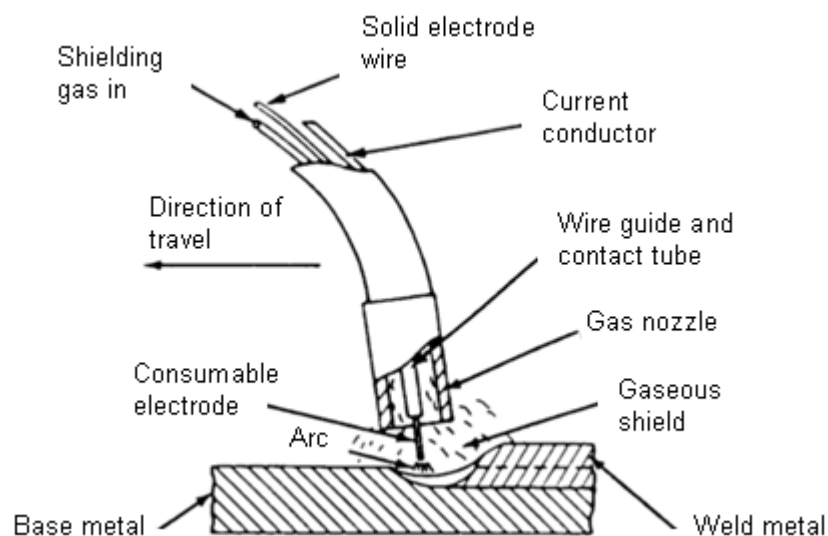
Figure 1-1 Schematic illustration of GMAW process [2]

Fusion welding of Al has several shortcomings, in particular the volume change due to the transition from liquid to solid results in shrinkage. The shrinkage could cause porosity or distortion which affects the strength of the weld joint. Porosities in the weld are also formed due to the high solubility of hydrogen in the molten material and its low solubility in the solid. Distortion and porosity lead to poor mechanical properties at the weld joint. Generally, GMAW produces poor quality welds such as porosity, solidification cracking and heat affected zone (HAZ) cracking. Friction stir welding eliminates these defects as it is a solid state joining process [3].

1.2 Rotary Friction Welding / Friction Stir Welding

1.2.1 Rotary Friction Welding

Rotary friction welding and friction stir welding are solid state joining processes that generate heat through mechanical friction and involve no melting of the base materials. Figure 1-2 illustrates the rotary friction welding process. Rotary friction welds are made by holding a rotating component in contact with a non-rotating component with a constant or increasing axial load, so that frictional heat is developed at the interface between the faying surfaces. When the interface reaches the appropriate welding temperature, rotation is stopped, and then the weld completed. There are restrictions on the shape of part that only parts with rotational symmetry can be welded using rotational motion [4, 5].
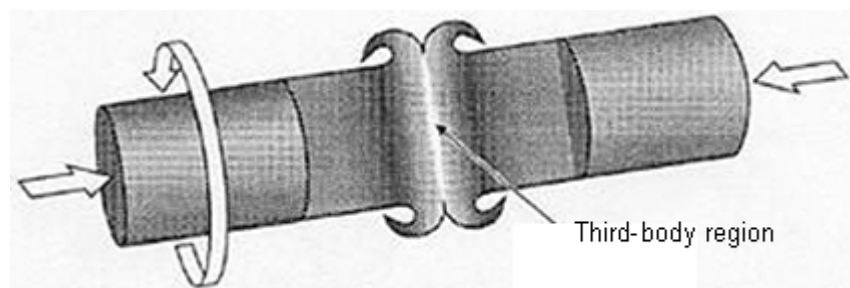
Figure 1-2 Schematic illustration of rotary friction welding process [5]

1.2.2 Friction Stir Welding

Friction stir welding (FSW) was invented at The Welding Institute (TWI) of UK in 1991. Figure 1-3 schematically illustrates the basic concept of FSW. A non-consumable rotating tool is plunged into the workpiece and between the neighboring edges of the

2

plates (workpiece) to be joined, and traversed along the line of joint. During FSW, frictional heat is generated between the tool and the workpiece, causing the latter to soften (plasticise) without gross melting. The plastised material is transferred from the leading edge to the trailing edge of the tool pin and is forged in the top zone, bonding the two pieces together.
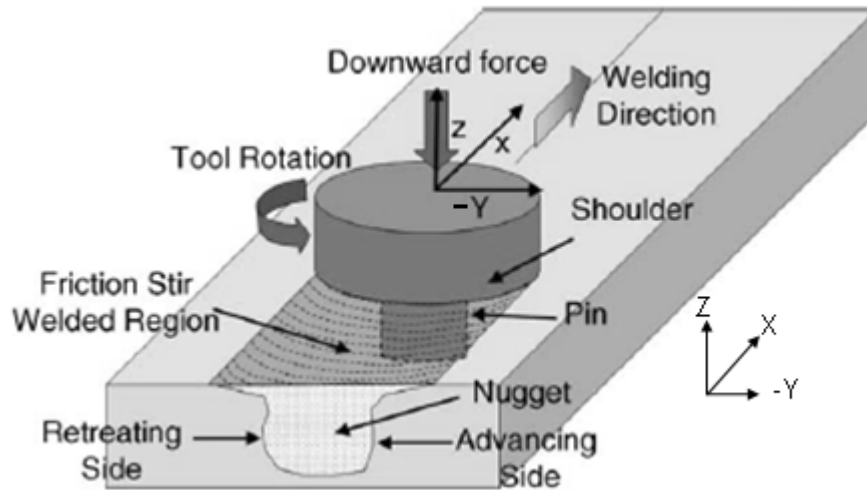
Figure 1-3 Schematic drawing of FSW process [6]

The process and terminology of FSW are schematically explained in Figure 1-3. The process includes three main procedures; tool pin plunging, tool shoulder plunging and tool pin/shoulder travelling. The advancing side (AS) is the side where the tool rotation and traveling direction are same, and the side where the tool rotation and traveling direction are opposite is referred to as the retreating side (RS). Figure 1-3 also shows the coordinate system (welding direction always parallel to X axis) used throughout this report.

FSW process parameters are schematically illustrated in Figure 1-4. They include tool geometry, tilt angle (θ), tool rotating speed (ω), tool travelling speed (V), tool plunging speed ($V_{plunging}$), plunge force (F), and depth of shoulder penetration (H).

Shortly after the invention of FSW in 1991, the process and tooling were systematically developed for welding various Al alloys at various material gauges. Two types of tools were developed by TWI and named conventional shoulder (tilted) tool and scroll shoulder (non-tilted) tool [6]. Tilting means that the tool shoulder is tilted (see Figure 1-4) with an angle of 2-3 degrees. The tool is machined to have a featureless shoulder face. A non-tilted type tool has no degree of tilting angle, but a scroll groove is cut into

the shoulder face. The optimum geometry for both types of tool is still being investigated.
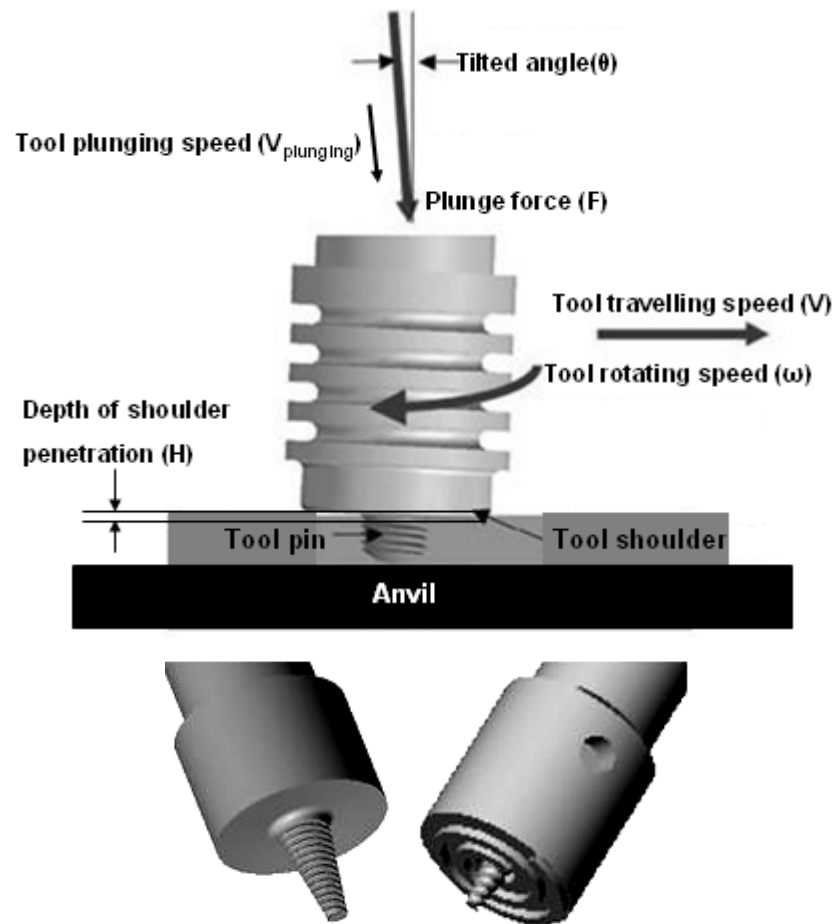
Figure 1-4 Typical tools and processing parameters used in the FSW process, conventional shoulder tool (bottom left) and scroll shoulder tool (bottom right) [7]

In the development of an improved scroll shoulder tool, Dawes and Thomas [8] reported that special care was necessary in setting the tool to just touch the workpiece surface. They also found that any additional workpiece contact would produce significant amounts of weld flash and result in a risk of voids occurring in the weldment. It is speculated that there is a relationship between the mass of weld flash and mass of displaced workpiece material, and that will need to be further investigated.

Figure 1-5 illustrates the transverse cross section of a FSW weld, where two main weld zones are classified; the shoulder flow zone and nugget zone. These two weld zones are formed due to the interactions of the workpiece with the tool shoulder and tool pin respectively, and most likely form independently [9, 10].
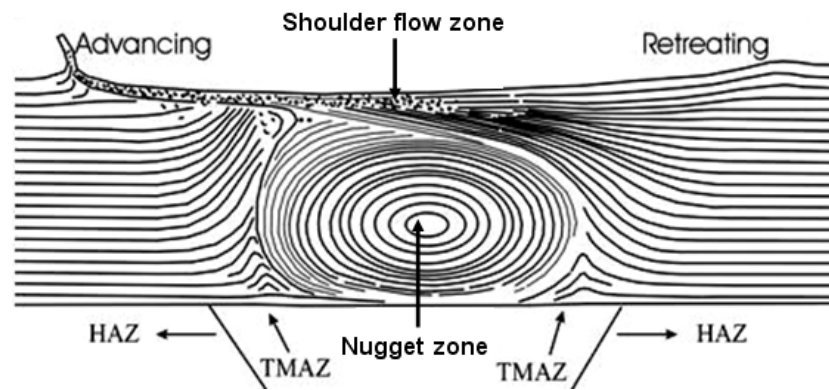
Figure 1-5 Schematic illustration of a weld region showing various macrostructural zones in FSW

An investigation of the FSW weld zone [11] has shown that recrystallization occurs in the nugget zone due to plastic deformation and frictional heating. A thermo-mechanically affected zone (TMAZ) is situated adjacent to the nugget zone. This transition zone experiences both high temperature and plastic deformation, but recrystallization does not occur in this zone due to insufficient deformation strain. The heat affected zone (HAZ) is beyond the TMAZ and it does not experience plastic deformation. Material in this zone has the same grain structure as matrix material [11].

A typical FSW weld has two unique features, which are the onion rings pattern and banded structures. Under some FSW conditions, an onion ring structure can be observed in the nugget zone. Figure 1-6 shows a transverse cross section of weld produced by FSW, where an onion rings pattern is easily identified and exists in the centre of the weld.
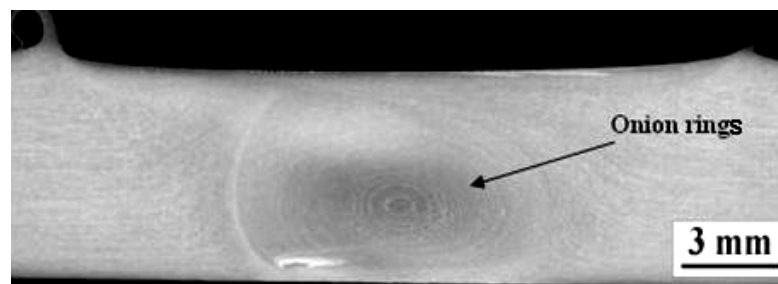
Figure 1-6 A transverse cross section of FSW A5083 Al weld shows onion rings pattern (produced at AUT laboratory, sectioning on Z-Y plane see Figure 1-3 for coordinate, advancing side on the right) [9]

By sectioning a FSW weld sample parallel to the welding direction and to the workpiece top surface (X-Y plane), a typical feature is shown in Figure 1-7, the serial semicircular trace (also known as banded structures) can be easily identified.
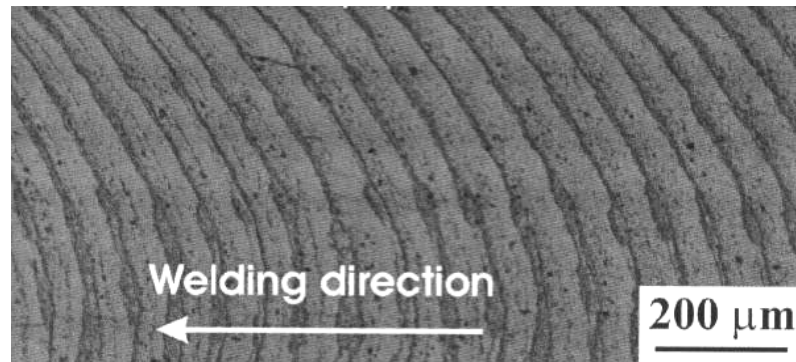
Figure 1-7 Banded structures in the nugget zone of a FSW A5083/6061 alloy weld (produced at AUT laboratory, sectioning on X-Y plane see Figure 1-3 for coordinate) [9]

FSW is considered to be the most significant development in metal joining in a decade as concluded by Mishra and Ma [6]. FSW is a 'green' technology due to its energy efficiency, environmental friendliness, and versatility. As it is a solid state joining technology, it provides many advantages compared with conventional fusion welding, such as the elimination of porosity and fumes, reduction of distortion in the weldments and excellent mechanical properties at the weld joint.

Despite successful applications of FSW in industries worldwide, the fundamental science associated with FSW is still developing [10]. This includes material flow formation and process control, which are essential for tooling development, process optimization and broadening the application of FSW. Therefore, further investigations in shoulder flow zone formation, particularly with use of a scroll shoulder tool, are required for a better understanding of thick sectioned Al plate FSW.

1.3   FSW Science

As FSW is a new technology, many aspects remain to be investigated. A physical understanding of the FSW process can be described by combining the complementary efforts of experimental examination and computational modelling. From open literature, many research projects have been conducted to observe and predict the material flow and weld structure formation. These projects have used various experimental techniques

and simulation methods, such as the tracer technique using a 'marker insert' [6]. However, no complete understanding of the FSW process has been presented over the last decade [6, 9, 12].

1.3.1 Shoulder Flow Zone Formation Using Scroll Shoulder Tool

Figure 1-8 illustrates the FSW process using a scroll shoulder tool and indicates the shoulder flow zone (blue solid line) and nugget zone (black dash line). Additionally, the components of the scroll shoulder tool and the denotation of shoulder flow zone material are demonstrated.
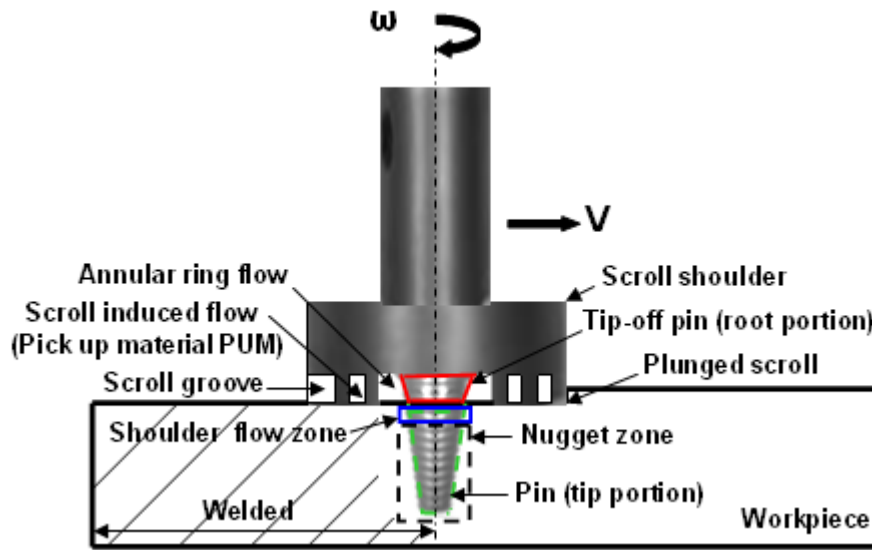
Figure 1-8 Schematic illustration of scroll shoulder tool FSW process, components of scroll shoulder and tapered thread pin tool and denotation of material flow (dimension of tool and weld zone are not to scale)

As can be seen in Figure 1-8, the scroll shoulder tool pin is divided into two sections 'tip-off' pin (root portion, red solid line) and pin (tip portion, green dash line). Its shoulder consists of a scroll groove cut into the shoulder face and a 'tip-off' pin embedded beneath the shoulder face. During scroll shoulder tool FSW processes, the workpiece material displaced by the penetrated tool is distributed in two ways; material is extruded outside the tool to form weld flash, and material is induced into the scroll groove beneath the shoulder. The workpiece material (WPM) which is driven into the scroll groove and accumulated within the scroll groove is denoted as Pick Up Material (PUM), and the central portion of PUM (PUM around the root portion of pin) is denoted as Annular Ring Material (ARM) in the present study.

7

Since TWI introduced the scroll shoulder tool concept, research has focused on improving its performance such as cutting more than one scroll onto the shoulder face [13, 14]. Investigation has shown that the scroll shoulder tool has three potential advantages; it can improve surface finish, increase welding speed, and operate normal to the workpiece surface [8]. However, the forming mechanism of the shoulder flow zone using a scroll shoulder tool still remains unidentified as they have different tool geometries. Weld zone formation using a conventional shoulder tool will be detailed later.

In the development of the scroll shoulder tool, Dawes and Thomas [8] studied the PUM induced by the tool pin during tool pin plunging stage. Figure 1-9 demonstrates the movement of the displaced workpiece material, relative to the tool, during the tool pin plunging stage.
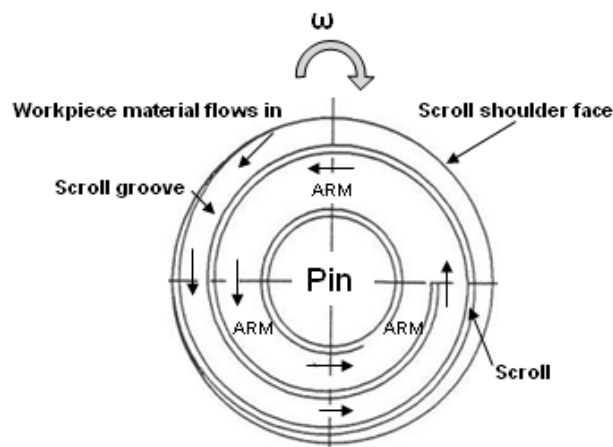
Figure 1-9 Schematic illustration of the material flow movement relative to the tool during the tool pin plunging stage and associated accumulation of annular ring material (ARM) [8]

Dawes and Thomas [8] reported that when the scroll shoulder tool pin is rotated and plunged into the workpiece, the workpiece material extruded by the pin is pushed up into the scroll groove. The workpiece material within the scroll groove will follow the groove moving towards the pin. The scroll (also called fence) is stopped short of the pin, the material flow that enters the spacing between the fence and the pin forms compressed ARM flow around the pin. As the pin travels along the weld path, the ARM flow around the pin is extruded across the workpiece surface to fill the cavity created by the travelling pin and form the weld. They, however, did not offer any experimental evidence of their theories. Furthermore, the formation of the shoulder flow zone in

terms of its relation to the scroll shoulder geometry and welding parameters was not investigated.

Knowledge for FSW thick section Al plate using a scroll shoulder tool is not as advanced as using the conventional shoulder tool, and there is little information available in the public domain. Colligan et al [15] studied scroll shoulder tool design by FSW 25.4mm thick 5083-H131 Al plate, using a scroll shoulder and tapered threaded pin tool with three flats cut on the thread pin surface. A schematic illustration of their tool design is shown in Figure 1-10.
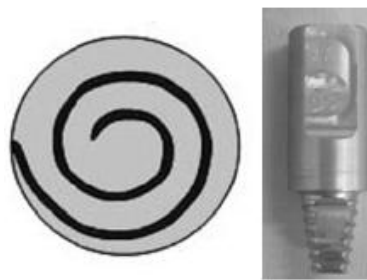
Figure 1-10 Schematic illustration of scroll shoulder face (left) and tapered threaded pin with three flats on the thread (right) used in Colligan's experiment

Colligan et al observed that the weld nugget produced by this type of tool in 5083 Al 25.4mm thick plate does not resemble the typical rounded nugget by the conventional shoulder tool, nor does the weld nugget exhibit the typical onion rings pattern. The onion rings pattern has been replaced by a series of semicircular bands that can be seen nested vertically in the transverse cross section of weld as shown in Figure 1-11 [15].
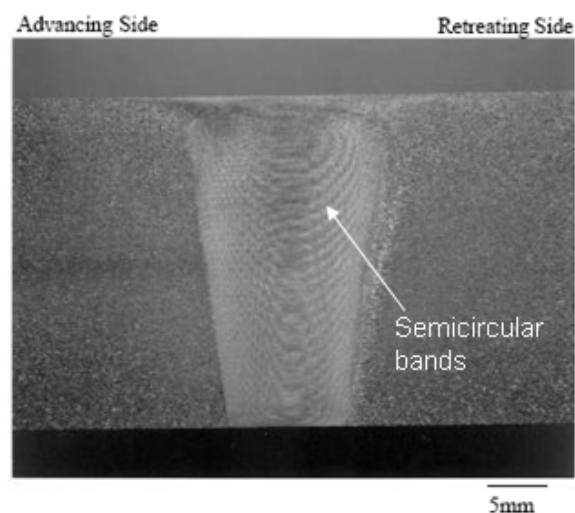
Figure 1-11 Typical 25.4mm thick 5083-H131 Al FSW weld transverse section, using scroll shoulder and three flats on thread tapered pin tool rotating at 250rpm and travel at 127mm/min [15]

Colligan et al also found that when the tool travels at lower speeds (25mm/min), the weld contained gross linear voids near the weld surface, which were aligned with the advancing side of the pin. As the travel speed was increased, the size of internal voids was reduced until, at a travel speed of 107mm/min, sound welds were achieved. Although upon radiographic examination, indistinct voids were detected near the start and end of each weld. A micrograph of the end defect is shown in Figure 1-12, where a cluster of voids on the wedge shaped region in the upper advancing side of the weld nugget can be identified. However, there is no detailed information regarding the material flow in the shoulder flow zone forming the weld [15].
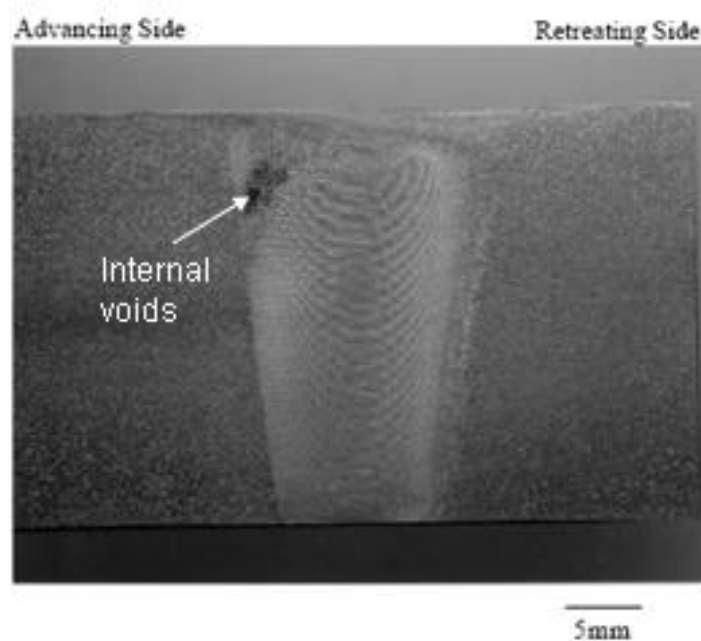
Figure 1-12 Transverse section of 25.4mm thick 5083-H131 Al FSW weld showing typical weld end defect, using scroll shoulder and three flats on thread tapered pin tool rotating at 250rpm and travelling at 107mm/min [15]

Information and knowledge of the formation of the shoulder flow zone is important for the design of FSW tools, particularly for thick plate FSW. An inappropriate use of the welding parameters, as will be described in the preliminary investigation section, will result in insufficient material flow in the shoulder flow zone which will lead to the formation of weld defects.

1.3.2 Preliminary Investigation at AUT University

Figure 1-13 shows a scroll shoulder tool and FSW welds of 20mm thick Al plate obtained in the preliminary investigation, and Figure 1-14 presents the enlarged view of the area 'A' of Figure 1-13 (b). As can be seen in Figure 1-13 (b) and (c), the severity of surface defects and internal voids formed in the weld varies when the scroll shoulder was used at different depths of shoulder penetration.
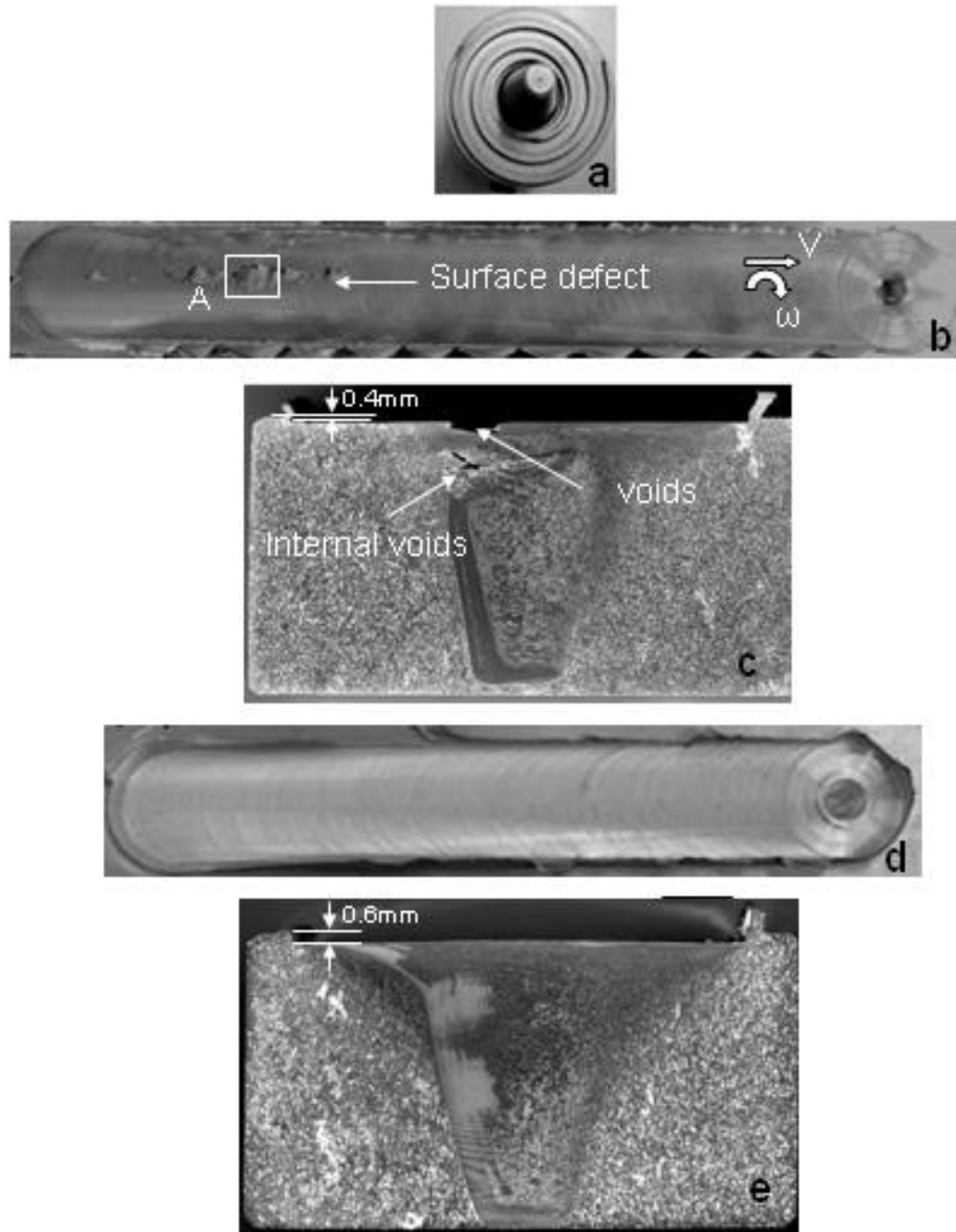
Figure 1-13 Photos of (a) scroll shoulder and tapered pin tool used in preliminary study; (b) and (d) surface defect and no-defect weld profiles; (c) and (e) weld transverse cross sections; obtained by FSW 20mm thick Al plates, using a scroll shoulder tool rotating at 250rpm and travelling at 40mm/min, with 0.4mm and 0.6mm depth of shoulder penetration respectively (AS on the left)

11

Figure 1-14 indicates the distribution of the nugget zone material and shoulder flow zone material, and shows a cavity along the advancing side caused by insufficient shoulder flow zone material. This cavity needs to be fully filled up by shoulder flow zone material to form a defect-free weld. It also gives a good geometric reference to the shoulder flow zone in the weld produced by a scroll shoulder tool for the present study.
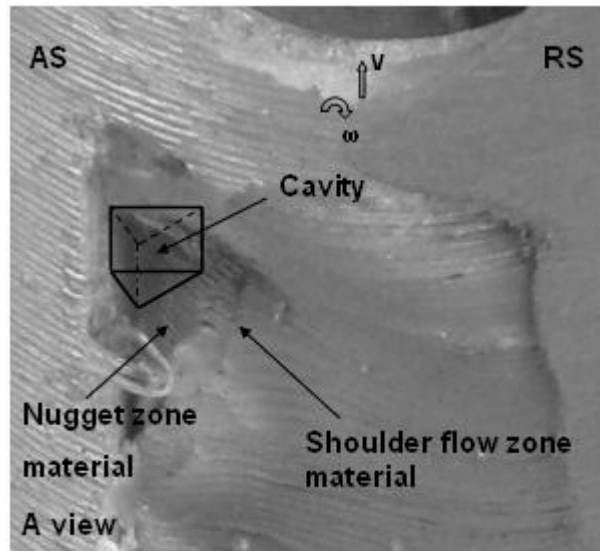
Figure 1-14 Enlarged view of area 'A' of Figure 1-13 (b), indicating the distribution of nugget zone material and shoulder flow zone material, showing a cavity caused by insufficient shoulder flow zone material swirling downward from the retreating side to the advancing side

By comparing Figure 1-13 (c) and (e), it was found that deeper shoulder penetration improved the material flow in the shoulder flow zone significantly, resulting in a defect-free weld. By speculation, it is proposed that with deeper shoulder penetration, more of the front part of the displaced workpiece material flows into the scroll groove, rather than being pushed away from the tool shoulder face. This deeper penetration may result in an increase of the accumulated workpiece material within the scroll groove beneath the shoulder after welding, which will improve the shoulder flow zone material flow. However, there is no evidence to support this speculation. Additionally, the shoulder flow zone forming mechanism has never been explored, although the occurrence of surface defects and internal voids in thick section Al FSW weld, produced by the scroll shoulder tool, have been observed and reported by two researchers [8, 15]. Therefore, further investigation into shoulder flow zone formation is necessary.

1.4   Research Objectives

As discussed earlier, shoulder flow zone formation using the scroll shoulder tool has not been comprehensive. It was not well understood how the scroll shoulder tool geometry and welding parameters (tool rotating speed, tool travelling speed and the depth of shoulder penetration) affect the formation of the shoulder flow zone in FSW thick section Al plate.

This research programme was to conduct a series of thick section Al plate FSW using a scroll shoulder tool at a range of welding parameters. Analysis of the mass of PUM and the weld obtained from these experiments will improve the understanding of the shoulder flow zone formation in terms of the relationship among the tool geometry, welding parameters and weld quality.

In addition, a 'marker insert' experimental technique was used to trace the shoulder flow zone material (same as PUM) movement and document the material flow pattern in the shoulder flow zone. The forming mechanism of the shoulder flow zone was revealed based on the flow pattern documented by the marker.

The major aspects of this research were to:

- Evaluate the effect of welding parameters on the mass of PUM induced by the tool during tool pin plunging, tool shoulder plunging and tool travelling;

- Investigate the effect of welding parameters on the formation of the shoulder flow zone. These will include the determination of the interface location (shoulder flow zone-nugget zone interface), estimation of the thickness of the shoulder flow zone, suggestion of the flow patterns in the shoulder flow zone and revelation of the relationship between the mass of PUM and weld quality. The relationship among the mass of PUM, the formation of shoulder flow zone, and the associated likelihood of defect weld formation, has not been explored yet. This knowledge is important in the design of scroll shoulder tools to ensure FSW weld quality;

- Trace the PUM movement, and identify the shoulder flow zone flow pattern in thick section Al FSW weld using a 'marker insert' technique; and

- Reveal the forming mechanism of the shoulder flow zone for the scroll shoulder tool.

2   State of the Art in FSW

This chapter reviews the literature on FSW in the aspects of tool design, processing parameters and current experimental techniques used in flow pattern observation. Additionally, material flow patterns and flow forming mechanism, factors affecting weld zone structure, and formation of shoulder flow zone using scroll shoulder tool will also be critically reviewed. The review also serves to identify the knowledge gaps and to support the chosen methodologies that have been incorporated into the present study.

2.1   FSW Tool Design and Processing Parameters

FSW involves complex material movement and plastic deformation. Tool geometry and welding parameters exert significant effects on the material flow pattern, thereby influencing weld quality [6, 11, 16]. Two major factors affecting the FSW process, tool geometry and welding parameters, are addressed.

2.1.1   Tool Design / Geometry

As discussed in chapter one (section 1.3.1), a FSW tool consists of a shoulder and pin. Since TWI introduced the conventional shoulder tool and scroll shoulder tool in 1991, the geometry of the tool shoulder and pin has now evolved significantly. The tool shoulder and pin design will be reviewed in the following section.

Tool shoulders are designed to produce heat (through friction and material deformation), transfer this heat to the weld region of the workpiece, and provide the downward forging action necessary for weld consolidation. Currently, two types of tool shoulders are commonly used, the conventional tool shoulder and scroll tool shoulder [6].

Figure 2-1 shows a conventional tool shoulder which is designed with a concave face machined on the tool shoulder face, and is currently the most common shoulder design in FSW. To induce shoulder flow zone material, this shoulder design requires the tool to be tilted 2 to 4 degrees from the normal of the workpiece, away from the direction of travel [6, 17, 18]. The effect of the conventional shoulder geometry on the weld zone formation will be reviewed later.
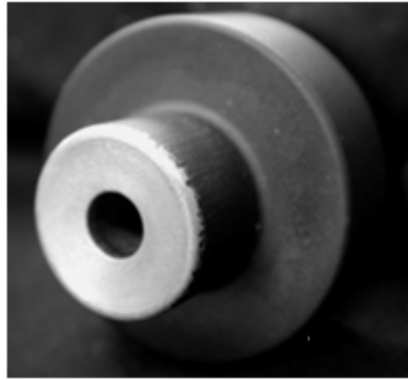
Figure 2-1 Photos of concave conventional tool shoulder [19]

Figure 2-2 shows two scroll shoulder profiles, one has a flat shoulder face and the other a convex face. Both profiles have a scroll groove cut from the edge of the shoulder toward the centre. The function of the scroll groove is to direct the deformed material from the edge of the shoulder to the pin, thus eliminating the need to tilt the tool, leading to the simplification of the FSW machine design. Additionally, the scroll on the convex shoulder moves material from the outside of the shoulder toward the pin. As a result, the outer edge of the convex shoulder tool is not required to be fully engaged with the workpiece. When any part of the scroll is engaged with the workpiece, it moves material toward the pin, and produces a sound weld [8, 13, 20-22].
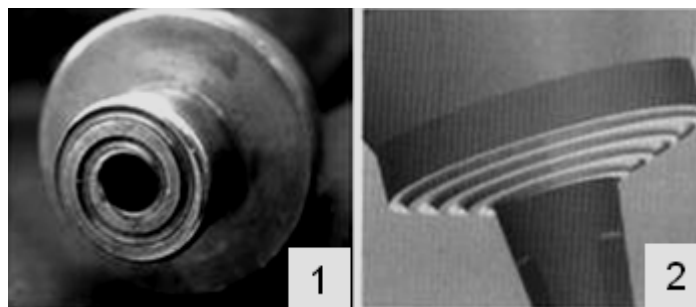
Figure 2-2 Photos of one scroll tool shoulder profiles (1) flat face, and (2) convex face [19, 20]

The scroll shoulder can also contain additional features to increase the amount of material deformation, and improve FSW weld quality. Figure 2-3 shows three types of shoulder features that have been published; they are scrolls, scoops, and concentric circles. Specified tool shoulder design can be achieved by machining selected shoulder features onto either the flat or convex shoulder profiles [6, 8, 23]. The effect of the scroll shoulder geometry on the shoulder flow zone formation will be reviewed in section 2.5.

16
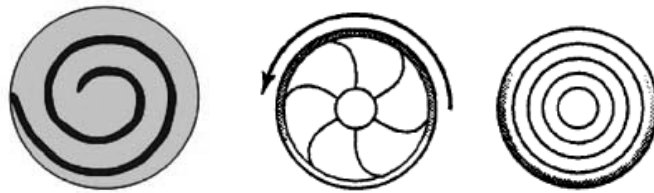
Figure 2-3 Schematic illustration of shoulder features (left) scroll, (mid) scoops, and (right) concentric circles [6, 8]

Tool pins are designed to disrupt the contacting surfaces of the workpiece, shear workpiece material in front of tool pin, and move material behind the tool pin. As illustrated in Figure 2-4, threads cut on the pin are used to transfer the material flow from the shoulder face down to the bottom of the pin. Additionally, Figure 2-5 shows six types of tool pin designs found in open literature [22].
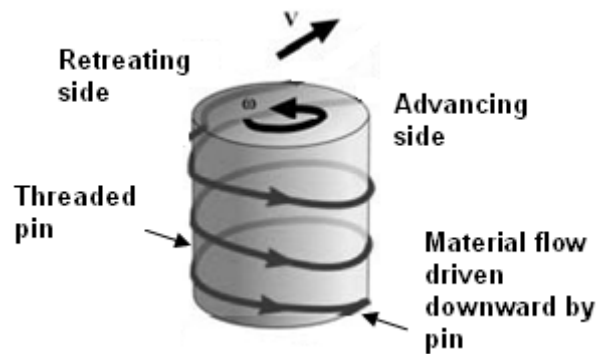
Figure 2-4 Schematic illustration of threaded pin drives material flow down to the bottom of the pin [24]
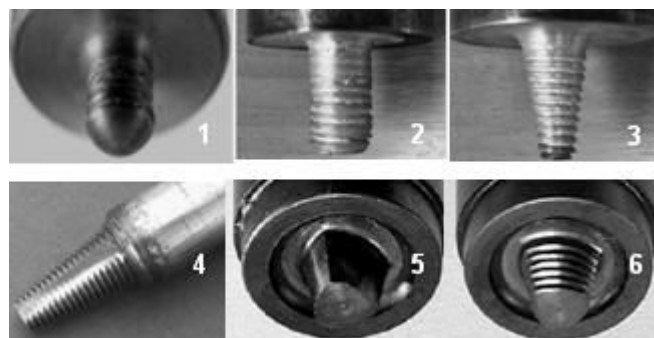
Figure 2-5 Photos of various tool pin designs (size of pins are not to scale), (1) Round-bottom cylindrical pin with diameter (ø) of 6mm, (2) Flat-bottom cylindrical pin with ø of 8mm, (3) Tapered pin with ø of 10mm at the base of cone, (4) Addition machined flats and tapered pin with ø of 12mm at the base of cone, (5) Trivex pin, and (6) MX Trivex pin [18, 20, 25-28]

A round-bottom cylindrical pin (see image 1 in Figure 2-5) has a round end, which reduces the tool wear during tool penetration and improves the quality of the weld root. A flat-bottom cylindrical pin design (see image 2 in the figure) has a bigger rotational radius at the edge of bottom pin than a round-bottom cylindrical pin, resulting in a higher velocity at the edge of bottom pin, thereby improving the tool performance. A tapered pin (see image 3 in the figure) has lower transverse loads than the same diameter cylindrical pin due to the reduction of the pin displaced volume. The cone shape pin has the largest moment load at the base of cone, where the tool pin is the strongest. Thus a cone shaped pin is preferred when compared with a cylindrical pin [18, 25, 28].

The addition of machined flats on a tapered pin (see image 4 Figure 2-5) has the effect of locally increasing the deformation of the plasticized material. Colligan et al [28] have demonstrated that a reduction in transverse forces and tool torque is directly proportional to the number of flats placed on the tapered pin. Additionally, Zettler et al [19] found that addition of flats on the pin can increase the weld nugget area and the workpiece temperature, which leads to the production of a fully consolidated weld structure.

Colegrove et al [27] studied the performance of the Trivex and MX Trivex tool pins (see image 5, 6 Figure 2-5) using two-dimensional computational fluid dynamics simulations. They found that the convex shape designs promote material slip, while maintaining the ability of the tool pin to stir the material, and reduce the magnitude of axial force. They also found that the Trivex tool pin has a marginally lower traversing force than the MX Trivex pin, as there are threads on the MX Trivex pin that increase the area carrying the shear stress, which result in an increase in the traversing force for this shape design.

In the FSW tool design process, one of the important steps is to determine the diameters of tool shoulder and pin. The sizes of tool shoulder and pin need to be large enough to generate sufficient frictional heat to plasticize the workpiece material to achieve a sound weld. In addition, the pin diameter needs to be large enough to withstand traverse loads and prevent pin fracture.

Tool pin length is determined by the workpiece thickness, tool set-up (tool tilt or non-tilt), and the desired clearance between the end of the tool pin and backing anvil. A ratio of tool shoulder diameter to pin diameter was suggested to assist tool design, and ratios between 2.5 and 3 to 1 were recommended by Dawes et al [25] for FSW 6mm thick Al plate. In addition, Dubourg et al [24] suggested that for FSW butt joints of Al plates between 1 to 8.3mm thick, the tool shoulder diameter is about 2.3 times the workpiece thickness plus a constant of 7 mm, and the tool pin diameter is equal to the workpiece thickness. Table 1 shows the dimensions of the scroll shoulder tool design used by Colligan and Pickens [15, 20] during FSW 25.4mm thick 6061 Al plate.

Table 1 Tool dimensions used by Colligan and Pickens in the investigation of the scroll shoulder tool design [20]

Shoulder diameter	Scroll depth	Scroll pitch	Scroll width	Pin diameter	Pin length
35.6mm	1.3mm	3.3mm	2.5mm	15.2mm	24.1mm

With increasing experience in FSW applications, complex shoulder and pin tool designs combined with an intelligent FSW machine have been implemented in industrial applications. Figure 2-6 illustrates the fixed, retractable and adjustable self-reacting pin tools. Fixed pin tools have a pin that does not move relative to the tool shoulder, and are generally used for both straight and complex curvature joints. A retractable pin tool can change pin position relative to the shoulder to accommodate varying material thicknesses and eliminate the 'pin hole' at the completion of a weld. Both fixed and retractable pin tools require a backside anvil to react to tool downward forces [29]. In contrast, the adjustable self-reacting pin tool is a dual-sided tool which has two shoulders with one contact on the top surface, and the other contact on the bottom. It must be operated with the tool vertical to the workpiece surface (similar to scroll shoulder tool), in which the workpiece to be joined is pinched between the upper and lower shoulders [30, 31].
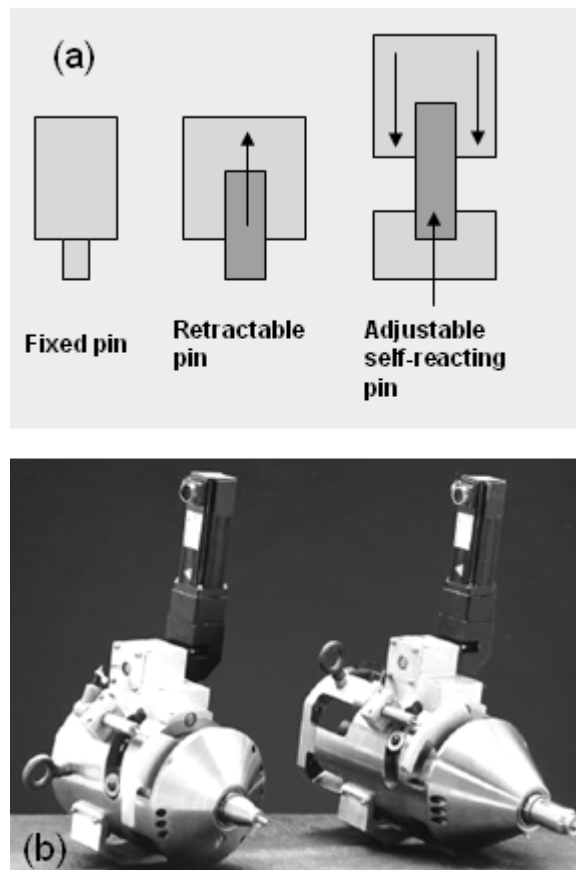
Figure 2-6 (a) Schematic illustration of Fixed, Retractable and Adjustable self-reacting pin tools, (b) Photo of Retractable pin tools [29, 30]

Complex motion FSW tool design focus on generating an effective mixing action between the tool and the workpiece, and most require specialized machinery. As can be seen from Figure 2-7, the Skew-stir tools increase the volume of material swept by the pin-to-pin volume ratio. This can be achieved by offsetting the axis of the pin from the axis of the spindle, thus producing an orbital motion to improve mixing action [32].
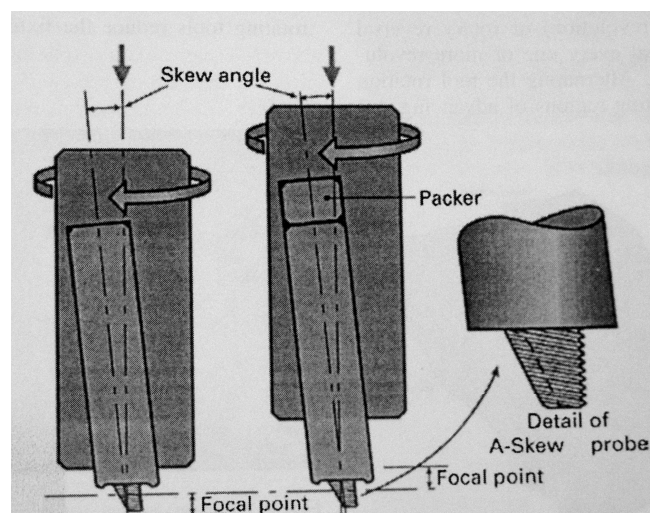
Figure 2-7 Schematic illustration of Skew-stir tools [32]

Com-stir tools combine rotary motion of the tool shoulder with orbital motion of the tool pin to maximize the volume of material swept by the pin-to-pin volume ratio. Figure 2-8 shows a FSW in progress using a Com-stir tool where the rotating pin with an orbital motion produces a wider weld, and increases fragmentation of the oxides that are originally presented on the two buffing faces [33].
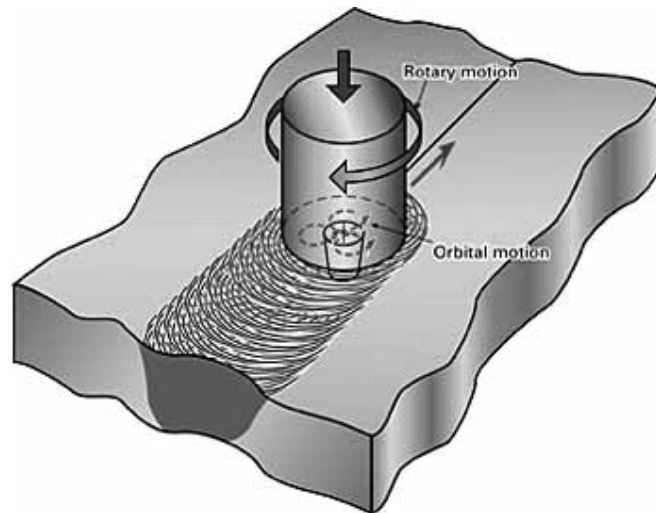
Figure 2-8 Schematic illustration of FSW process using a Com-stir tool [33]

Figure 2-9 shows a FSW process using a Two counter-rotating tools. Two counter-rotating tools can be used to FSW thick plates by counter-rotating the tools on either side of the plate. Two counter-rotating tools can reduce the clamping force required to secure the workpiece due to a decrease in net torque applied by the tools [34, 35].
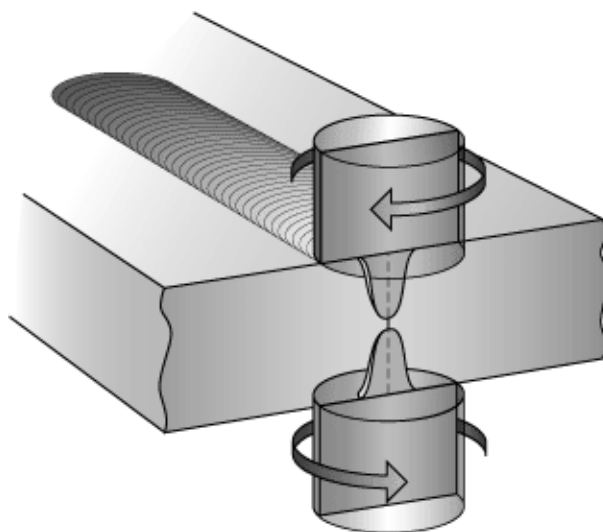
Figure 2-9 Schematic illustration of a simultaneous double-sided FSW process using a Two counter-rotating tools [35]

2.1.2 Processing Parameters

The FSW process has to be applied with equipment and controlled at processing parameters including ω, V and H etc. (see Figure 1-4). Some investigators [6, 31] have suggested that an increase in rotating speed (ω) generally decreases the welding resistant force, but with a non-proportional increase in rotating speed. Additionally, Arbegast's study [29] has also shown that the scroll shoulder tool rotating speed (hundreds of revolutions per minute) is much slower than conventional shoulder tool (over a thousand rpm) as they have different tool geometry.

In general terms, increasing travelling speed (V) will result in an increase of the welding resistant force [6, 16]. As reviewed in section 1.3.1, during FSW thick 5083-H131 Al plate, Colligan et al [15] found that a lower V (25mm/min) results in gross linear voids near the weld surface while higher V (107mm/min) leads to the appearance of internal voids in the shoulder flow zone. Travelling speed is a sensitive parameter in FSW using a scroll shoulder tool. However, the effect of tool travelling speed on weld zone formation is not well understood.

As for tilt angle (θ), Loftus et al [36] observed that increase θ form 1.5 to 3 degrees increased the welding resistant force by 20 percent in a conventional shoulder tool FSW. However, there is no tilt angle between the scroll shoulder tool rotating axis and the normal axis of the workpiece.

Nandan and Mclane [16, 37] have suggested that setting an appropriate plunge force (F) is the most desirable approach to be used in FSW workpieces of varying thickness. Colligan [20] found that the deeper the scroll shoulder tool is penetrated, the larger the plunge force is generated.

Smith [31] has found that the position control is a viable strategy to control the FSW process and assure the weld quality by means of setting a designated depth of shoulder penetration (H) below the workpiece surface. Fuller [22] has also suggested that a 0.1 to 0.5 mm depth of shoulder penetration is an optimal depth for the position control during scroll shoulder tool FSW. The effect of depth of shoulder penetration on the weld zone formation using a scroll shoulder tool has not been studied yet.

A few researchers [8, 14, 15, 19, 20, 38] have investigated the design of the scroll shoulder tool in the aspects of material flow induction, weld zone formation, and flow pattern identification. The range of processing parameters they used are as follows:

- ω=200 to 500rpm

- V=25 to 200 mm/min

- H=0.1 to 0.5mm

2.2 Experimental Techniques for Material Flow Investigation

FSW results in intense plastic deformation of the workpiece material. Material flow can not be viewed during FSW, except where specific approaches are conducted to preserve the real-time flow pattern. In this section, current experimental techniques that have been applied to investigate material flow during FSW will be reviewed.

2.2.1 'Marker Insert' Technique

'Marker insert' technique is one method of tracking material flow during FSW. It involves using a marker material, which is different from the material being welded, as a tracer. In the past few years, different marker materials, such as Al alloys that etch differently from the base Al alloy, copper foil, small steel shots, Al–SiC and Al–W composites, and tungsten wire, have been used to track the material flow during conventional shoulder tool FSW [6].

London et al [39, 40] reported that there are three main requirements for a microstructure marker: (i) it should be easily distinguished from the surrounding alloy after welding; (ii) it should readily flow with the alloy being welded; (iii) and it should be a size of scale that will not adversely affect normal FSW material flow behaviour.

2.2.2   'Dissimilar Materials' Technique

In addition to the 'marker insert' technique, several studies have used FSW of dissimilar materials to visualize the complex flow phenomenon. Ouyang and Kovacevic [41] examined the material flow behaviour by butt FSW 12.7 mm thick 2024 and 6061Al plates. They revealed three different regions in the welded zone. The first is the mechanically mixed region characterized by the relatively uniformly dispersed particles of different alloy constituents. The second is the stirring-induced plastic flow region consisting of alternative vortex-like lamellae of these two Al alloys. The third is the unmixed region consisting of fine and equiaxed 6061Al alloy grains.

2.2.3   Tool 'Stop Action' Technique

Colligan [42] studied the material flow behavior during FSW of aluminum alloys by means of steel shot tracer technique and 'stop action' technique. After stopping the welding process, each weld was subsequently radiographed to reveal the distribution of the tracer material around and behind the pin. He concluded that not all the material in the tool path was actually stirred and rather a large amount of the material was simply extruded around the retreating side of the welding tool pin and deposited behind.

'Stop action' technique includes manually stopping the FSW machine, to retract the tool pin from the workpiece, or to embed the tool pin in the workpiece for flow pattern investigation. However, one shortcoming of this technique is the time delay, as the rotating tool pin is not stopped instantaneously. To be specific, the pin could go from a very high rotating speed (hundreds or thousands) to zero. During the time required for this deceleration of the rotating pin, some material flow must have occurred.

2.2.4   'Pin-Breaking' Technique

A 'pin-breaking' technique has been developed by Chen et al [43] by means of machining a sharp corner at the pin-shoulder intersection (see Figure 2-10 below). As can be expected, a tool pin modified in this way can easily break and separate from the tool shoulder instantaneously, after which the real-time flow pattern around the broken pin can be preserved for detailed study. The application of this technique will be reviewed later in section 2.3.4.
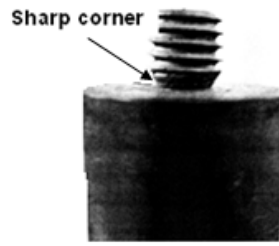
Figure 2-10 Photo of a FSW tool used in AUT laboratory showing the sharp corner at pin-shoulder intersection

The different experimental techniques used were aimed at understanding the basic physics of the material flow occurring during FSW. The application of those techniques in real-time material flow patterns observation will be reviewed in the next section.

2.3 Material Flow Patterns and Flow Forming Mechanism

Material flow during FSW is complex and depends on the tool geometry, process parameters, and the material to be welded. A few articles [44, 45] has suggested that material flow around the tool pin can be considered as material being forced and displaced from the leading side of the pin to the trailing side of the pin, under the rotational and translational action of the tool, resulting in a non-symmetrical flow field (nugget zone). Additionally, material flow in the shoulder flow zone is heavily affected by the tool shoulder and in particular the shoulder forging function.

Currently, the majority of the research focuses on the formation of the nugget zone using a conventional shoulder tool. There are two leading material flow formation hypothesis lodged in the literature, as illustrated in Figure 2-11 and Figure 2-12, to propose the formation of the nugget zone. One is the nugget flow patterns are attributed to the material flow with vortex-like and swirl features at the back of the tool pin (see Figure 2-11). The other is that the plasticized material is extruded and sheared by the rotating pin then deposited at the back of the pin, and this deposited material which has a semi-cylindrical shape forms the nugget zone, as illustrated in Figure 2-12 [46, 47].
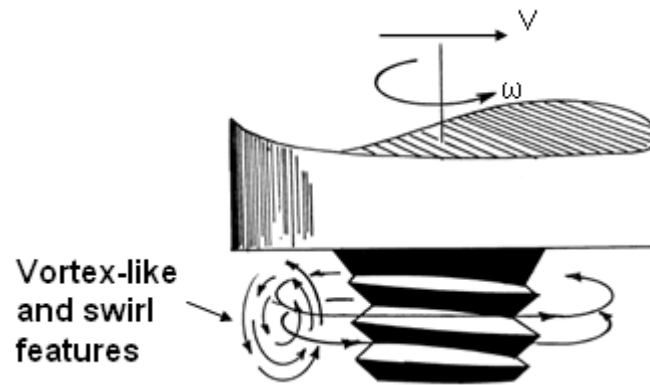
Figure 2-11 Schematic illustration of the material flow has vortex-like and swirl features in the back of tool pin forming nugget zone [48]
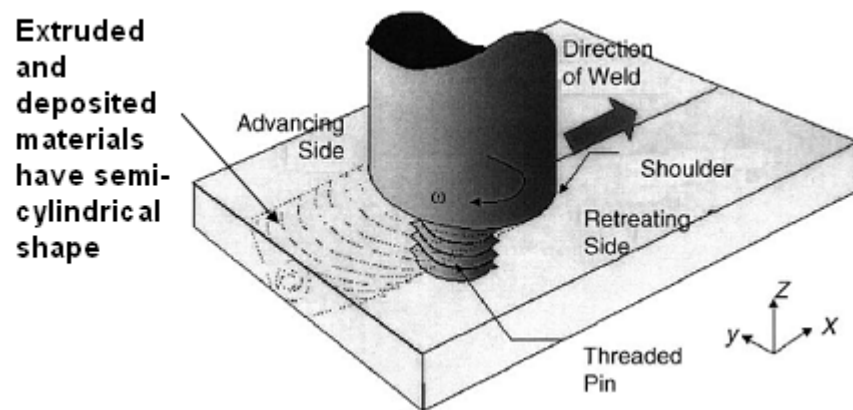
Figure 2-12 Schematic illustration of the material extrusion and deposition in the back of tool pin, deposition in the nugget zone has a semi-cylindrical shape [49]

In the following section, a few studies that focused on the experimental observation of the material flow behaviour will be summarized; then the overall flow patterns and some general trends will be presented. In addition, the forming mechanism of the weld zones and the correlations between the material flow pattern and the flow forming mechanism will also be addressed.

2.3.1 Onion Rings and Banded Structures

As introduced in section 1.2.2, a FSW weld consists of a shoulder flow zone and nugget zone. Under some FSW conditions, an onion ring pattern (see Figure 1-6) can be observed within the nugget zone in the transverse cross section (Z-Y plane see Figure 1-3 for coordinate) of weld. While a banded structure (see Figure 1-7) is viewed in the longitudinal direction (both X-Y and X-Z planes). These features are closely related to

26

the material flow and weld structure formation during FSW. The understanding of the formation of onion rings pattern is vital to the overall understanding of the FSW process [12].

Krishnan [47] studied the forming mechanism of the onion ring pattern. He suggested that the formation of the onion ring is found to be a geometric effect due to the fact that cylindrical sheets of material are extruded during each rotation of the tool, and cutting a transverse section (Z-Y plane) of the material produces an onion ring pattern. He simulated the formation of the onion ring using a clay model as shown in Figure 2-13. The model involves pressing two different coloured semicylinder clays together, to imitate the cylindrical sheets of metal extruded by FSW tool. By sectioning the model through the A-A plane (see Figure 2-13), the onion ring pattern can be distinguished in the cross section of the model as shown in Figure 2-14.
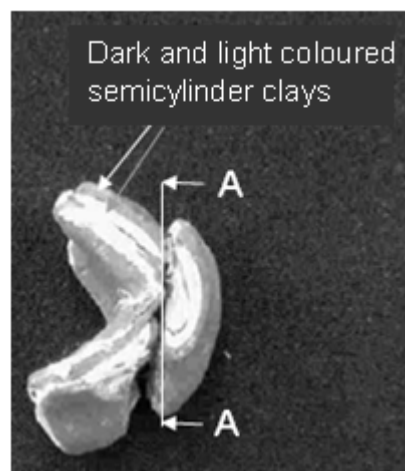
Figure 2-13 Clay model showing that semicylinders are pressed together to model the microstructural features in a FSW [47]
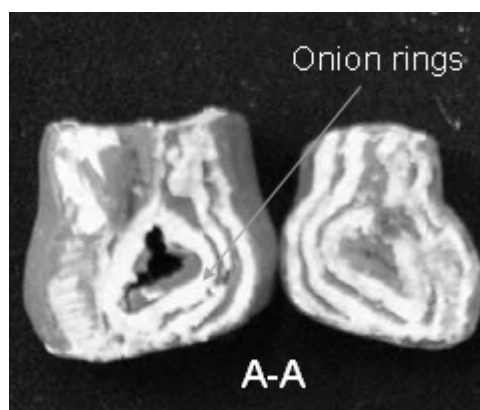
Figure 2-14 A-A section through the semicylinders in Figure 2-13 produces the onion rings [47]

27

Krishnan [47] also identified the flow pattern in the longitudinal cross section (X-Z plane) of the FSW weld as shown in Figure 2-15, and described the pattern as regularly spaced curved lines (similar to banded structures). As can be observed from the figure, there is a featureless region upon the spaced curved lines.
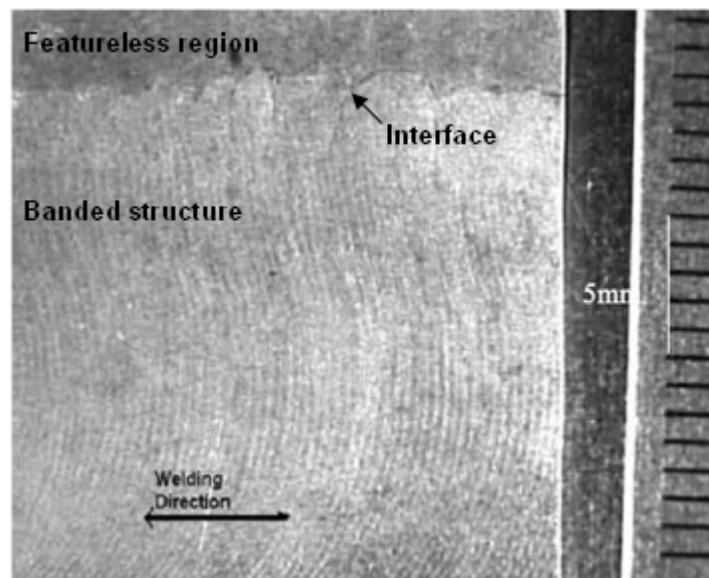
Figure 2-15 Longitudinal cross section of weld (sectioning on X-Z plane, see Figure 1-3 for coordinate), showing regularly spaced curved lines (banded structure) away from the welding direction within nugget zone, obtained at ω=400rpm and V=120mm/min [47]

2.3.2 Vortex-Like Flow Character

Guerra et al [50] studied the material flow character during FSW 6061Al using a conventional shoulder tool, and applying both the 'marker insert' and 'stop action' techniques. They inserted a thin 0.114mm high-purity copper foil along the faying surface of the weld. After a stable weld had been established, the pin rotation was manually stopped to produce a pin frozen in the workpiece. The workpiece was then sectioned for material flow pattern observation.

Figure 2-16 shows a plan view made at the midsection of the weld with a copper foil along the faying surface, and Figure 2-17 presents the enlarged view of the region ahead of the pin at the top of Figure 2-16. After study of the distribution of copper foil fragments in these figures, Guerra et al [50] found that the workpiece material (similar to markers) was moved around the pin during FSW by two processes. Firstly, the workpiece material on the front advancing side of the weld enters into a zone that rotates and advances simultaneously with the pin. Secondly, the workpiece material on

28

the front retreating side of the pin is extruded by the pin between the rotational zone and the parent material, and then fills in between material sloughed off from the rotational zone in the wake of the weld. This finding was supported by means of the 'stop action' technique and 'marker insert' technique by Colligan et al [42].
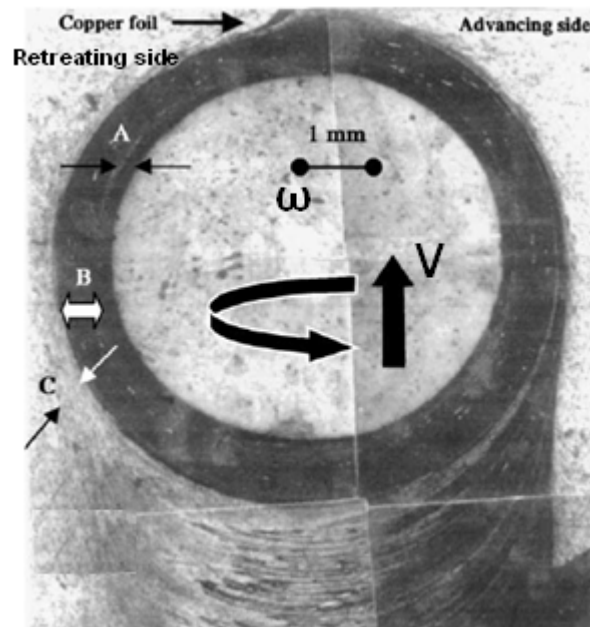
Figure 2-16 X-Y plane (see Figure 1-3 for coordinate) view at mid thickness of weld with a frozen pin, a copper foil (at the top part of figure) is inserted along the faying surface of 6061 Al plates, 'A' gap without material, 'B' rotational zone that rotates with the pin, 'C' transitional zone of material that is entrained by the rotating pin, small bright particles in 'B' are tracer particles from the copper foil [50]
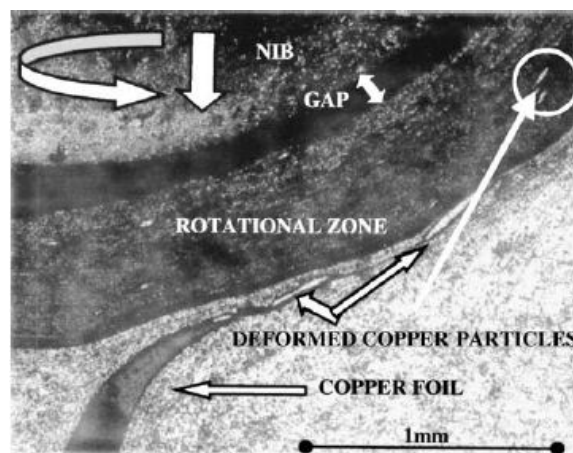
Figure 2-17 Enlarged view of region ahead of pin at the top of Figure 2-16, showing copper foil on the edge entering into rotational zone, and the copper foil is immediately broken into small particles, which appear at various places in the rotational zone [50]

Figure 2-18 shows the distribution of the copper foil particles in the transverse cross section of the weld. As can be seen from the figure, copper foil particles are distributed at various vertical and horizontal positions throughout the rotational zone in the weld which implies swirling movement of the copper foil particles. Accordingly, Guerra et al suggested that there is large vortex-like movement of workpiece material within the rotational zone. In addition, they also explained the cause of vortex movement is due to the wash and backwash of the threads. This explanation correlated well with schematic illustrations of vortex-like material flow movement by Prado et al [48] shown in Figure 2-11. Additionally, the suggestion of flow vortex-like motion by Guerra et al was also supported by Ke et al [51] by butt friction stir welding 6061 T6 and LF6 Al alloy, and Ouyang and Kovacevic [41] by butt friction stir welding of 2024 Al to 6061 Al plates.
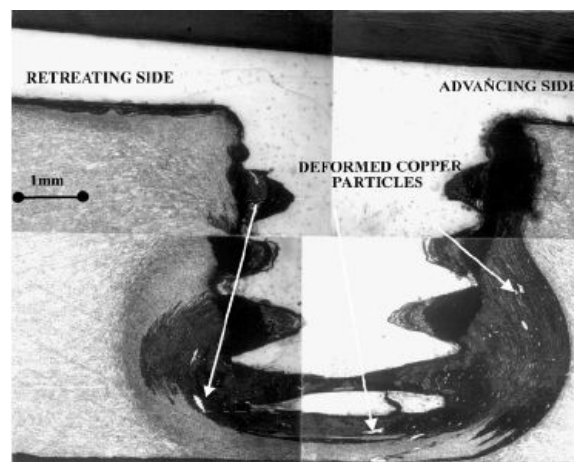
Figure 2-18 Transverse cross section of weld, bright copper particles can be seen throughout the dark rotational zone surrounding the pin [50]

As can be seen from the figures obtained by Guerra et al shown above, the material flow movement has been traced by 0.114mm high-purity copper foil inserted along the welding centre line during FSW of 6061 Al plate. Additionally, Guerra et al's findings also strongly support the hypothesis that flow patterns are attributed to material flow with vortex-like and swirl features at the back of the tool pin.

2.3.3 Extrusion Process Material Flow Behaviour

Reynolds et al [52] investigated the material flow behaviour by applying the 'marker insert' technique in FSW of 2195Al-T8 using a conventional shoulder tool. In their study, markers made of 5454Al-H32 were embedded in the pathway of the rotating tool as shown in Figure 2-19. The markers distribution after welding was revealed by

milling off successive slices of 0.25 mm thick from the top surface of the weld, etching with Keller's reagent, and metallographic examination.
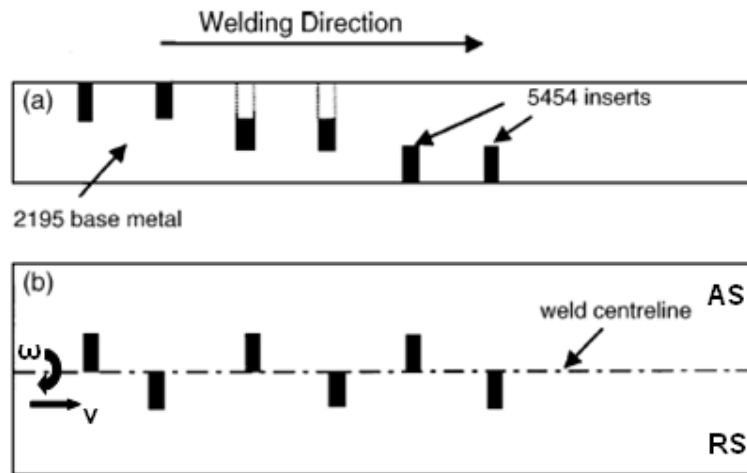
Figure 2-19 Schematic drawing of markers configuration and welding direction, (a) X-Z plane view (see Figure 1-3 for coordinate) showing the top, middle and bottom markers and tool travelling direction, (b) X-Y plane view showing advancing side (AS), retreating side (RS) of markers and tool rotating clockwise [52]

Reynolds et al found that the bulk of the marker material moved to a final location behind the original position, and only a small amount of the material on the advancing side was moved to a final position in front of its original position as shown in Figure 2-20. Additionally, they also found that the shoulder diameter is almost identical to the width of the deformed region as defined by distortion of the marker.
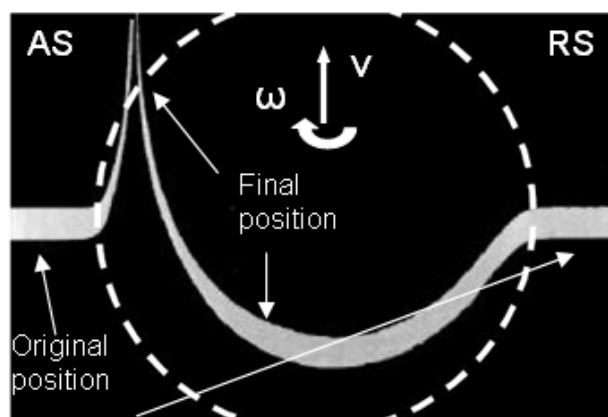
Figure 2-20 Composite picture (X-Y plane view) of marker materials distribution after welding, taken at 0.25mm from the top of the weld, showing original and final position of markers, where the dashed circle indicates tool shoulder diameter [52]

Further, Reynolds et al observed that there is a well-defined interface between the advancing side and retreating side as shown in Figure 2-21 and indicated by the arrow line. This shows that the workpiece material is not really stirred across the interface during the FSW process, when observed on a macroscopic level. This finding is different to the experimental results obtained by Chen et al [43] by means of the 'pin-breaking' technique, where there is not an interface between the advancing side and retreating side. Additionally, Reynolds et al also concluded that the post-welded marker materials distributed at the back of the pin have a semi-cylindrical shape.
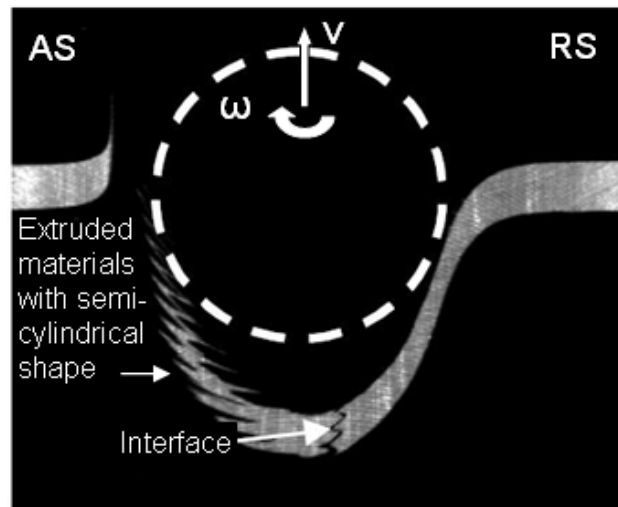
Figure 2-21 Composite picture (X-Y plane view) of marker materials distribution after welding, taken at 4mm from the top of the weld, indicating the interface between advancing and retreating side, showing the extruded markers with semi-cylindrical shape, where the dashed circle indicates footprint of threaded pin diameter [52]

Reynolds et al suggested that the FSW process can be roughly described as an 'in-situ' extrusion process wherein the tool shoulder, the pin, the weld backing plate, and cold base metal outside the weld zone form an 'extrusion chamber' which moves relative to the workpiece. This suggestion is supported by means of the 'marker insert' technique using steel shot as tracer by Colligan et al [42], and the 'Metalworking Model' technique based on the resultant microstructure and metal flow features by Arbegast [53]. However, Mishra and Ma [6], suggested that FSW is material dependent, such as A356 cast Al will not behave like a simple extrusion process in FSW, which is in contrast to Reynolds et al's proposition. Additionally, Reynolds et al's finding strongly supports the hypothesis that nugget flow patterns are attributed to the plasticized material being extruded by the tool pin and then deposited at the back of the pin in a layer to layer manner, and this deposited material has a semi-cylindrical shape.

2.3.4 Forming Mechanism of Nugget Zone

As reviewed above, nugget zone formation using a conventional shoulder tool has been investigated largely based on the observation of metallographic patterns in the cross sections of welds. However, those suggestions do not completely explain the forming mechanism of the nugget zone.

Recently, Chen et al [43] investigated the material flow around the tool pin, and the method of material deposition into the cavity at the trailing end of the pin to form the nugget zone. In their study, FSW experiments were conducted using a 'pin-breaking' technique, causing the pin to break suddenly and to embed it into the workpiece. A better explanation of the weld zone forming mechanism was presented by Chen et al along with the direct observation of both two-dimensional weld cross sections and three-dimensional pin-workpiece couples. The macrograph taken at the middle-thickness plane of the broken pin is shown in Figure 2-22. They found that a highly deformed shear zone exists around the embedded pin. As can be observed from the figure, workpiece material in this zone has been sheared and extruded around the pin.
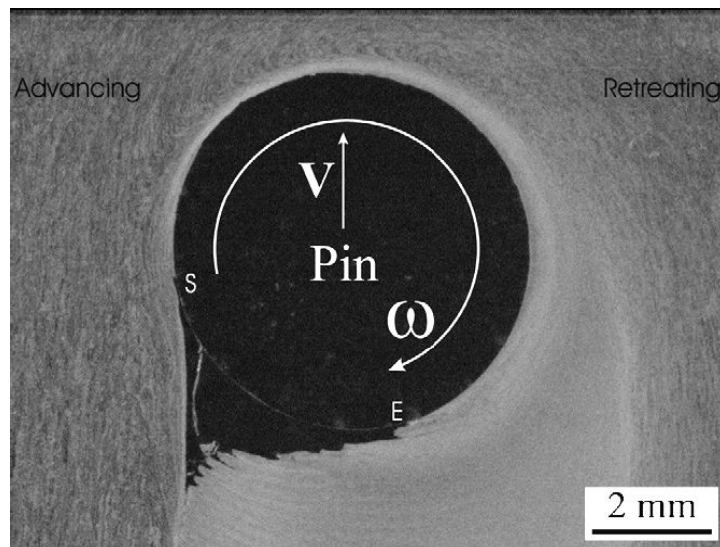
Figure 2-22 A longitudinal cross section of FSW weld (5083 Al alloy) with the broken pin embedded, sectioned along mid plane and parallel to X-Y plane (see Figure 1-3 for coordinate), welding condition: ω=760rpm, V=120mm/min, and θ=3° [43]

Chen et al also found that at the back of the pin, the sheared material will detach away from the pin moving to the advancing side to fill the cavity created by the pin moving forward. These experimental results are correlated well with the computing simulation results obtained by Bendzsak et al [54] using a thermo-mechanical flow model (STIR-

3D). Based on those observations, Chen et al [43] suggested that the nugget zone is formed in such a way that a portion of the shear zone forms a layer which detaches in the trailing-retreating location of the pin, one layer in each revolution. The majority of the shear layer detaches from the pin leaving little material to rotate with the pin. The detached layers continue to flow, pushed by the incoming material in the shear zone, subsequently filling the stable and forward moving cavity in a layer to layer manner to form the nugget zone.

More recently, Chen and Cui [46] studied the forming mechanism of banded structures. They conducted experiments using a modified 'pin-breaking' technique, in which a conventional shoulder tool with zero tilt angle was used in to eliminate the shoulder flow zone material flowing into the nugget zone. Figure 2-23 shows a three-dimensional SEM image of the pin-workpiece couples, and pin-workpiece couples was sampled from a weld produced by FSW 8mm thick 5083 Al plate with the top 4mm of the weld plate sectioned off.
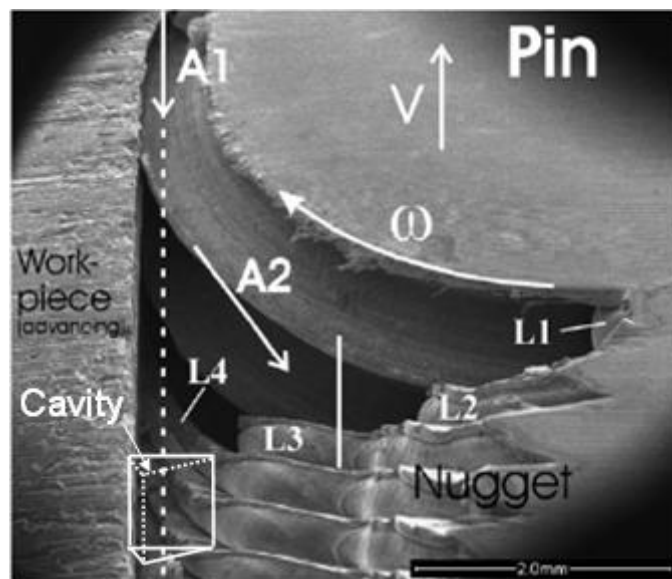
Figure 2-23 SEM image of a pin–workpiece couple sampled from a weld made with V = 5.2 mm/ s, ω = 710 rpm (thus λ = 440 μm) , and θ=0°; advancing side (AS) on left; (i) pin moving directions indicated; (ii) L1–L4 indicate layers immediately following the rotating pin; (iii) A1 – the sample further sectioned along; (iv) A2 – direction of viewing in a higher magnification [46]

Chen and Cui found that four layers (L1-L4 as indicated in the figure) were rotating and detaching from the pin clearly showing the bands (shear layers) forming the weld nugget behind the pin. They explained that the shear material in a thread space was spread into a layer, primarily as a result of the equivalent downward motion of the

thread flank. The bands being equal to the tool advance per revolution (λ = tool welding speed (V)/rotational speed (ω)), which is due to a geometrical restriction [46].

As can be observed from Figure 2-23, the bands (shear layers) swirled downward from the retreating side to the advancing side and formed a cavity as indicated. This cavity was formed by using a conventional shoulder tool FSW at a zero tilt angle and after pin breaking suddenly. It can be also noticed that the cavity is along the advancing side of weld and has a deeper downward distance from the workpiece surface on the advancing side than on the retreating side, which is similar to the experimental results obtained during the preliminary investigation of the present study shown in Figure 1-14.

As reviewed above, the nugget zone is formed by the shear layer detached from the pin in a layer to layer manner. Under some FSW conditions as discussed in section 2.3.1, banded structures can be identified in the nugget zone within the longitudinal cross section of weld. It does show a strong correlation between the flow pattern and flow forming mechanism. Therefore, it is possible to reveal the shoulder flow zone forming mechanism by identifying the flow pattern within the shoulder flow zone.

2.3.5   Forming Mechanism of Shoulder Flow Zone

As introduced in section 1.2.2 and illustrated in Figure 1-5, the shoulder flow zone is located in the top of the weld zone. The shoulder flow zone formation using a conventional shoulder tool has been investigated by many researchers. Studies have suggested that the shoulder flow zone is formed by sheared and compressive material flow around the tilted pin [9, 55].

Sheared material flow is induced by the applied normal force and the rotating shoulder, in which a friction force is created on the shoulder-workpiece interface resulting in a large amount of frictional heat generation, leading to a high degree of workpiece material plasticity and material movement, and hence shear flow is obtained. The compression of the material flow is created by tilting the shoulder such that a tilt angle of the tool shoulder results in a transverse force applied on the workpiece and along the welding direction, leading to a compressing and forging action on the material flow. The shear action transfers the workpiece material from the retreating side to the advancing side. As the tool travels, the plasticized workpiece material is sheared and

forced around the pin to fill the channel left by the travelling tool pin to form the shoulder flow zone. During conventional shoulder tool FSW, material flow forged by the rotating shoulder to fill the channel has a bulk flow characteristic.

Chen et al [9] conducted a series of FSW experiments to examine the effects of tool shoulder size and tilt angle on the shoulder flow zone formation. They found that a higher tilt angle resulted in adequate material flow within the shoulder flow zone which led to a reduction of the weld defect size, as can be observed from Figure 2-24.

(a) θ = 0° (b) θ = 1°

(c) θ = 3° (d) θ = 4°
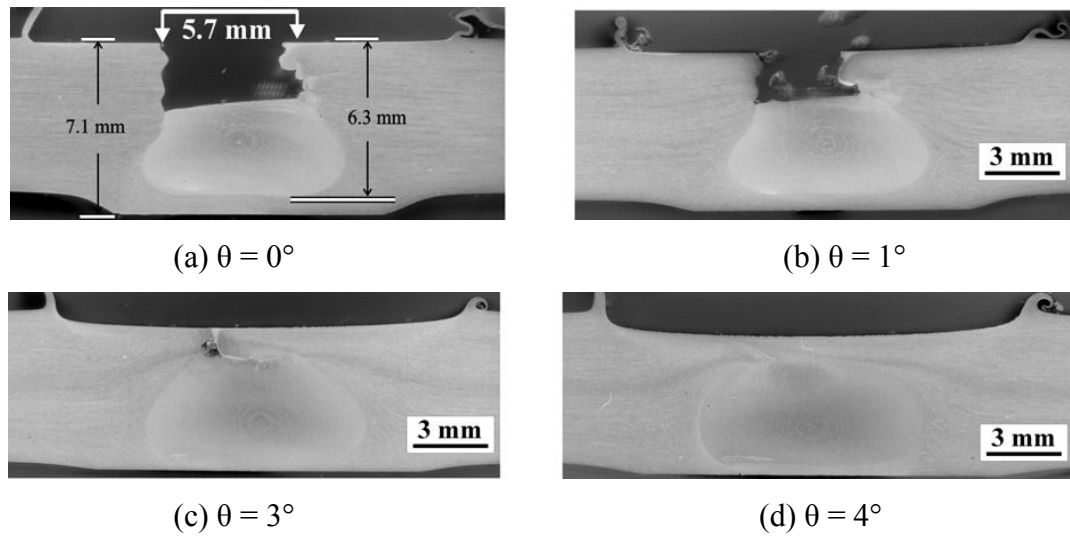
Figure 2-24 Cross section of Al alloy 5083 welds made using a conventional shoulder tool with shoulder diameter=16 mm and tilt angle (θ) as indicated [9]

Chen et al also observed that a smaller shoulder resulted in insufficient material flow in the shoulder flow zone and hence a channel defect would form in the weld as shown in Figure 2-25. They concluded that the plasticized material flow compressed by the forward motion of shoulder contributed to the complete formation of shoulder flow zone. This finding is well supported by Elangovan et al [56] in investigation of the effect of shoulder diameter on the shoulder flow zone formation.

(a) $D_{shoulder}$ = 20 mm (b) $D_{shoulder}$ = 16 mm
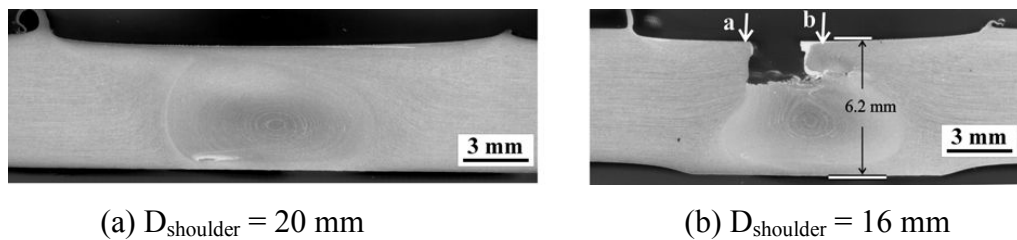
Figure 2-25 Cross sections of Al alloy 5083 welds made using a conventional tool with shoulder diameter as indicated and θ = 2° [9]

2.4 Factors Affecting Weld Structure / Weld Imperfection

As reviewed above, weld zone formation has been studied intensively using a conventional shoulder tool and direct observation of weld zone metallographic patterns. Although the exact forming mechanism of material flow has not been fully understood, it is well known that weld zone material flow behaviour is strongly dependent on tool geometry, welding parameters and base material [6, 16]. Factors affecting weld zone formation and weld imperfections will be reviewed in this section.

2.4.1 Tool Geometry and Welding Parameters Affecting Defect Formation

Fujii et al [57] studied the effect of FSW tool shapes and welding parameters on the mechanical properties and microstructure of the weld. They conducted experiments by butt FSW 6061 Al plates using three different tool pin profiles as shown in Figure 2-26.
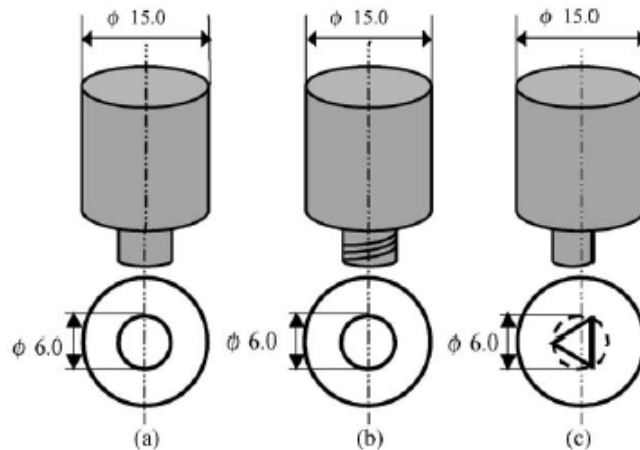
Figure 2-26 FSW tool shape (a) column without threads, (b) column with threads, (c) triangular prism [57]

Fujii et al found that the tensile strength of FSW joints is almost the same for the three different tools. Accordingly, they concluded that the tool shape does not significantly affect the microstructures and mechanical properties of the joints. This finding is supported by Elangovan et al [56, 58] in a study of the effect of tool profile on the weld zone formation.

Figure 2-27 shows the macrostructure of welds produced at various travelling speeds and with various tool shapes, and obtained by Fujii et al. It can be observed from the figures, there is a defect appearing in the weld obtained by a triangular prism tool FSW

at 1500rpm (ω) and 1000mm/min (V). However, there are no defects in the welds produced by the same tool rotating at the same speed (ω) but a lower travelling speed of 100 and 400mm/min. This indicates that a faster tool travelling speed (V) results in an increase in the likelihood of welding defects which correlates with an other study conducted by Kim et al [59]. However, the effect of travelling speed on the shoulder flow zone formation using a scroll shoulder tool remains unclear, and is worthy of further research.
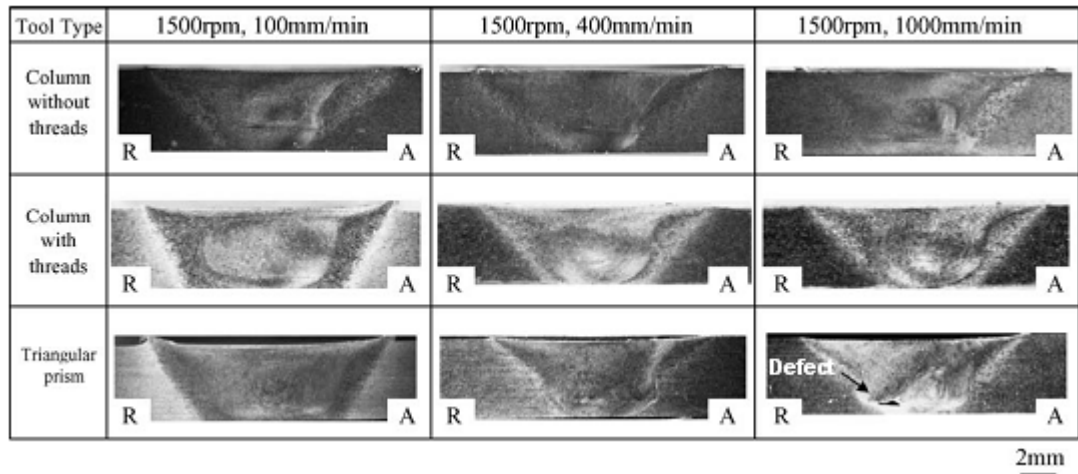
Figure 2-27 Macrostructure of cross sections of 6061 Al FSW joints, showing the weld quality at various welding parameters and tool types [57]

Recently, Kumar and Kailas [55] studied the shoulder flow zone forming mechanism by FSW 7020-T6 Al plate using a special experimental setting. Figure 2-28 shows the experimental setting used by Kumar and Kailas, where the interaction of the conventional shoulder tool with the base material is continuously increased, leading to an increase in the depth of shoulder penetration and axial load.
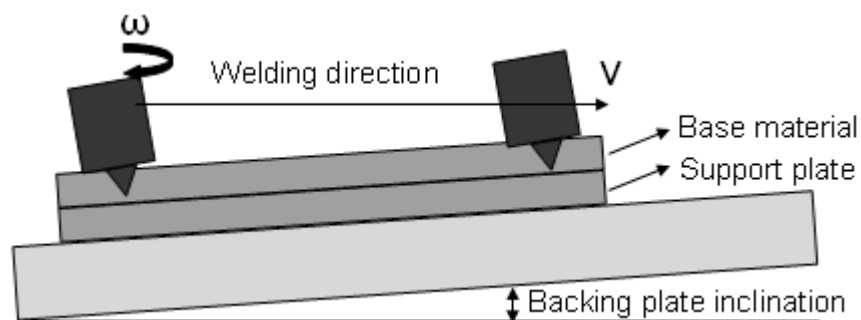
Figure 2-28 Schematic illustration of experimental setting; the backing plate is kept at an angle such that the axial load can be linearly increased (from 4 to 10.9 kN) by linearly increasing the interference between tool and material being welded [55]

Figure 2-29 shows the cross section of welds produced at increasing depths of shoulder penetration and downward loads, and obtained by Kumar and Kailas. It can be seen that the shoulder flow zone defect size reduced as the downward loads increased, and above a 'normal' load of 7.4 kN (Figure 2-29 f) defects have disappeared.
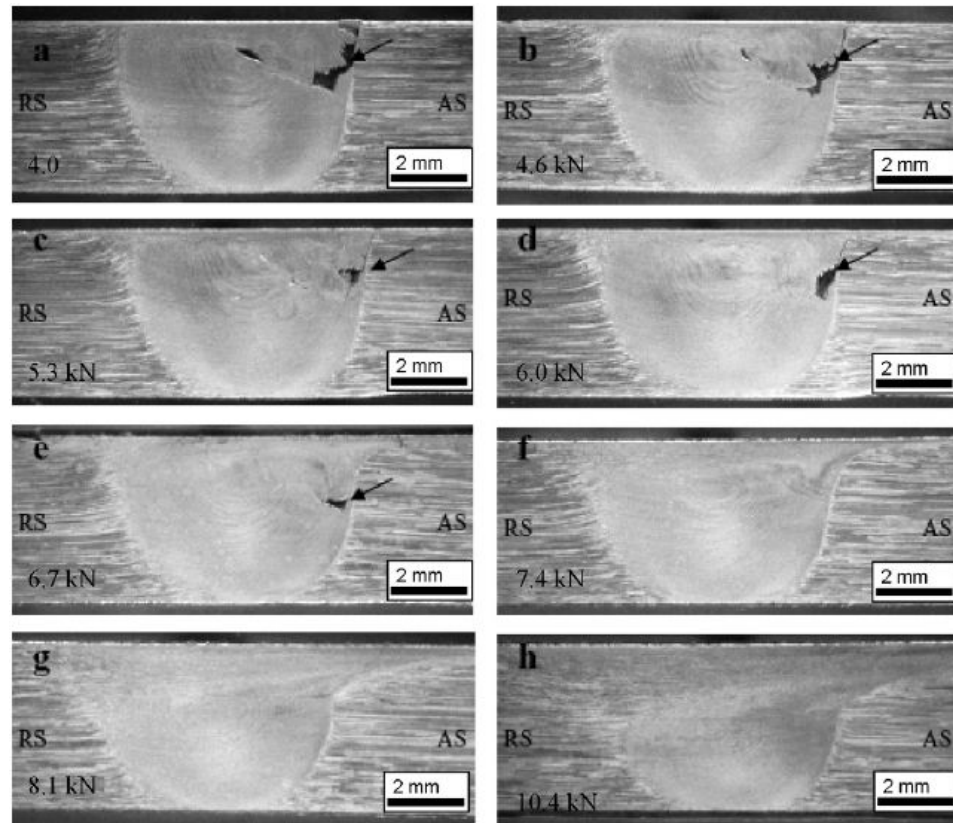
Figure 2-29 Evolution of a shoulder flow zone formation as a function of the downward force, arrow marks indicate the presence of voids in the weld [55]

Kumar and Kailas explained that the primary reason for the defect in the welds, at the initial stages, where the axial load was less than 7.4 kN, is shallow shoulder penetration (lack of shoulder contact with the base material). When the depth of shoulder penetration was increased the axial load increased and when the axial load was above 7.4 kN, the shoulder flow zone material from the leading edge was confined in the weld cavity, and then a sufficient amount of frictional heat and hydrostatic pressure was generated to produce a defect-free weld. Accordingly, they concluded that deeper shoulder penetration leads to a decrease in the likelihood of welding defects. This conclusion is supported by the findings of Dubourg et al [60] in a study of the effect of welding parameters on the FSW weld quality. However, the effect of depth of shoulder penetration on the shoulder flow zone formation using a scroll shoulder tool remains unknown.

2.4.2 Workpiece Materials Influencing Material Flow

Chen et al [61, 62] investigated the material flow pattern by FSW two types of Al alloy and comparing the cross sections of these two welds. Figure 2-30 shows two cross sections of weld produced by FSW AA5083 and A356 plates at 800rpm (ω), and 1mm/min or 3mm/min (V). As can be observed from the figures, the nugget zone of AA5083 weld exhibited the typical onion rings pattern. On the other hand, an onion rings pattern has not been observed in the A356 weld.
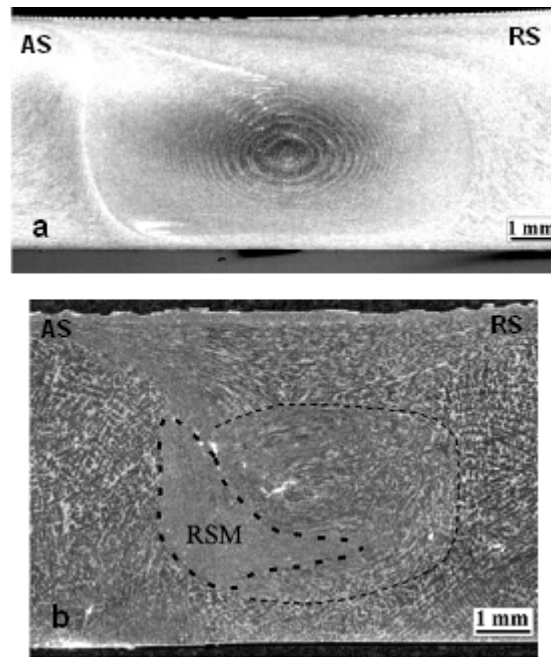
Figure 2-30 Cross section of FSW welds (a) AA5083, $D_{shoulder}$ = 20 mm, V = 1 mm/s, ω= 800rpm and θ= 2°, displaying onion rings in nugget zone (b) A356, $D_{shoulder}$ = 16 mm, V = 3 mm/s, ω = 800rpm and θ = 2°, showing the absence of clear onion rings in nugget zone (outlined) [61, 62]

As can be seen in Figure 2-30 (b), the boundary of the weld nugget on the retreating side is less clear in the macrograph due to a low degree of deformation and thus the zone has been marked. Furthermore, there is a region marked RSM where the original dendritic feature has disappeared completely, due to heavy deformation. Chen et al concluded that the type of metal workpiece is another factor that can influence the material flow characteristics significantly as different materials have different mechanical and thermal properties. This conclusion is strongly supported by Zettler et al [38] in the study of the effect of alloy types on material flow patterns during FSW 2024-T351 and 6013-T6 Al plates.

2.4.3 Types of FSW Defects and Defects Control

Leonard et al [63] investigated the imperfections of FSW welds, and they reported that there are three common defects encountered during FSW. Figure 2-31 shows these three typical defects, which are internal voids, joint line remnants, and root flaws. They observed that internal voids normally occurred on the advancing side of the weld, and internal void formation was due to insufficient forging pressure and excessive welding speed, and internal voids could be significantly reduced using an appropriate tool shoulder-pin design and welding speed.
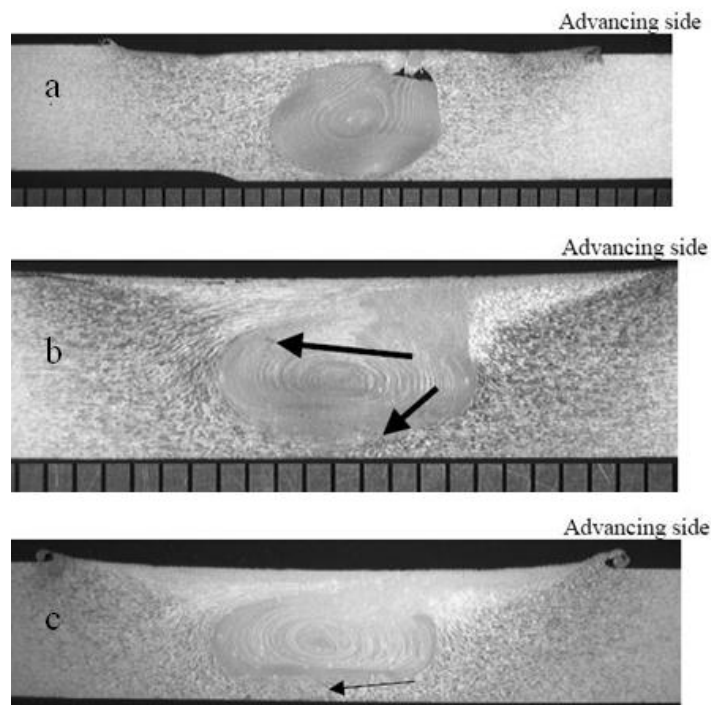
Figure 2-31 Cross sections of defect weld (a) internal voids, (b) joint line remnants, and (c) root flaws [63]

Leonard et al also found that joint line remnant defects were due to a semicontinuous layer of oxide through the weld nugget. They recommended several strategies to reduce this type of weld imperfection, such as sufficient cleaning of the workpiece, correct tool location versus weld joint-line, suitable shoulder diameters and tool welding speeds etc. Further, they also concluded that there were quite a few causes of root flaws, including variation of plate thickness, incorrect tool position, and improper tool design. They advised that a sufficient depth of shoulder penetration could eliminate root defects. Leonard et al's findings and suggestions are well supported by Arbegast [64] in investigation of FSW weld defect mechanism.

In addition, due to different types of defect weldments obtained in this study, FSW weld defects are also defined as weld cavity (a triangular prism shape discontinuity along the weld profile as indicated in Figure 1-14), weld void (a small empty space along the top cross section of weld, see Figure 1-13 c) and weld internal void (a small empty space inside the cross section of weld, see Figure 1-13 c) throughout this report.

2.5 Formation of Shoulder Flow Zone Using Scroll Shoulder Tool

As introduced in section 1.2.2 and illustrated in Figure 1-5, the shoulder flow zone is located in the top of the weld zone. Some articles [6, 11, 16] has suggested that the shoulder flow zone is mainly influenced by the shoulder geometry and welding parameters. The tool shoulder plays a critical role not only in inducing shoulder flow zone material, but also in ensuring proper containment and consolidation of the shoulder flow zone.

Since TWI introduced the scroll shoulder tool concept, several studies [6, 8, 14, 65] have been conducted to evaluate the material flow induction and weld zone formation in the shoulder flow zone using this type of tool. A small quantity of publications regarding shoulder flow zone formation will be reviewed in this section.

2.5.1 Induction of Pick Up Material (PUM) / Effect of Welding Parameters on Mass of PUM

As reviewed in section 1.3.1, Dawes and Thomas [8] studied the PUM (pick up material) induced by the tool pin. They described how the PUM is induced during the tool pin plunging stage (FSW process includes tool pin plunging, tool shoulder plunging and tool travelling; three main procedures as introduced in chapter one). However, experiments to trace PUM movement were not conducted. Additionally, they also investigated shoulder flow zone formation by FSW 6.35mm thick 5083 Al plate using a scroll shoulder tool. As can be seen in Figure 2-32, the weld surface undercutting was absent, and the surface proud flash was eliminated, thus the weld surface finish was improved.
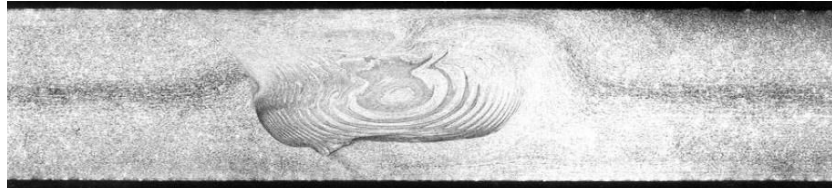
Figure 2-32 Transverse cross section of weld produced by butt FSW 6.35mm thick A5083 plates using a scroll shoulder tool, and operated normal to the workpiece surface, with the tool shoulder set to just touch the workpiece surface [8]

Dawes and Thomas found that the scroll shoulder tool has three advantages; it can improve surface finish, increase welding speed, and operate normal to the work surface. However, they also found that the disadvantage of the scroll shoulder tool was that special care is required to set the tool such that it just touches the workpiece surface. Any additional workpiece contact will produce significant amounts of weld flash and result in a risk of voids occurring in the weld.

Toskey et al [13] studied the effect of scroll shoulder tool design on joint quality by FSW 11mm thick 5083 Al C-channel structures. Figure 2-33 shows the adjustable self-reacting pin tool (as introduced in section 2.1.1) that they used, and Figure 2-34 demonstrates the FSW experiment in progress.
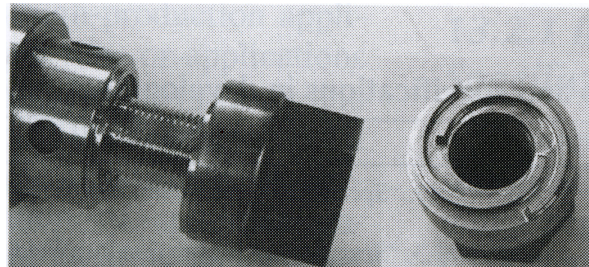
Figure 2-33 An adjustable self-reacting pin tool used in welding 11mm thick 5083 Al C-channel structures [13]
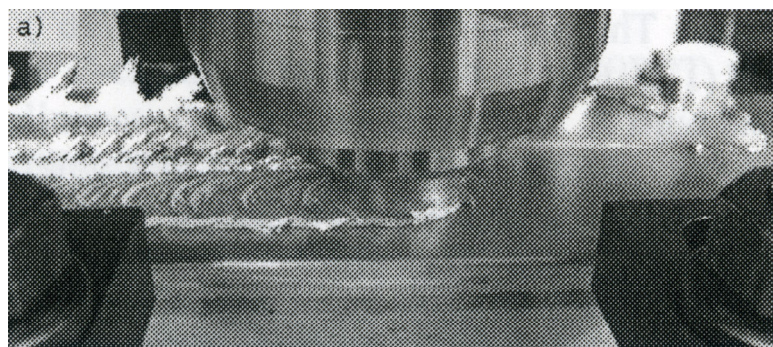
Figure 2-34 FSW 11mm thick 5083 Al C-channel structures in progress, showing 'snowplowing' around the tool [13]

Toskey et al observed that the scroll shoulder tool resulted in a 'snowplowing' effect, where material on the workpiece top surface was pushed to the outside edge of the shoulder rather than pulled into the scroll groove beneath the shoulder. They speculated that an 'over-plunging' of the tool shoulder resulted in the 'snowplowing' effect. However, they did not report the depth of shoulder penetration they used in this experiment or conduct further investigation to verify the cause of the 'snowplowing' effect they speculated.

As reviewed above, Dawes and Thomas [8] described the induction and the movement of the PUM during the first stage of the FSW procedure, and their descriptions have not been verified by experimental results. In addition, during tool shoulder plunging and tool travelling (two other FSW procedures), the induction and the movement of the PUM are still unclear. Further, neither Dawes [8] nor Toskey [13] have quantified the mass of PUM to establish how much workpiece material could be driven into the scroll groove beneath the shoulder. They have also not evaluated the effect of welding parameters, such as the depth of shoulder penetration, on the mass of induced PUM. The relationship among the mass of PUM, the formation of shoulder flow zone, and the associated likelihood of defect weld formation, has not been explored yet. This knowledge is important in the design of scroll shoulder tools to ensure FSW weld quality.

2.5.2   Effect of Welding Parameters on Shoulder Flow Zone Formation

As reviewed in section 1.3.1, Colligan et al [15] investigated the effect of welding parameters on the shoulder flow zone formation by FSW a 25.4mm thick 5083-H131 Al plate, using a scroll shoulder and tapered threaded pin tool with three flats cut on the thread pin surface. They evaluated the shoulder flow zone formation by varying the tool travelling speed from 25 to 127mm/min and keeping the tool rotational speed constant at 250rpm. The results they obtained (demonstrated in Figure 1-11 and Figure 1-12) show that a risk of a defect forming in the weld zone occurs at both lower (25mm/min) and higher (107mm/min) tool travelling speeds. These results are in contrast to the finding of Fujii et al [57] reviewed earlier.

Colligan et al [15] also studied scroll shoulder tool design by FSW an 18.4mm thick 2195-T8P4 Al plate, using a scroll shoulder and tapered threaded pin tool with three

flats cut on the thread pin surface. Figure 2-35 shows a transverse cross section of FSW 2195 Al weld produced by the tool travelling at a speed of 66mm/min, and a 200rev/min spindle speed. They found that the weld produced by the scroll shoulder and flat pin tool in 2195-T8P4 Al alloy appears to have a defect-free weld and a 'bulls eye' pattern of concentric circles in the upper portion of weld zone.
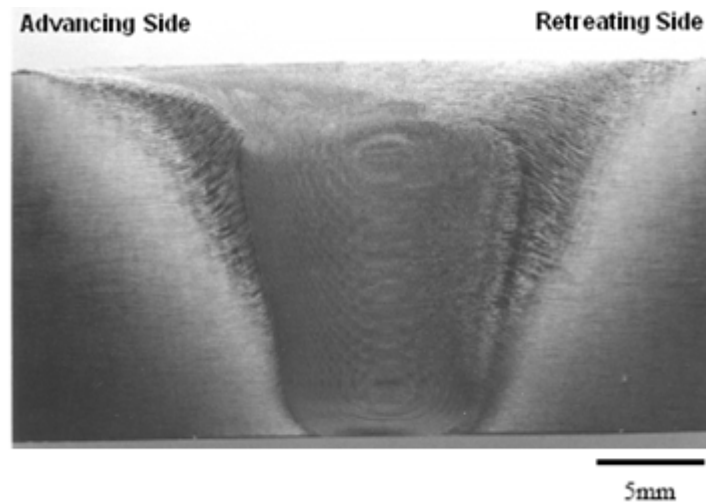
Figure 2-35 Transverse section of 18.4mm 2195-T8P4 Al FSW weld produced by a scroll shoulder tool rotating at 200rpm and travelling at 66mm/min, showing a 'bulls eye' pattern in the weld [15]

Figure 2-36 shows a cross section of FSW 2195 Al weld obtained by Colligan et al [15] using a scroll shoulder tool travelling at a speed of 78.7mm/min, and a 200rev/min spindle speed. They observed that the weld structure implied an insufficient consolidation of material or internal voids in the upper advancing side of weld zone. This indicates that a faster tool travelling speed (V) resulted in an increased likelihood of welding defects. In addition, they also found that a layer to layer flow pattern appeared in the upper advancing side of weld zone as indicated in the figure.
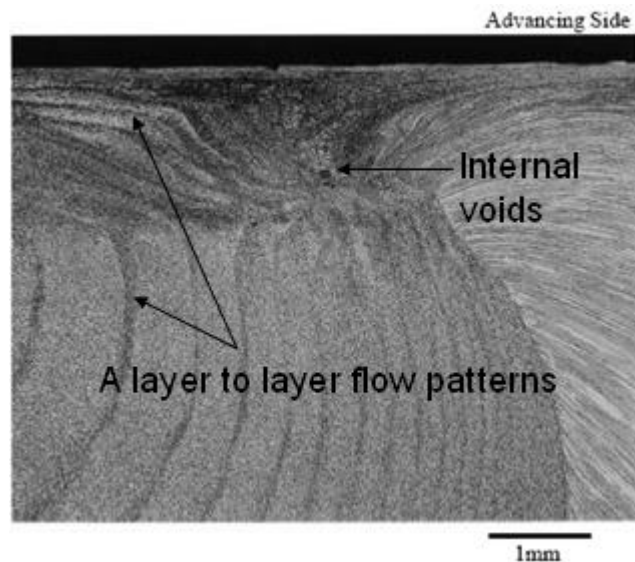
Figure 2-36 Transverse section of 18.4mm 2195-T8P4 Al FSW weld, showing a layer to layer flow pattern and a defect appearing in the upper advancing side of weld zone, using a scroll shoulder tool rotating at 200rpm and travelling at 78.7mm/min [15]

As can be noticed from the results provided by Colligan et al [15] shown above, the effect of the tool travelling speed on the weld zone formation are in contrast to each other in FSW 5083-H131 Al and 2195-T8P4 Al plates. It still remains unclear why both faster and lower travelling speeds increase the likelihood of defects forming in the shoulder flow zone. The effect of tool travelling speed on the shoulder flow zone formation is however not well understood.

As reviewed in section 2.5.1 (last section), both Dawes [8] and Toskey's [13] experimental results demonstrated the effect of the depth of shoulder penetration on the shoulder flow zone formation. Dawes and Thomas [8] suggested that a near zero depth of shoulder penetration (setting tool to just touch the workpiece surface) could lead to the elimination of the weld flash and an improvement of the weld finish. However, the depth of 0.1 to 0.5mm shoulder penetration was strongly recommended by Fuller [22] using a scroll shoulder tool, which is different to Dawes and Thomas' suggestion. Additionally, Toskey et al's [13] speculation ('over-plunging' of the tool shoulder) correlates with Dawes and Thomas' [8] proposition. Nevertheless, how the depth of shoulder penetration affects the material flow forming the shoulder flow zone is still unclear. The information regarding the effect of welding parameters on the shoulder flow zone formation is important in the selection of welding parameter to assure FSW weld quality.

2.5.3   Shoulder Flow Zone Flow Patterns and Forming Mechanism

Zettler et al [19, 38] studied the effects of tool pin geometry on the material flow formation by FSW 4mm thick AlMgSc alloy, using a scroll shoulder and tapered pin tool. Figure 2-37 shows the tool they used and Figure 2-38 presents a longitudinal cross section of the weld produced by this tool.
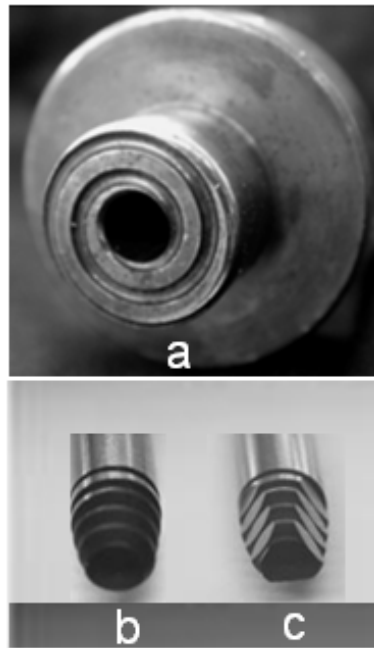
Figure 2-37 Photos of scroll shoulder tool; (a) one scroll flat shoulder, (b) tapered threaded pin, (c) tapered three flats cut on thread pin used by Zettler et al [19]
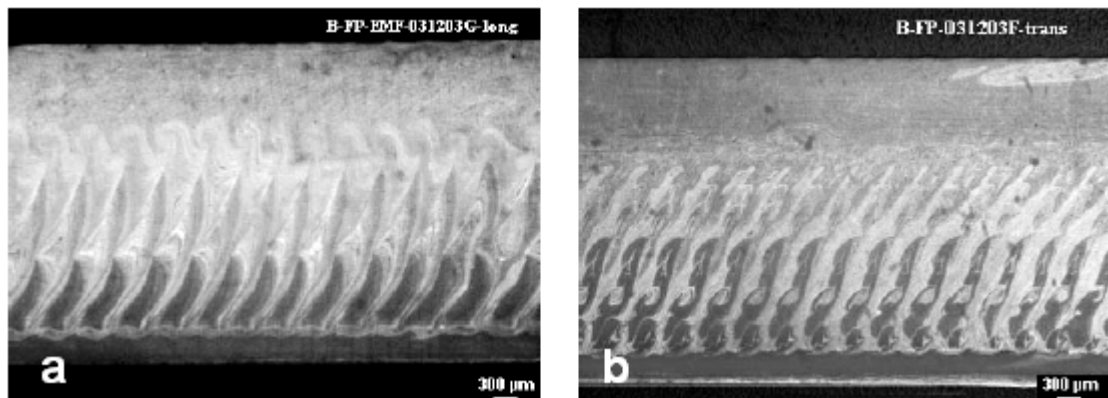
Figure 2-38 Transverse section (sectioning through Z-Y plane, see Figure 1-3 for coordinate) of AlMgSc alloy weld produced by tool shown in Figure 2-37, (a) using pin 'b', and (b) using pin 'c', FSW at ω=700rpm and V=350mm/min, showing the banded structure in the join line of weld [38]

Zettler et al reported that the banded structure shown in Figure 2-38 was obtained by sectioning a post-weld through the Z-Y plane which is a transverse cross section of the weld (seen perpendicular to the welding direction). However, this is an unusual flow

47

pattern as Chen and Krishnan [46, 47] have suggested that the banded structure normally can be observed in the longitudinal cross section of weld sectioned through the X-Y or X-Z plane (seen parallel to the welding direction). The flow pattern of the shoulder flow zone produced by scroll shoulder tool still remains unclear.

Burford et al [14] investigated the influence of scroll shoulder tool geometry on the metal deformation and surface roughness in the uppermost layers of the weld. They conducted an experiment by FSW 3.2mm thick 7055-T6 Al plate, using two types of scroll shoulder tool as shown in Figure 2-39.
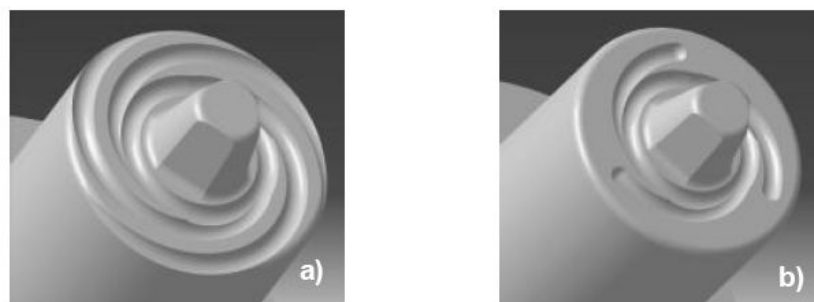
Figure 2-39 Scroll shoulder tools a) conventional scroll tool- shoulder configuration with scrolls extending out to the edge of the shoulder face, b) wiper scroll tool-the same shoulder configuration with the wiper feature (area) added, which serves to bound the extent of the scrolls [14]

Representative longitudinal cross sections along the centre lines of welds produced by the tools shown in Figure 2-39 are presented in Figure 2-40. After comparing the microstructure adjacent to the upper surface of the weld produced by these two tools, Burford et al concluded that a conventional scroll tool produced a greater extent of non-uniform deformation along with greater surface roughening than wiper scroll tool. They explained that the scrolls used in a conventional scroll tool were open at the edge of a given workpiece surface which results in more collection of contaminates, such as oxides, etc., leading to greater surface roughening. However, the specific flow pattern in the shoulder flow zone induced by scroll shoulder tool is still unclear.
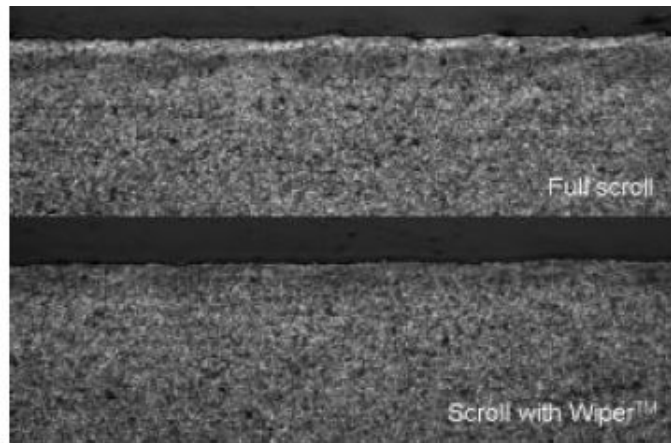
Figure 2-40 Longitudinal cross section of 3.2mm thick 7055-T6 Al FSW welds (50X magnification) produced by tools shown in Figure 2-39, (top) using conventional scroll tool, and (bottom) using wiper scroll tool, rotating at 800rpm and travelling at 4.2mm/s [14]

Scialpi et al [66] studied the effect of scroll shoulder tool geometries on the mechanical properties of FSW weld. In their work, they butt joined two 1.5mm 6082-T6 Al sheets by FSW, using a modified scroll shoulder tool as shown in Figure 2-41.
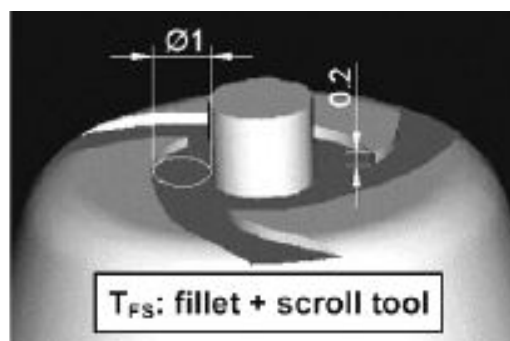
Figure 2-41 A scroll shoulder and non-threaded pin tool used by Scialpi et al, and tool dimensions are in mm [66]

Scialpi et al observed that the transverse cross section of weld, as shown in Figure 2-42 below, did not show a typical onion ring pattern. They speculated that this is due to the high spindle speed and use of a non-threaded pin. They also observed that the scroll shoulder tool produced a weld with higher strength and elongation characteristics than other tools in longitudinal tensile tests. However, the exact flow pattern in the shoulder flow zone induced by scroll shoulder tool has not been documented yet.
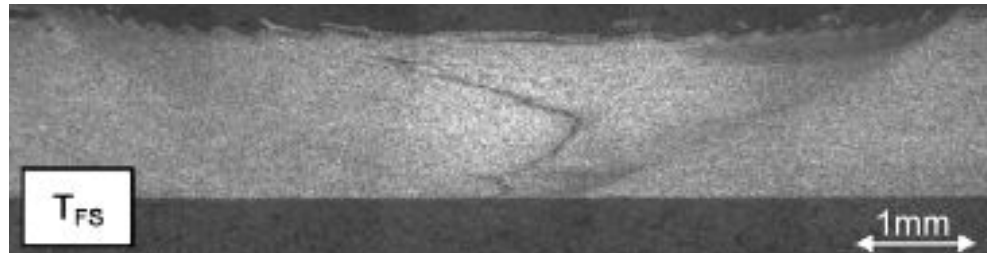
Figure 2-42 Macrographs of transverse section of FSW 1.5mm thick 6082-T6 Al sheets weld produced by scroll shoulder tool shown in Figure 2-41, FSW at ω=1810rpm and V=460mm/min [66]

As reviewed in this section, although a certain amount of weld zone flow patterns have been obtained by researchers, the exact flow pattern in the shoulder flow zone using a scroll shoulder tool is still unknown. Further, as reviewed in the last section, a layer to layer flow pattern in the upper advancing side of weld zone was obtained by Colligan [15]. However, the exact flow pattern in the shoulder flow zone has not been identified. Material flow patterns are vital in revealing the forming mechanism of the material flow.

Further, as reviewed in section 2.5.1, Dawes and Thomas [8] only described the induction of the PUM during the first stage of the FSW procedure. The induction and the movement of the PUM, during tool shoulder plunging and tool travelling (two other FSW procedures), are still unclear. In particular, how PUM is induced, then flows into the weld and consolidates with nugget flow to form a weld, has not been investigated. The forming mechanism of the shoulder flow zone using a scroll shoulder tool still remains unknown. This information and knowledge is important in the development of scroll shoulder tools.

2.6 Summary

Since TWI invented FSW in 1991, progresses in FSW technology have been mainly related to new tool development and a better understanding of the process. As can be seen in the sections reviewed, various types of tool have been widely adopted to join various materials. A number of techniques, such as the 'marker insert' and 'stop action' techniques, have been utilized to view the flow pattern and improve understanding of material flow formation during FSW. Whilst there are many factors that can influence the material flow during FSW, the main factors include tool geometry, welding

parameters and material types. However, the material flow during FSW is complicated and the understanding of the deformation process is limited.

As reviewed in this chapter, the relationship between the mass of PUM and the formation of shoulder flow zone, and the associated likelihood of defect weld formation, have not been explored yet. This knowledge is important in the design of scroll shoulder tools to ensure FSW weld quality. Therefore, the effect of welding parameters on the mass of PUM induced by the tool, during tool pin plunging, tool shoulder plunging and tool travelling, will need to be investigated in the present study.

Further, it still remains unclear why both faster and lower travelling speeds increase the likelihood of defects forming in the shoulder flow zone. The effect of tool travelling speed on the shoulder flow zone formation is however not well understood. Additionally, how the depth of shoulder penetration affects the material flow forming the shoulder flow zone is still unclear. The information regarding the effect of welding parameters on the shoulder flow zone formation is important in the selection of welding parameter to assure FSW weld quality, and will need to be investigated in the present study.

Furthermore, the exact flow pattern in shoulder flow zone induced by scroll shoulder tool is still unknown and has not been identified. Material flow patterns are vital in revealing the forming mechanism of the material flow, and will need to be determined and re-documented in the present study.

Moreover, the induction and the movement of the PUM, during tool shoulder plunging and tool travelling (two other FSW procedures), are still unclear. In particular how PUM is induced, flows into the weld and consolidates with nugget flow to form a weld, have not been investigated. The forming mechanism of the shoulder flow zone using a scroll shoulder tool still remains unknown. This information and knowledge is important in the development of scroll shoulder tools, and will also need to be revealed in the present study.

In conclusion, the various types of FSW tool, a range of welding parameters and the different types of experimental techniques have been used to conduct experiments and analyse results which improve understanding of material flow formation during FSW.

However, the knowledge gaps which include the aspects of the effect of welding parameters on the mass of induced PUM and the formation of the shoulder flow zone, exact flow pattern in shoulder flow zone, and the forming mechanism of the shoulder flow zone in thick section Al FSW using a scroll shoulder tool still exist and require further investigation as proposed in section 1.4. FSW experiments are conducted by using a 'marker insert' technique to analyse thick sections of 6061 Al welds, which are welded with a flat scroll shoulder and tapered pin tool at a range of welding parameters to fulfil the research goals and will be detailed in the next chapter.

3 Methodology and Experimental Procedure

The literature review presented in chapter two has identified certain knowledge gaps and formulated this study's research objectives which are important in the design of scroll shoulder tools to ensure FSW weld quality. Research objectives in the present study included the evaluation of the effect of welding parameters on the mass of induced PUM and the shoulder flow zone formation, the identification of the flow pattern in the shoulder flow zone, and the revelation of the forming mechanism of the shoulder flow zone during thick section Al FSW using a scroll shoulder. This chapter details the design of the FSW tool and experiments, the use of the 'marker insert' technique, and the approaches used for PUM quantification and sample metallography to achieve research goals. Additionally, the equipment, experimental set-up and workpiece materials used in this study are also described.

3.1 Quantification of the Mass of Induced PUM

As identified from the literature review and proposed in chapter one, the first research objective of the present study was to verify the hypothesis that the welding parameters have a significant influence on the mass of PUM induced by the tool during tool pin plunging, tool shoulder plunging and tool travelling. Tools and a series of FSW experiments were designed and executed to achieve these research goals which are detailed in the following section.

3.1.1 Tool Design

Figure 3-1 shows the FSW tool with one scroll flat shoulder and tapered left-hand-threaded pin that was used in the present study. The dimensions used in this tool design were scaled down from those dimensions adopted by Colligan [20] in FSW 25.4mm thick 6061Al plate as reviewed in chapter two section 2.1.1. The shoulder diameter was 30mm with one scroll groove cut into the shoulder face. The depth, width and pitch of the scroll groove were 1.3mm, 2.0mm and 3.5mm respectively. Furthermore, the length of the thread on the tapered pin was 19.8mm with diameters at the pin root (starting point of the thread) and tip (ending point of the thread) equal to 9.8mm and 5mm respectively. The coarse thread cut into the tapered pin has a depth, width and pitch of

0.5mm, 0.55mm and 1.35mm respectively. An engineering drawing which details these dimensions is provided in Appendix 1.

As shown in Figure 3-1, *tool 1*'s shoulder and pin were assembled such that the starting point of the thread on the tapered pin was embedded beneath the shoulder face at 1.3mm (the depth of scroll groove), in which the 'actual' length (between the shoulder face and pin tip) of the threaded pin was 18.5mm (original length 19.8mm).
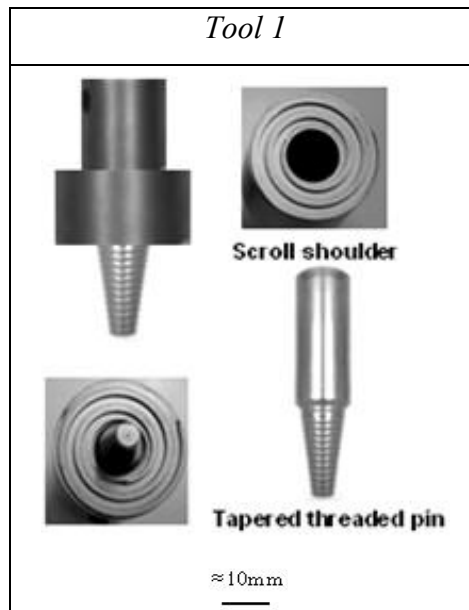
Figure 3-1 Photos of assembled *tool 1*, scroll shoulder and pin couples used at AUT lab in the present study

FSW process included three main procedures; tool pin plunging, tool shoulder plunging and tool travelling (introduced in chapter one). In order to eliminate the PUM induced by the tool during the first stage of FSW procedure (tool pin plunging), *tool 1* was modified to construct *tool 2*. The modified tool was used in the experiments to evaluate the mass of PUM induced by the tool during tool shoulder plunging and tool shoulder travelling. As shown in Figure 3-2, the modification made to *tool 1* to construct *tool 2* is such that the 'actual' length of the thread pin on *tool 1* was reduced to zero. However, *tool 2* still has 1.3mm length of threaded pin remaining beneath its' shoulder.
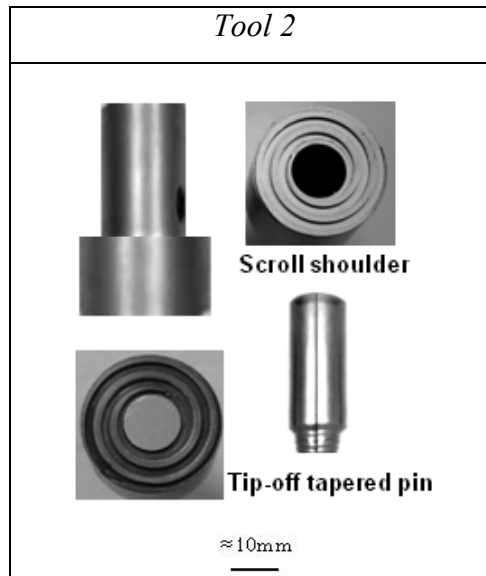
Figure 3-2 Photos of assembled *tool 2*, scroll shoulder and pin couples used at AUT lab in the present study

H13 tool steel (Fe-5.25 Cr-1.4 Mo-1 Si-1 V-0.4 C) [67] was used to make the scroll shoulder and tapered pin tool. To provide a tool capable of FSW without breakage, both the scroll shoulder and the tapered threaded pin were heat treated to HRc 45. The tool strength was proven to be sufficiently strong by the successful use of the tool during FSW of 20mm thick 6061 Al plates in the preliminary investigation of the present study.

3.1.2 Experiments to Evaluate the Mass of Induced PUM

It was hypothesised that welding parameters have a large effect on the mass of PUM induced by the tool during tool pin plunging, tool shoulder plunging and tool travelling. In order to test the hypothesis, three different types of FSW trials ('A', 'B' and 'C') and a total of eight FSW experiments were designed and completed.

Welding parameters used in trial 'A', 'B' and 'C' were illustrated in Figure 1-4 and are shown in Table 2. In order to achieve comparable results, welding parameters used by Colligan [15, 20] and in the preliminary studies were adopted. Tool rotating speed was kept constant at 250rpm in a clockwise direction. Procedures for each trial will be detailed later. Each experiment was conducted and repeated three times at each welding condition to obtain an average result.

Table 2 FSW parameters used in trial 'A', 'B' and 'C' to determine the mass of induced PUM (ω = 250rpm, L = welding distance, T_{dwell} = tool dwell time)

Trial	Tool	Weld No.	Parameters of FSW					
			$V_{plunging}$	H	$T_{dwell\,(1)}$	V	L	$T_{dwell\,(2)}$
'A'	1	1	3mm/min	0mm	1min	-	-	-
		2	6mm/min	0mm	1min	-	-	-
'B'	2	3	3mm/min	0.4mm	1min	-	-	-
		4	3mm/min	0.5mm	1min	-	-	-
		5	3mm/min	0.6mm	1min	-	-	-
		6	3mm/min	1.0mm	1min	-	-	-
'C'	2	7	3mm/min	0.4mm	1min	40mm/min	40mm	1min
		8	3mm/min	0.4mm	1min	56mm/min	40mm	1min

As illustrated in Figure 3-3, trial 'A' was conducted to evaluate the effect of tool plunging speed on the mass of PUM induced by the tool during tool pin plunging. Two welds (welds 1 and 2) were made by *tool 1* using two different tool plunging speeds.
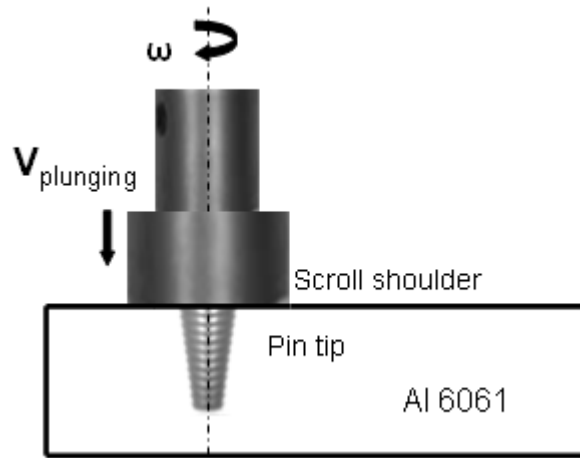
Figure 3-3 Schematic illustration of trial 'A', showing *tool 1*'s pin plunged into workpiece at a position where *tool 1*'s shoulder just touches the workpiece using various $V_{plunging}$, to evaluate effect of $V_{plunging}$ on the mass of PUM induced by tool during tool pin plunging

Trial 'A' procedures are specified as follows. Firstly, the scroll groove of the *tool 1*'s shoulder was fully cleaned out before each experiment was started (this applied to trial 'B' and 'C' too). Secondly, the rotating *tool 1* was plunged into the workpiece at the chosen $V_{plunging}$ (tool plunging speed) until its shoulder was brought to just touch the workpiece (zero shoulder penetration), and then tool plunging was terminated. Finally,

the rotating tool dwelled one minute for material flow stabilization and then was stopped.

Figure 3-4 illustrates trial 'B', which was implemented to study how the depth of shoulder penetration influenced the mass of PUM during tool shoulder plunging. To achieve this, four welds (welds 3, 4, 5 and 6) were made using *tool 2* at four different depths of shoulder penetration.
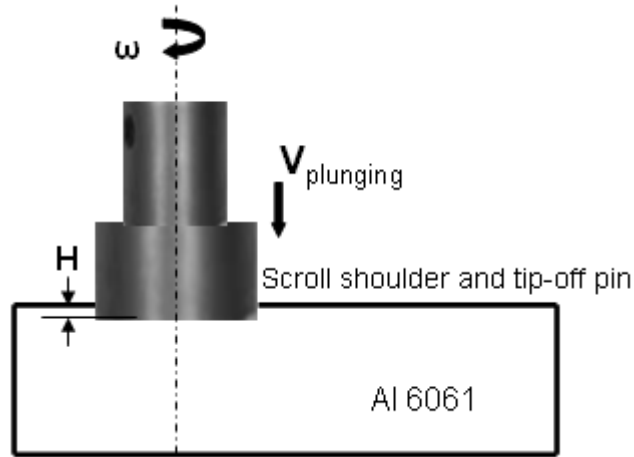
Figure 3-4 Schematic illustration of trial 'B', showing *tool 2*'s shoulder plunged into workpiece at various H, to evaluate effect of H on the mass of PUM induced by tool during tool shoulder plunging

Trial 'B' procedures are described as follows. Firstly, rotating *tool 2* (fully emptied scroll groove) was plunged into the workpiece at the chosen H (depth of shoulder penetration) with a constant $V_{plunging}$ (tool plunging speed=3mm/min), and then tool plunging was terminated. Finally, the rotating tool dwelled for one minute and was stopped.

As illustrated in Figure 3-5, trial 'C' was performed to investigate the effect of the tool travelling speed on the mass of PUM induced by the tool during tool shoulder travelling. To attain this, two welds (welds 7 and 8) were made by *tool 2* using two different tool travelling speeds. Due to very limited spacing of the scroll groove, trial 'C' was conducted by *tool 2* travelling to a distance of 40mm only.
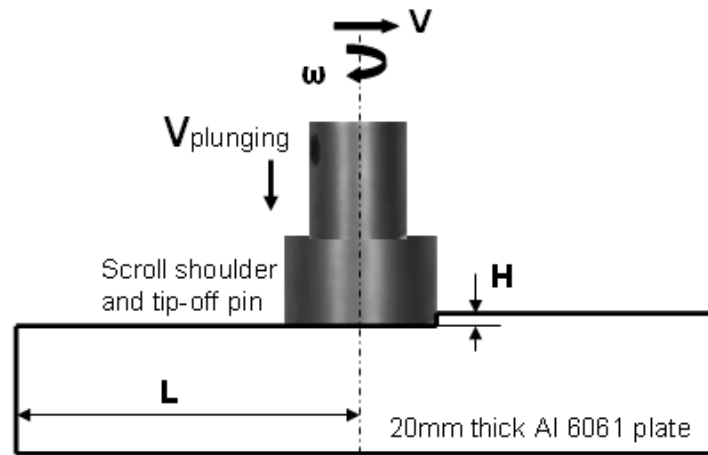
Figure 3-5 Schematic illustration of trial 'C', showing *tool 2*'s shoulder plunged into workpiece at 0.4mm depth (H) and travelled 40mm (L) at various V, to evaluate effect of V on the mass of PUM induced by tool during tool travelling

Trial 'C' procedures are detailed as follows. Firstly, the rotating *tool 2* (fully emptied scroll groove) was plunged into the workpiece at a 0.4mm depth of shoulder penetration with a constant $V_{plunging}$ (tool plunging speed=3mm/min), tool plunging was terminated and then the rotating tool dwelled one minute for material flow stabilization. Secondly, the rotating tool travelled 40mm at the chosen V (tool travelling speed) and then tool travelling was terminated. Finally, the rotating tool dwelled for another minute and was stopped.

For trial 'A', 'B' and 'C', the mass of PUM was determined by measuring and deducting the weight of the pre-weld tool from the used tool after each weld was completed. The procedures and equipment used in the determination of the mass of PUM will be detailed in the next section.

3.1.3 Approaches to Determine the Mass of PUM

After each welding experiment (welds 1, 2, 3, 4, 5, 6, 7, and 8) was completed, the used tool was weighed up by a METTLER TOLEDO PB602-S/FACT Precision Balance as shown in Figure 3-6. It has a precision of 0.01g and applies Fully Automatic Calibration Technology (FACT) to assure the accuracy of the weighting results [68].

Figure 3-6 Photo of a METTLER TOLEDO PB602-S/FACT Precision Balance used at AUT lab in the present study

The used tool (with Al accumulated within the scroll groove-induced PUM) was fully cleaned using chemical cleaning. The chemical solution used to clean the used tool was caustic soda, composed of 100g NaOH (99% purity) and 1L water. Figure 3-7 shows the cleaning set up, where the used tool was submerged in the caustic soda solution and heated to 90 C° to speed up the cleaning process.
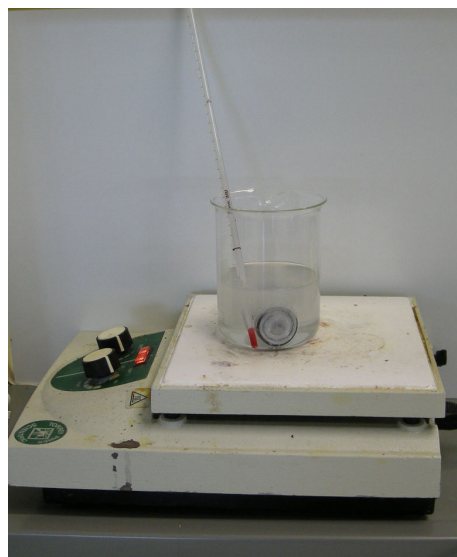
Figure 3-7 Photo of 'used tool' cleaning in progress used at AUT lab in the present study

The mass of induced PUM was determined by measuring the mass of the tool pre-weld and after welding. The procedure was as follows:

- Measure the mass of pre-weld tool (fully emptied scroll groove)
- Measure the mass of used tool (including the induced PUM)

The net mass of induced PUM was established by subtracting the mass of the used tool from the mass of the pre-weld tool.

As introduced in chapter one, during scroll shoulder tool FSW, the workpiece material displaced by the penetrated tool is distributed in two ways; material is extruded outside the tool to form welding flash, and material is induced into the scroll groove beneath the shoulder. In order to evaluate the mass balance between the mass of induced PUM and the mass of displaced workpiece material (WPM) during the three FSW procedures (tool pin plunging, tool shoulder plunging and tool travelling), the theoretical mass of displaced WPM during these three different procedures was calculated individually. In addition, the maximum mass of displaced WPM that could theoretically accumulate within the tool scroll groove was also calculated. All the experimental and theoretical results will be presented in the next chapter to show the effect of welding parameters on the mass of induced PUM. Raw data is also provided in Appendix 2.

3.1.4 Welding Machine, Workpiece Material and Experimental Set-Up

FSW experiments were done using a Tos Olomouc FA3AV milling machine at AUT's workshop as shown in Figure 3-8. This machine has a 5.8 kW maximum power output, and is able to vary spindle rotation speeds and set a desirable speed value for both vertical and horizontal movement. In addition, the machine has a vertical position setting of 0.02mm per step.
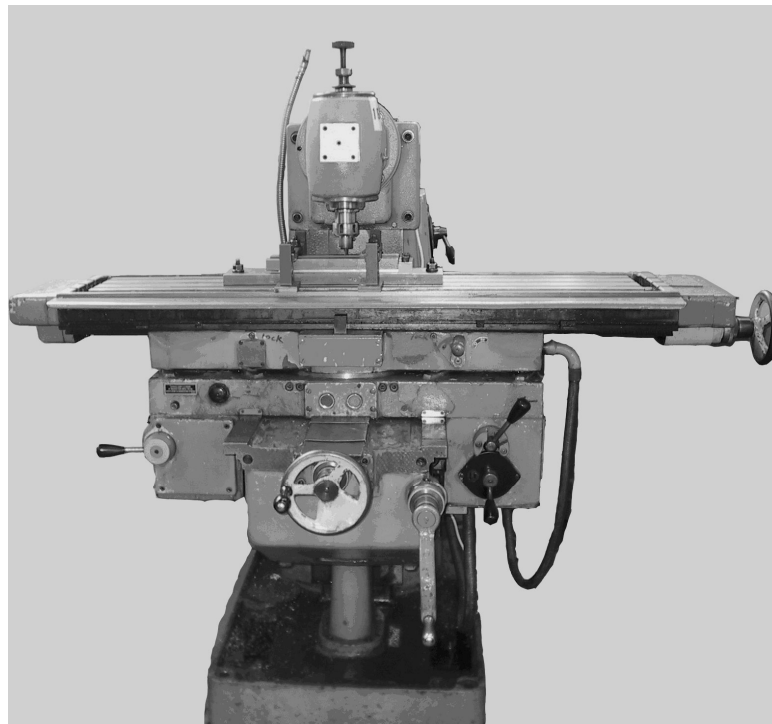
Figure 3-8 Tos Olomouc FA3AV milling machine used for FSW trials in the present study

As shown in Figure 3-9, a 20mm thick, rolled 6061 Al plate, where magnesium and silicon are the principal alloying elements, was chosen as the experimental material. Table 3 [69, 70] shows the chemical composition of 6061 Al alloy in wt%. In the experiments, the welding path direction was made both perpendicular and parallel to the rolling texture direction.

Figure 3-9 Photo of 20mm thick 6061 Al plates used in the present study

Table 3 Nominal chemical composition of 6061 Al alloy (wt.%) [69]

Mg	Si	Cu	Cr	Mn	Fe	Al
0.8-1.2	0.4-0.8	0.05-0.4	0.04-0.35	<0.15	<0.7	Bal.

Figure 3-10 shows the welding set-up. The Al plate (workpiece) to be welded was clamped on four corners to an anvil that was bolted to the machine bed. Rigid clamping was achieved by putting two top bars and one block on the workpiece to resist its vertical and horizontal movement. The tool was assembled in the machine spindle perpendicular to the workpiece and remained at a fixed position. Rather than the tool travelling through the workpiece, the machine bed moved and tool position was preset and fixed.
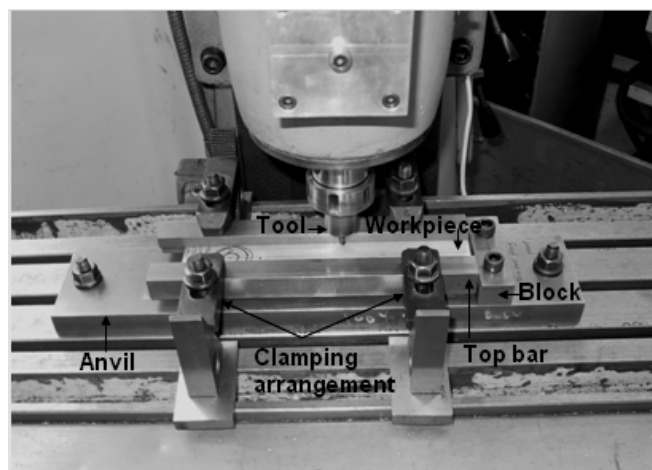
Figure 3-10 Experimental set-up used in the present study

3.2 Evaluation of the Formation of Shoulder Flow Zone

The knowledge gaps, regarding the formation of the shoulder flow zone using a scroll shoulder tool, have been identified in chapter two and incorporated into the research objectives proposed in chapter one. The second research objective of this study is to examine the hypothesis that the depth of shoulder penetration and tool travelling speed affect the shoulder flow zone formation significantly. A series of FSW experiments was designed and conducted to fulfil these research goals as detailed in the following section.

3.2.1 Experiments to Evaluate the Formation of Shoulder Flow Zone

In order to examine the hypothesis introduced above, a FSW trial ('D') with a total of six FSW experiments were designed and completed. Welding parameters used in trial 'D' were illustrated in Figure 1-4 and shown in Table 4. In order to attain equivalent results, the welding machine, workpiece material, experimental set-up and part of the welding parameters used in trial 'A', 'B' and 'C' were followed in trial 'D'. Tool rotating speed was kept constant at 250rpm in a clockwise direction. Trial procedures will be detailed later.

Table 4 FSW parameters used in trial 'D' to evaluate the shoulder flow zone formation (ω = 250rpm, L = welding distance, T_{dwell} = tool dwell time)

Trial	Tool	Weld No.	Parameters of FSW					
			$V_{plunging}$	H	$T_{dwell\,(1)}$	V	L	$T_{dwell\,(2)}$
'D'	1	9	3mm/min	0.4mm	1min	40mm/min	150mm	1min
		10	3mm/min	0.5mm	1min	40mm/min	200mm	1min
		11	3mm/min	0.6mm	1min	40mm/min	200mm	1min
		12	3mm/min	0.4mm	1min	56mm/min	150mm	1min
		13	3mm/min	0.5mm	1min	56mm/min	200mm	1min
		14	3mm/min	0.6mm	1min	56mm/min	200mm	1min

As illustrated in Figure 3-11, trial 'D' was conducted to evaluate the effect of the depth of shoulder penetration and tool travelling speed on shoulder flow zone formation. Six welds (weld 9, 10, 11, 12, 13 and 14) were made by *tool 1* using the various welding parameters shown in Table 4.
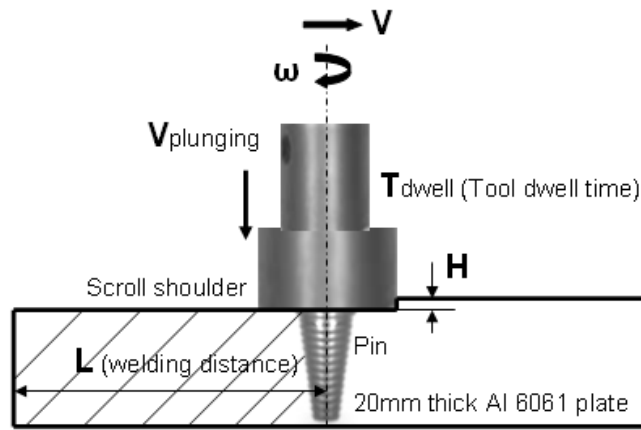
Figure 3-11 Schematic illustration of trial 'D', using *tool 1* at various H, and V to evaluate the effect of H and V on the shoulder flow zone formation

Trial 'D' procedures are described below. Firstly, the rotating *tool 1* was plunged into the workpiece at a chosen H (depth of shoulder penetration) with a constant $V_{plunging}$ (tool plunging speed=3mm/min), and tool plunging was terminated and then the rotating tool dwelled one minute for material flow stabilization. Secondly, the rotating tool travelled either 150mm or 200mm at the chosen V (tool travelling speed), then tool travelling was terminated. Finally, the rotating tool dwelled for another minute and was stopped.

After each weld was completed, each post-weld was sectioned to produce a metallographic sample for the shoulder flow zone formation investigation. The procedures and equipment used in the preparation of the metallographic sample will be detailed later.

3.2.2 Metallography in Trial 'D'

After each welding experiment (weld 9, 10, 11, 12, 13, and 14) was completed, each post-weld piece was sectioned in both the transverse and longitudinal direction (through the welding centre line) to produce cross sections of the weld. Figure 3-12 demonstrates the position and orientation used in the sectioning of post-weld pieces produced from trial 'D'.
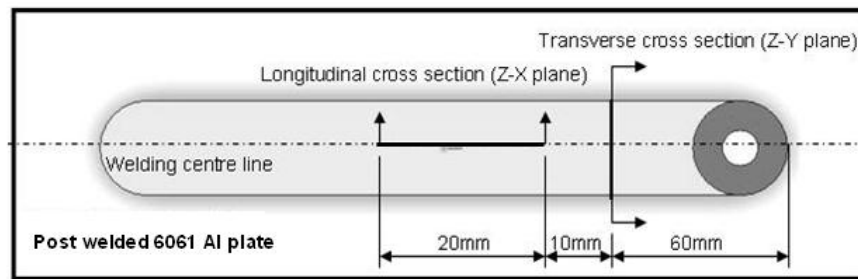
Figure 3-12 Schematic illustration of the position and the orientation used in sectioning post-weld pieces produced from trial 'D'

The metallographic samples of transverse cross sections of the welds obtained from trial 'D' were prepared for macrostructure observation. These samples provided an overall view of the weld quality produced from trial 'D'. Figure 3-13 shows the manual mounting gear set and polishing machine used in macrostructure sample preparation. The sample preparation procedure is as follows:

- Mount sectioned sample in a polymer resin
- Grind the surface of the sample, using Silicon Carbide Paper, from 120 to 2400 grit using water as lubricant
- Polish the sample to 6μ using a polishing disk with 6μ diamond paste
- Clean the samples with alcohol
- Chemically etch samples by swabbing in Tuckers Reagent (45% HCl, 15% HNO$_3$, 15% HF and 25% H$_2$O) for 30 seconds
- Clean samples with alcohol

Figure 3-13 Manual mounting gear set (left), grinding machine (middle) and polishing machine (right) used in macrostructure samples preparation at AUT lab in the present study

The metallographic samples of longitudinal cross sections of the welds obtained from trial 'D' were prepared for microstructure examination. These microstructures showed the flow pattern, and interface between the shoulder flow zone and nugget zone. Figure 3-14 shows an automatic mounting and polishing machine used in microstructure specimen preparation. The following steps were taken in sample preparation:

64

- Mount sectioned sample using an automatic mounting machine
- Grind the surface of the sample, using Silicon Carbide Paper, from 120 to 2400 grit using water as lubricant
- Polish samples to 1μ using an automatic polishing machine
- Clean the samples with alcohol
- Chemically etch samples by swabbing in Kellers Reagent (1.5%HCl, 2.5% HNO_3, 1% HF and 95% H_2O) for 20 seconds
- Clean sample with alcohol
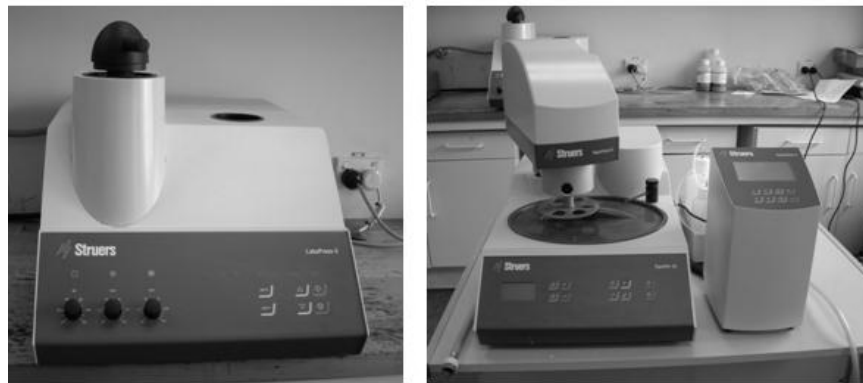
Figure 3-14 Automatic mounting machine (left) and polishing machines (right) used in microstructure sample preparation at AUT lab in the present study

After the macrostructure samples had been appropriately etched and cleaned, the overall quality of the weld structure was evaluated by observing the metallographic sample under the Olympus stereomicroscope shown in Figure 3-15.

Figure 3-15 Olympus stereomicroscope used in macrostructure samples observation at AUT lab in the present study

The flow pattern and weld zone interface in microstructure samples were identified using a Nikon optical microscope (shown in Figure 3-16). It has objective lenses of a magnification of 5 times to 100 times and images were taken accordingly. Observational results of all metallographic samples will be presented in the next chapter to show the effect of welding parameters on shoulder flow zone formation.

Figure 3-16 Nikon optical microscope used in microstructure sample observation at AUT lab in the present study

3.3   Identification of the Shoulder Flow Zone Flow Pattern

As identified from the work presented in chapter two and proposed in chapter one, the third research objective of this study was to prove the hypothesis that the shoulder flow zone flow pattern could be traced and documented by the 'marker insert' technique, although there is no open literature regarding the use of this technique to identify the flow pattern induced by the scroll shoulder tool. A 'marker insert' FSW experiment was designed and conducted to accomplish this research goal and is detailed in the following section.

3.3.1 'Marker Insert' Technique

Figure 3-17 illustrates the 'marker insert' experiment where a workpiece inserted with copper foil was constructed and the proposed marker movement was demonstrated. The 'marker insert' specimen was constructed such that a piece of copper foil was inserted along the advancing side of the workpiece with a 13mm offset from the welding centre line, and aligned with the top surface of the workpiece.

The workpiece material used in the 'marker insert' experiment was the same as trial 'D' (6061 Al thick plate). Copper foil [71], 0.114mm (0.0045in) thick and 99.99+% (metals basis) purity, was used as a maker to trace the shoulder zone flow.
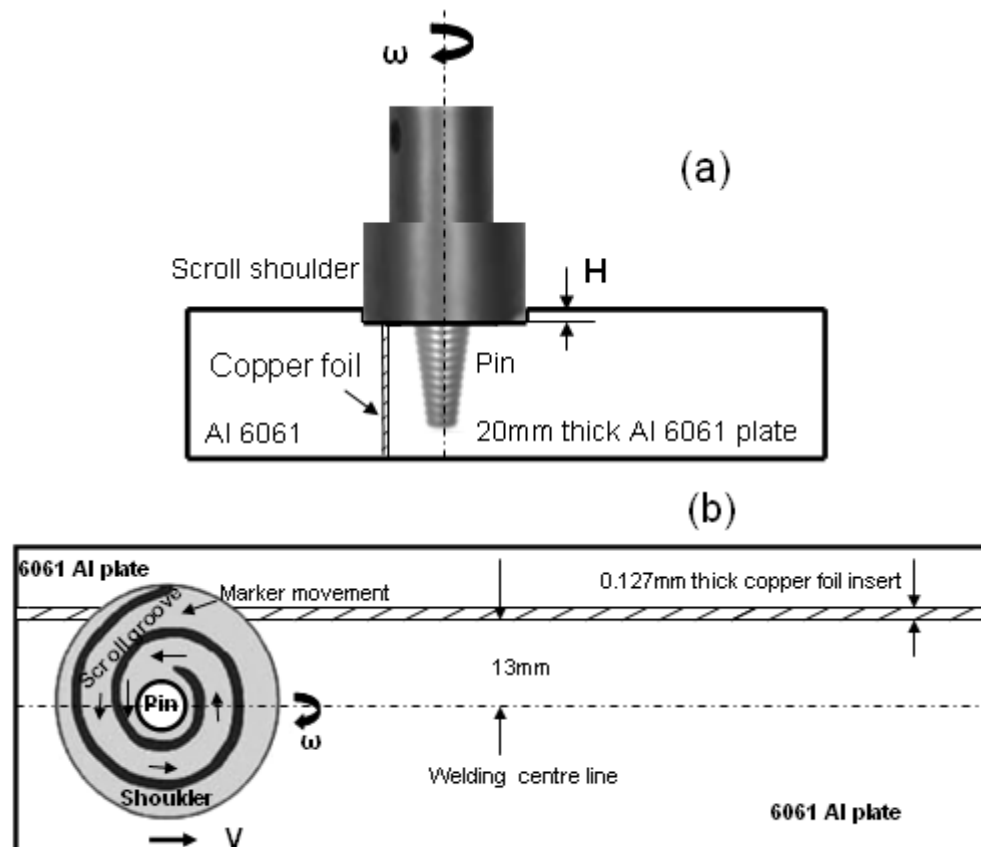
Figure 3-17 Schematic illustrations of the 'marker insert' experiment (trial 'E'), the workpiece to be welded with copper foil inserted, and the direction of the marker movement, (a) viewed on Z-Y plane, (b) viewed on X-Y plane, with welding direction parallel to X axis

The hypothesised 'marker' (same as PUM) movement expected in this experiment is described as follows. Firstly, the edge of the scroll groove entrance beneath the shoulder could reach and cut the copper foil after the tool shoulder was plunged into the workpiece. Secondly, whilst the scroll shoulder tool was travelling forward, the copper

67

foil could be sliced into fragments by the entrance edge of the rotating scroll groove. Thirdly, the copper foil fragments could follow the scroll groove and be driven into the centre spacing of the scroll shoulder (spacing of the annual ring material flow as illustrate in Figure 1-9). Finally, the marker fragment could be driven downward by the threaded tool pin and distributed within the weld zone. If copper foil fragments were found in the weld zone, it could be concluded that the zone upon the copper fragment was shoulder flow zone.

3.3.2 Experiment to Identify the Shoulder Flow Zone Flow Pattern

In order to prove the hypothesis introduced above, a 'marker insert' FSW experiment (trial 'E') was designed and completed. Welding parameters used in trial 'E' were illustrated in Figure 1-4 and shown in Table 5. Welding machine, workpiece material, experimental set-up and part of the welding parameters used in trial 'A', 'B' 'C' and 'D' were followed in trial 'E'. Tool rotating speed was kept constant at 250rpm in a clockwise direction. Trial procedures will be detailed below.

Table 5 FSW parameters used in trial 'E' to identify the shoulder flow zone flow pattern (ω = 250rpm, L = welding distance, T_{dwell} = tool dwell time)

Trial	Tool	Weld No.	Parameters of FSW					
			$V_{plunging}$	H	$T_{dwell\,(1)}$	V	L	$T_{dwell\,(2)}$
E	1	15	3mm/min	0.5mm	1min	40mm/min	200mm	1min

As illustrated in Figure 3-17 and shown above, trial 'E' was conducted to trace the marker movement and document the flow pattern in the shoulder flow zone. One weld (weld 15) was made by *tool 1* using the chosen welding parameters shown in Table 5.

Trial 'E' procedures are described as follows. Firstly, the rotating *tool 1* was plunged into the workpiece (inserted with copper foil) at a 0.5mm depth of shoulder penetration with a constant $V_{plunging}$ (tool plunging speed=3mm/min), tool plunging was terminated and the rotating tool dwelled one minute for material flow stabilization. Secondly, the rotating tool travelled 200mm at a constant V (tool travelling speed=40mm/min) at which point tool travelling was terminated. Finally, the rotating tool dwelled for another minute and was stopped.

After the weld was completed, the post-weld was sectioned to produce a metallographic sample for identification of the shoulder flow zone flow pattern. The procedures and equipment used in the preparation of the metallographic sample will be detailed in the next section.

3.3.3 Metallography in Trial 'E'

After the 'marker insert' experiment (trial 'E', weld 15) was completed, the post-weld piece was sectioned to obtain one transverse cross section and three different longitudinal cross sections of the weld. Figure 3-18 illustrates the position and orientation used in sectioning of post-weld pieces produced from trial 'E'.
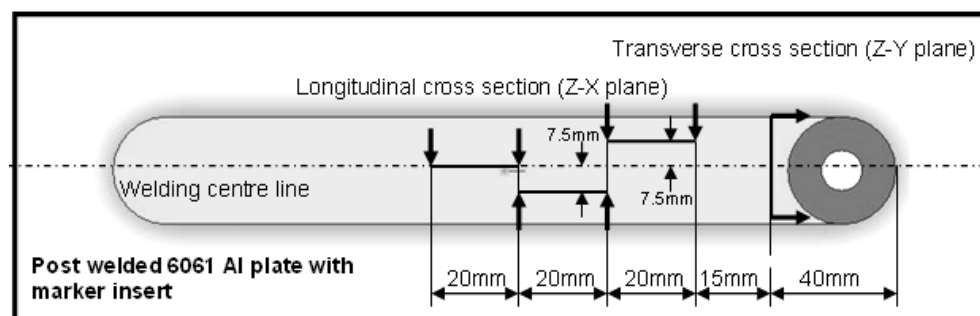
Figure 3-18 Schematic illustration of the position and the orientation used in sectioning post-weld pieces produced from trial 'E'

The metallographic samples of transverse cross sections of the welds obtained from trial 'E' were prepared for macrostructure observation. These macrostructures identified the location of the inserted copper foil and provided an overall view of the weld quality produced from trial 'E'. Mounting gear, polishing machine and the procedure used in macrostructure sample preparation were the same as trial 'D'.

The metallographic samples of longitudinal cross sections of the welds obtained from trial 'E' were prepared for microstructure examination. These microstructures showed the flow pattern, interface between the shoulder flow zone and nugget zone, and distribution of the copper foil. Automatic mounting gear, polishing machine and procedure used in microstructure sample preparation were the same as trial 'D'.

After the macrostructure samples had been appropriately etched and cleaned, the location of the inserted copper foil and the overall quality of the weld structure were

evaluated by observing the metallographic sample under the Olympus stereomicroscope shown in Figure 3-15.

The flow pattern, interface between the shoulder flow zone and nugget zone, and the distribution of the copper foil in the microstructure samples were identified using the Nikon optical microscope shown in Figure 3-16. Observational results of all metallographic samples will be presented in the next chapter to reveal the flow pattern in the shoulder flow zone.

4   Results

This chapter details the measured mass of PUM (already defined as pick up material in chapter one) induced by the scroll shoulder tool, and the effect of welding parameters on the formation of the shoulder flow zone. Additionally, shoulder flow zone flow patterns identified using the 'marker insert' technique will also be presented.

Shoulder flow zone formation results demonstrated a positive linear relationship between the mass of induced PUM and weld quality in the shoulder flow zone. The shoulder flow zone flow pattern induced by the scroll shoulder tool has been documented for the first time with a 'marker insert' technique.

4.1   Quantification of the Mass of Induced PUM

The quantitative results of the effect of various welding parameters on the net mass of PUM induced by the tool during tool pin plunging, tool shoulder plunging and tool travelling will be presented in this section. The experiment was conducted three times for each set of welding parameters, and the average of three net mass of PUM was determined (raw data see Appendix 2). In order to evaluate the mass balance between the mass of induced PUM and the mass of displaced WPM (workpiece material displaced by the penetrated tool as defined in chapter one) during FSW, the theoretical mass of displaced WPM, the percentage of the displaced WPM converted into PUM and the maximum mass of displaced WPM that could theoretically accumulate within the tool scroll groove will also be presented (raw data see Appendix 2).

4.1.1   Mass of PUM Induced during Tool Pin Plunging

As described in section 3.1.2 and shown in Figure 3-3, the net mass of PUM induced by the tool pin (*tool 1*, pin only) was quantified at two different plunging speeds. Figure 4-1 shows two post-weld profiles and used tools (*tool 1*). It can be seen from these figures that more Al was filled into the scroll groove of the used tools in weld 1 than in weld 2. This shows the effect of tool plunging speed on the mass of PUM induction.

Table 6 shows the individual and average of three net mass of induced PUM and theoretical mass of displaced WPM during *tool 1*'s pin plunging. The table also

demonstrates the relationship among the tool pin plunging speed, the mass of induced PUM and the mass of displaced WPM. Based on the information presented in Figure 4-1 and Table 6, it can be found that the faster the tool pin is plunged, the less mass of PUM is induced, and the lower percentage of displaced WPM is converted into PUM.
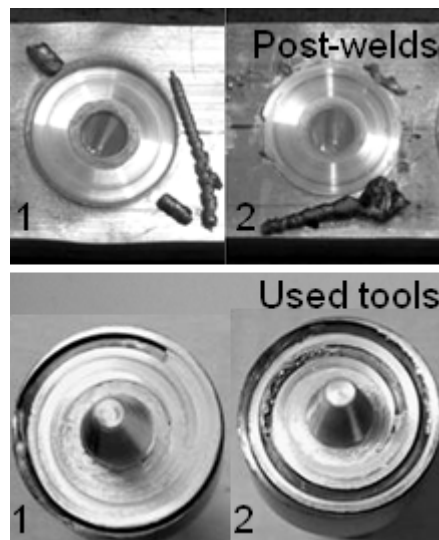
Figure 4-1 Photos of post-weld profiles and used tools (*tool 1*) produced after tool pin is plunged into workpiece at zero depth of shoulder penetration, and using (1) 3mm/min; (2) 6mm/min plunging speeds

Table 6 Individual and average (Avg.) of three net mass of PUM induced by *tool 1*, after tool pin plunging at two different speeds, and percentage of displaced WPM converted into PUM, labelled used *tool 1* is indicated in Figure 4-1

Weld No.	Tool plunging speed	Avg. net mass of induced PUM	Mass of displaced WPM	% of WPM converted into PUM
1	3mm/min	(0.88+0.71+0.78)/3=**0.79** g	**1.82** g	**43.4** %
2	6mm/min	(0.50+0.60+0.46)/3=**0.52** g	**1.82** g	**28.6** %
The maximum mass of displaced WPM that could theoretically accumulate within the tool scroll groove = **1.29**g (*tool 1* and *tool 2* have same spacing of scroll groove beneath the shoulder, see Appendix 2)				

4.1.2   Mass of PUM Induced during Tool Shoulder Plunging

As depicted in section 3.1.2 and illustrated in Figure 3-4, the net mass of PUM induced by the tool shoulder (*tool 2*, shoulder only) at four different depths of shoulder penetration was quantified. Figure 4-2 shows four post-weld profiles and used tools

(*tool 2*). It can be identified from the used tools that the degree of Al filling into the scroll groove increased significantly from weld 3 to weld 6, and the scroll groove used in weld 6 seems to have been fully filled up.

Table 7 shows the individual and average of three net mass of PUM and mass of displaced WPM during *tool 2* plunging. The table also shows the relationship among the depth of shoulder penetration, the mass of induced PUM and the mass of displaced WPM. Based on the information presented in Figure 4-2 and Table 7, it shows that the deeper the scroll shoulder is penetrated into the workpiece, the more mass of PUM is induced, and the higher percentage of displaced WPM is converted into PUM.
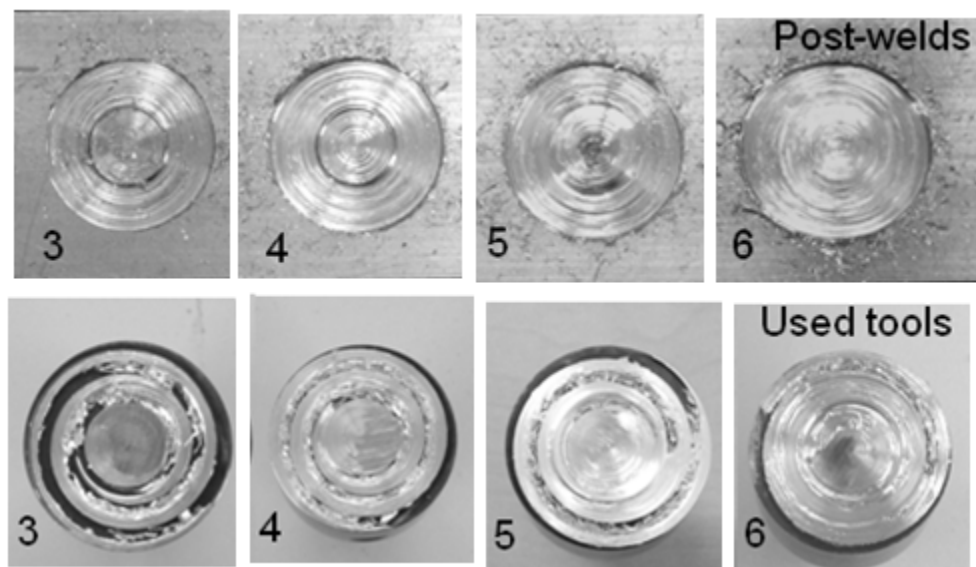
Figure 4-2 Photos of post-weld profiles and used tools (*tool 2*) obtained after the tool shoulder was plunged into workpiece at (3) 0.4mm; (4) 0.5mm; (5) 0.6mm; (6) 1.0mm depth of shoulder penetration; using 3mm/min plunging speeds

Table 7 Individual and average of three net mass of PUM induced by *tool 2*, after tool shoulder plunging at four different depths of shoulder penetration, and percentage of displaced WPM converted into PUM, labelled used *tool 2* is indicated in Figure 4-2

Weld No.	Depth of shoulder plunging	Avg. net mass of induced PUM	Mass of displaced WPM	% of WPM converted into PUM
3	0.4 mm	(0.15+0.16+0.14)/3=**0.15** g	**0.68** g	**22** %
4	0.5 mm	(0.40+0.48+0.35)/3=**0.41** g	**0.85** g	**48.2** %
5	0.6 mm	(0.63+0.66+0.54)/3=**0.61** g	**1.03** g	**59.2** %
6	1.0 mm	(1.18+1.34+1.23)/3=**1.25** g	**1.71** g	**73.1** %

4.1.3 Mass of PUM Induced during Tool Travelling

As illustrated in section 3.1.2 and demonstrated in Figure 3-5, the net mass of PUM induced by the tool (*tool 2*, shoulder only) was quantified at two different speeds. Due to very limited spacing of the scroll groove, the depth of shoulder penetration (H) and welding distance (L) were set at 0.4mm and 40mm respectively. Figure 4-3 shows two post-weld profiles and used tools (*tool 2*). It can be noticed from the used tool figure that more Al was filled into the scroll groove of the used tools in weld 7 than in weld 8. This shows the effect of tool travelling speed on the mass of PUM induction.

Table 8 shows the individual and average of three net mass of PUM and mass of displaced WPM after *tool 2* travels 40mm (welding distance). The table also shows the relationship among the tool travelling speed, the mass of induced PUM and the mass of displaced WPM. Based on the information presented in Figure 4-3 and Table 8, it can be summarized that the faster the tool travels, the less net mass of PUM is induced, and the lower percentage of displaced WPM is converted into PUM.
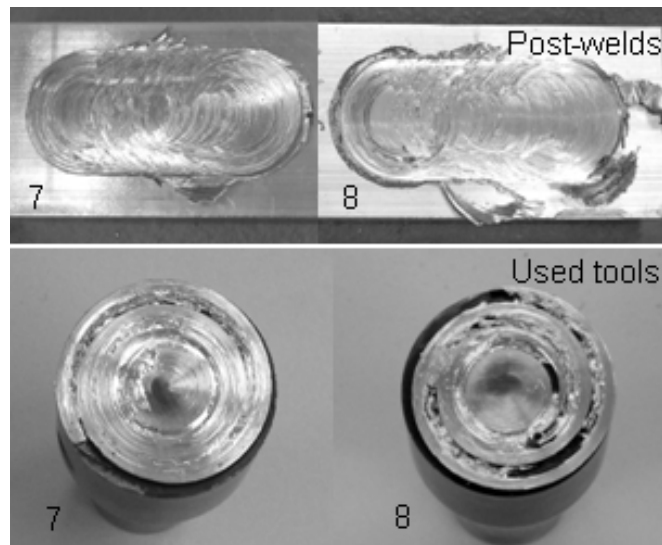
Figure 4-3 Photos of post-weld profiles and used tools (*tool 2*) acquired after *tool 2* was plunged into workpiece at 0.4mm depth of shoulder penetration; travelling 40mm at (7) 40mm/min; (8) 56mm/min two different speeds

Table 8 Individual and average of three net mass of PUM induced by *tool 2*, after tool travelling 40mm at two different speeds, and percentage of WPM converted into PUM, labelled used *tool 2* is indicated in Figure 4-3

Weld No.	Tool travelling speed	Avg. net mass of induced PUM	Mass of displaced WPM	% of WPM converted into PUM
7	40 mm/min	(1.08+1.20+1.05)/3=1.11 g	1.3 g	85.4 %
8	56 mm/min	(0.53+0.56+0.71)/3=0.60 g	1.3 g	46.2 %

4.1.4 Summary

The results have been obtained through the quantification of the net mass of PUM induced by the tool. They are:

1. Average net mass of induced PUM decreases from 0.79g to 0.52g, and the percentage of displaced WPM converted into PUM decreases from 43.4% to 28.6%, at **tool plunging speeds** of 3mm/min and 6mm/min respectively. This shows that the faster the tool pin is plunged, the less net mass of PUM is induced, and the lower percentage of displaced WPM is converted into PUM during tool pin plunging

2. Average net mass of induced PUM increases from 0.15g to 1.25g, and the percentage of displaced WPM converted into PUM increases from 22% to 73.1%, at **depths of shoulder penetration** from 0.40mm to 1.0mm respectively. This shows that the deeper the scroll shoulder is penetrated into the workpiece, the more mass of PUM is induced, and the higher percentage of displaced WPM is converted into PUM during tool shoulder plunging.

3. Average net mass of induced PUM decreases from 1.11g to 0.6g, and the percentage of displaced WPM converted into PUM decreases from 85.4% to 46.2%, at **tool travelling speeds** of 40mm/min and 56mm/min respectively. This shows that the faster the tool travels, the less net mass of PUM is induced, and the lower percentage of displaced WPM is converted into PUM during tool travelling at these two different speeds.

4.2   Effect of Welding Parameters on Shoulder Flow Zone Formation
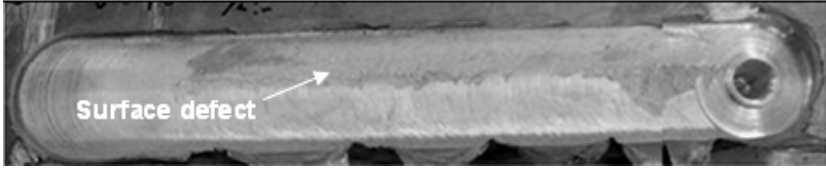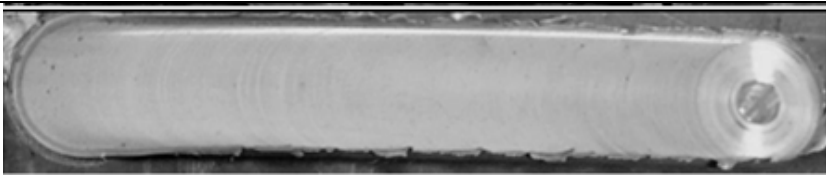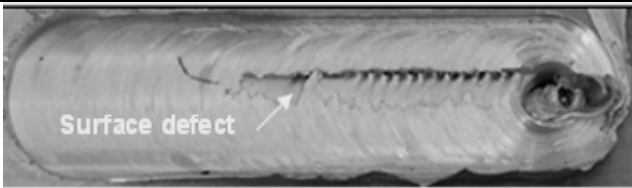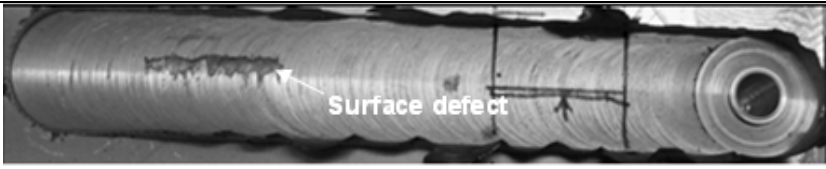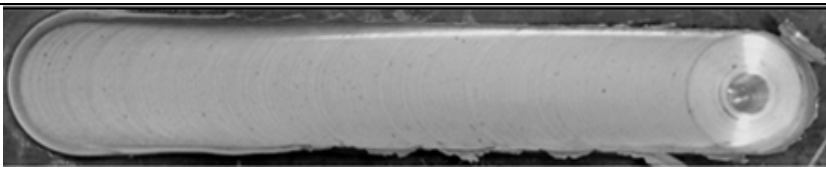
As described in section 3.2.1 and shown in Figure 3-11, the effect of the depth of shoulder penetration and tool travelling speed on the shoulder flow zone formation using a scroll shoulder tool was studied. FSW parameters used in these experiments were shown in Table 4. The study was implemented by directly observing the weld surface profiles, weld transverse cross sections (Z-Y plane see Figure 1-3 for coordinate) and weld longitudinal cross sections (Z-X plane).

The results of the investigation into the effect of various welding parameters on the shoulder flow zone formation will be presented in this section. Additionally, flow patterns in the shoulder flow zone will also be demonstrated.

4.2.1   Post-Weld Profile

The post-weld profiles are labelled and shown to scale in Figure 4-4, and the welded length of welds 9 and 12 is 150mm while others is 200mm. The figure shows varying degrees of surface defects (surface quality) in welds 9, 10, 12 and 13.

It would appear that after comparing the weld profile obtained by tool FSW at the same travelling speeds, the post-weld surface quality improves as the depth of shoulder penetration increases. Using a depth of 0.6mm shoulder penetration, surface defects have disappeared (see weld 11 and weld 14). In addition, it was also found from Figure 4-4 that the post-weld surface quality worsens as the tool travelling speed increases after comparing the weld profile produced by the tool at the same depth of shoulder penetration (welds 9 vs.12 and welds 10 vs. 13).
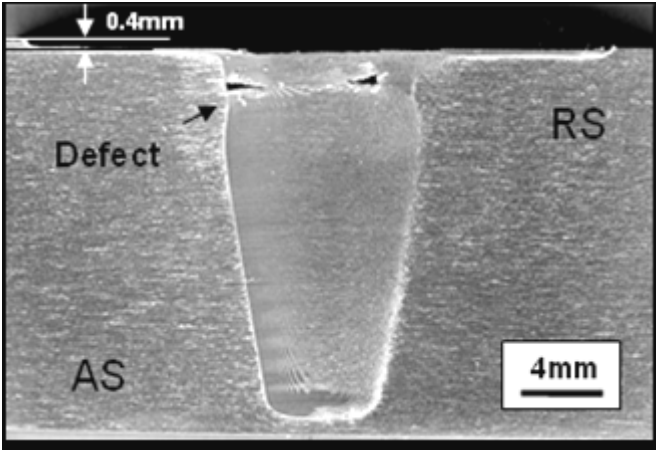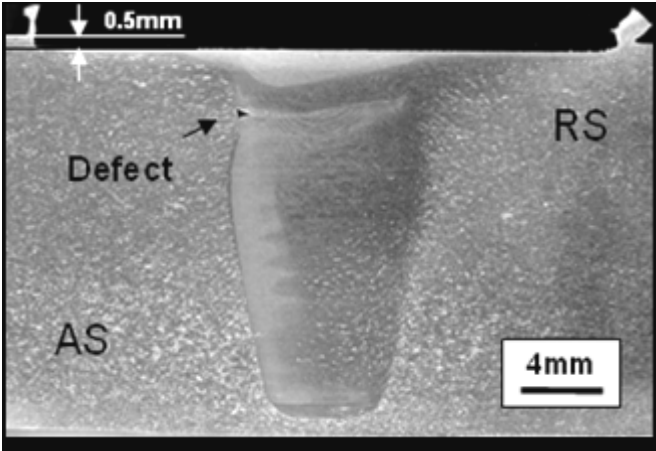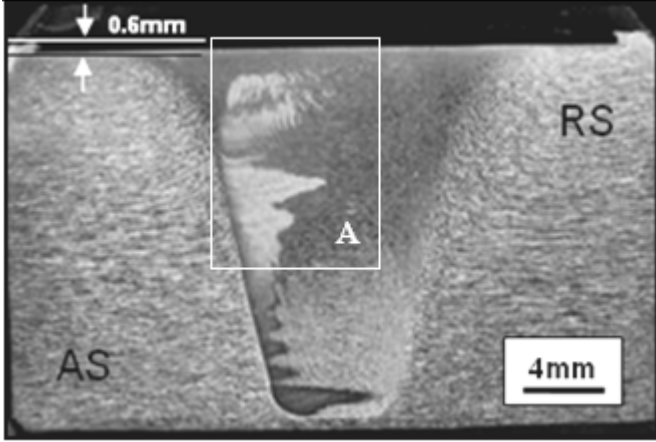
Weld No.	Post-weld profiles	Conditions
9		ω=250rpm V=**40**mm/min H=**0.4**mm
10		ω=250rpm V=**40**mm/min H=**0.5**mm
11		ω=250rpm V=**40**mm/min H=**0.6**mm
12		ω=250rpm V=**56**mm/min H=**0.4**mm
13		ω=250rpm V=**56**mm/min H=**0.5**mm
14		ω=250rpm V=**56**mm/min H=**0.6**mm

40mm
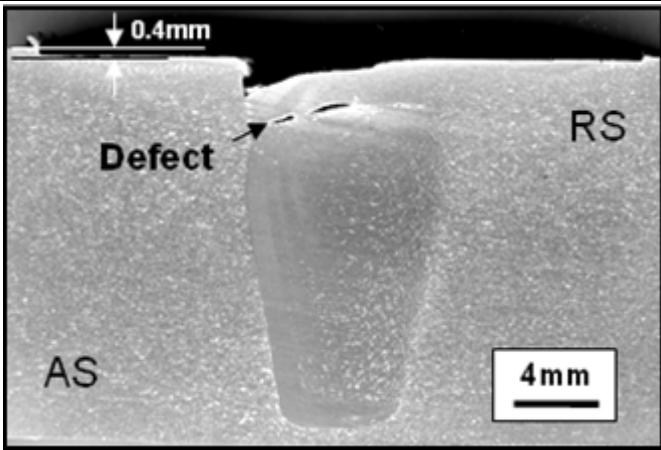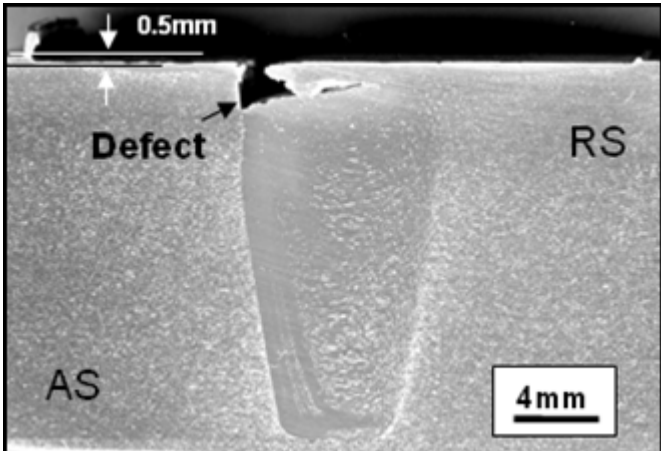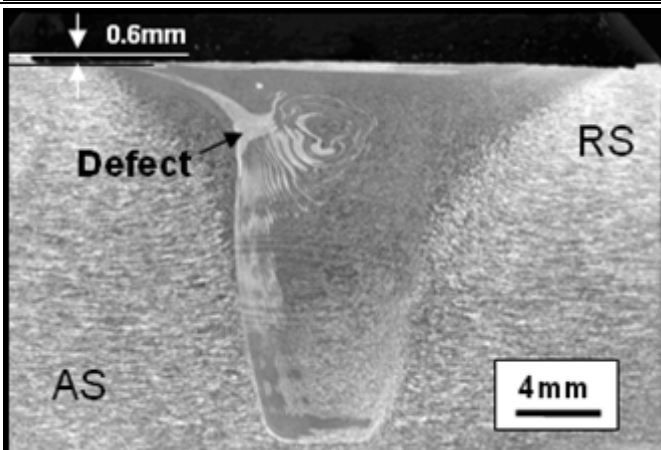
Figure 4-4 Post-weld profiles showing weld surface quality, using scroll shoulder and tapered thread pin tool; welding parameters as indicated

4.2.2   Macrostructure in Transverse Cross Section

Macrostructures of post-weld transverse cross sections, indicated in Figure 3-12, are shown in Figure 4-5 and Figure 4-6 at tool travelling speeds of 40mm/min and 56mm/min respectively. Each figure shows the size variation of internal voids versus depth of shoulder penetration. It would appear that, from evaluating the transverse cross section of the welds shown in Figure 4-5 and Figure 4-6, the post-weld internal void size reduces as the depth of shoulder penetration (H) increases.

Weld No.	Macrostructure of transverse cross section of post-welds	Conditions
9		ω=250rpm V=**40**mm/min H=**0.4**mm
10		ω=250rpm V=**40**mm/min H=**0.5**mm
11		ω=250rpm V=**40**mm/min H=**0.6**mm (welding line normal to workpiece texture direction)

Figure 4-5 Macrostructure of transverse cross section of post-welds (sectioning on Z-Y plane), showing defect (internal voids) occurred in weld 9 and 10, and no-defect (weld 11) weld structures, using scroll shoulder and tapered thread pin tool; welding parameters as indicated

Weld No.	Macrostructure of transverse cross section of post-welds	Conditions
12		ω=250rpm V=**56**mm/min H=**0.4**mm
13		ω=250rpm V=**56**mm/min H=**0.5**mm
14		ω=250rpm V=**56**mm/min H=**0.6**mm (welding line normal to workpiece texture direction)

Figure 4-6 Macrostructure of transverse cross section of post-welds (sectioning on Z-Y plane), showing defect structures (voids and internal voids) occurred in weld 12, 13 and internal void occurred in weld 14 (enlarged version of internal voids in weld 14 shown in area 'B' of Figure 4-11), using scroll shoulder and tapered thread pin tool; welding parameters as indicated

After inspecting the transverse cross section of welds produced by the tool at the same depth of shoulder penetration (welds 9 vs.12 and welds 10 vs. 13 shown in Figure 4-5 and Figure 4-6), it was also observed that the post-weld voids size increases as the tool

travelling speed increases. It can also be noticed that the majority of voids and internal voids appear on the advancing side of weld in the shoulder flow zone.
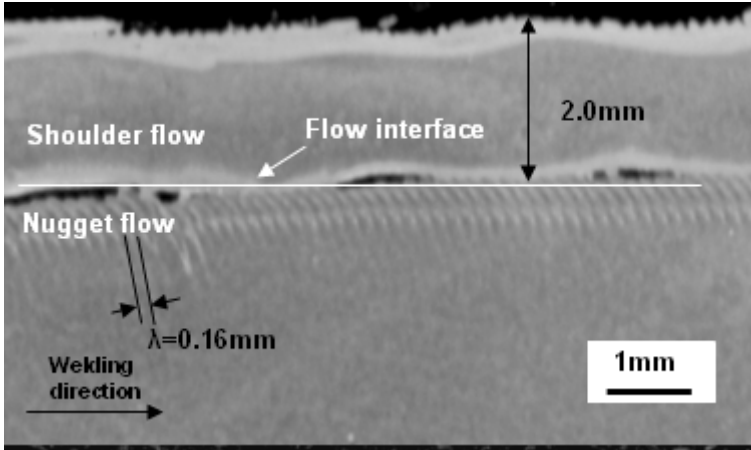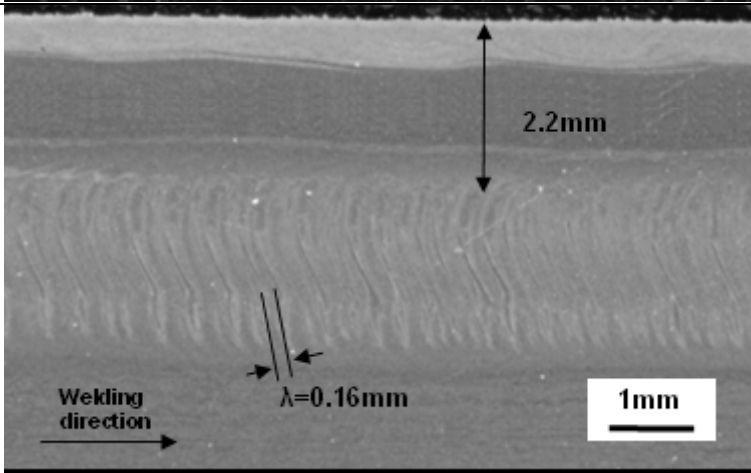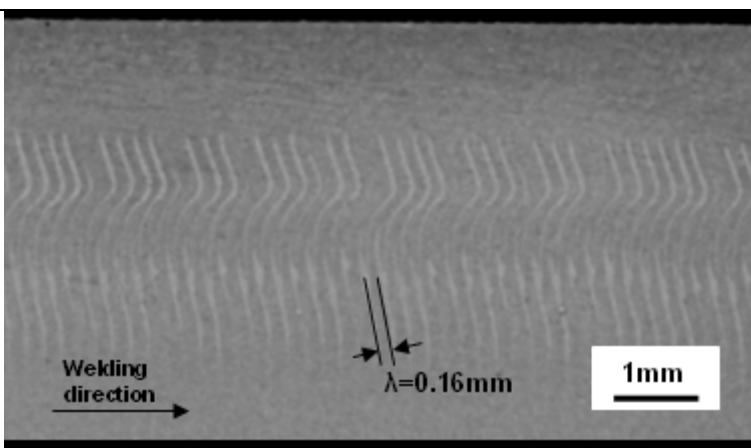
Another observation is that either a quarter or half onion ring pattern appears on the advancing side of the welds 11 and 14 transverse cross sections shown in Figure 4-5 and Figure 4-6. These two welds were produced by a scroll shoulder tool travelling perpendicular to the workpiece texture direction and using two different tool travelling speeds. Additionally, it was also found from the figures that the majority of the weld zones in transverse cross section are not symmetric about the welding centre line.

4.2.3 Microstructure in Longitudinal Cross Section

The microstructures of the post-weld longitudinal cross sections, indicated in Figure 3-12, are shown in Figure 4-7 and Figure 4-8. It can be observed from the figures that a simple banded structure occurs within the weld cross section. The spacing (λ) of these bands is equal to the tool advance per revolution, and hence V/ω (travelling speed over rotating speed of the tool). These bands in the centre are curved away from the tool travelling direction.

Another observation is that defects (internal voids) appear on welds 9, 13 and 12 as shown in Figure 4-7 and Figure 4-8. These internal voids indicate the interface between the shoulder flow zone and nugget zone in the longitudinal cross section of weld. Hence the thickness of the shoulder flow zone in the weld can be determined by measuring the distance between the top surface of weld and the defect (internal voids) interface.

After comparing the weld cross sections obtained by tool FSW at the same travelling speeds (see welds 12 and 13 in Figure 4-8), it can be noticed from that the thickness of the shoulder flow zone increases as the depth of shoulder penetration increases. Furthermore, after comparing the weld cross sections obtained at the same depth of shoulder penetration (see welds 9 and 12 in Figure 4-7 and Figure 4-8), the thickness of shoulder flow zone also increases as the travelling speed increases (welds 9 vs.12 and welds 10 vs. 13).

Weld No.	Microstructure of longitudinal cross section of post-welds	Conditions
9		$\omega=250$rpm V=**40**mm/min H=**0.4**mm $\lambda=V/\omega=40/250$ =0.16mm
10		$\omega=250$rpm V=**40**mm/min H=**0.5**mm $\lambda=V/\omega=40/250$ =0.16mm
11		$\omega=250$rpm V=**40**mm/min H=**0.6**mm $\lambda=V/\omega=40/250$ =0.16mm

Figure 4-7 Microstructure of longitudinal cross section of post-welds (sectioning through welding centre line, on X-Z plane), indicating the interface between shoulder flow zone and nugget zone in weld 9, and the spacing of banded lines (λ), showing defect weld structures (internal voids occurred on weld 9) and no-defect weld (weld 10 and 11), using scroll shoulder and tapered thread pin tool; welding parameters as indicated
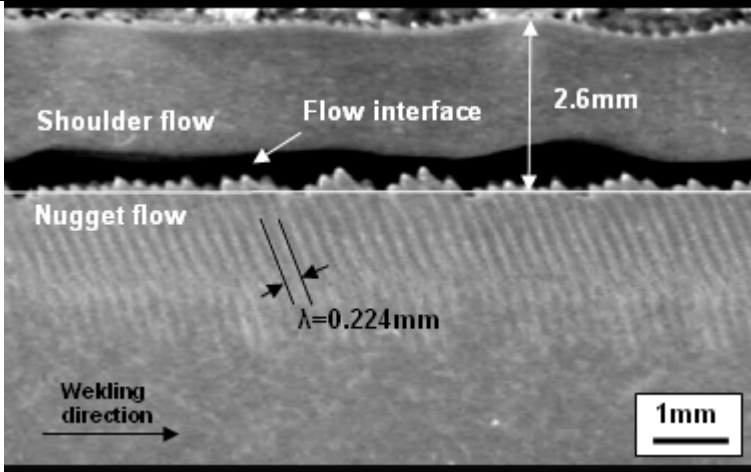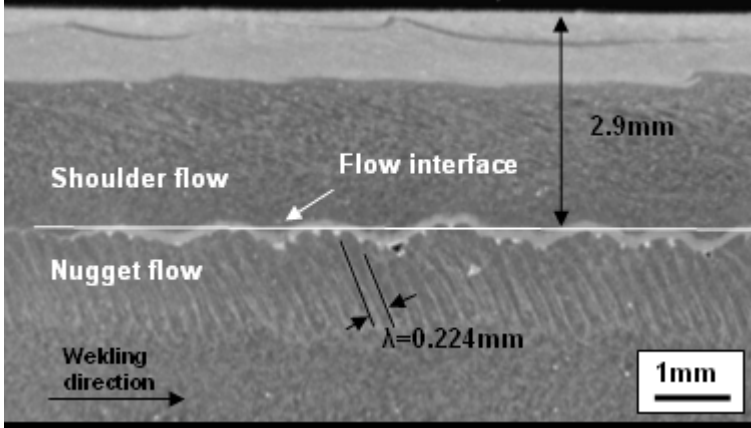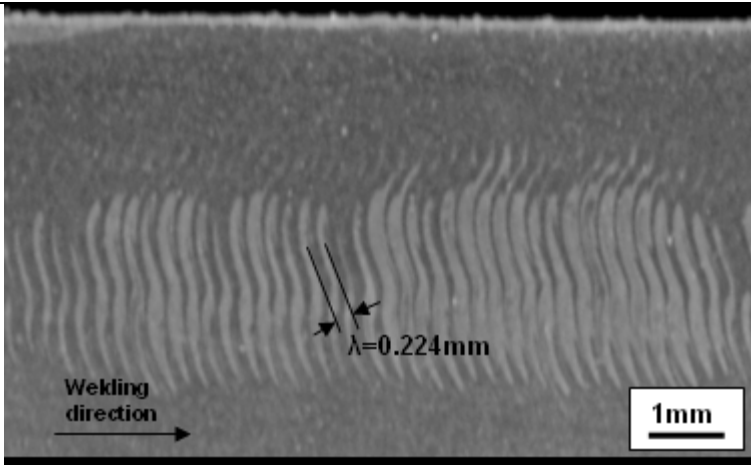
Weld No.	Microstructure of longitudinal cross section of post-welds	Conditions
12		ω=250rpm V=**56**mm/min H=**0.4**mm λ=V/ω=56/250 =0.224mm
13		ω=250rpm V=**56**mm/min H=**0.5**mm λ=V/ω=56/250 =0.224mm
14		ω=250rpm V=**56**mm/min H=**0.6**mm λ=V/ω=56/250 =0.224mm

Figure 4-8 Microstructure of longitudinal cross section of post-welds (sectioning through welding centre line, on X-Z plane), indicating the interface between shoulder flow zone and nugget zone (weld 12 and 13), and the spacing of banded lines (λ), showing defect weld structures (internal voids occurred in weld 12 and 13), and no-defect weld structures (weld 14), using scroll shoulder and tapered thread pin tool; welding parameters as indicated

Further, as shown in Figure 4-7 and Figure 4-8, the shallowest shoulder flow zone thicknesses for each of the two groups of post-welds (sectioning through welding centre line) are around 2.0mm and 2.6mm. These two values were measured from weld 9 and 12, which were produced by a scroll shoulder tool at a 0.4mm depth of shoulder penetration and travel speeds of 40 and 56mm/min respectively. These two values of shoulder flow zone thickness will be used to estimate the thickness of the shoulder flow zone in weld 11 and weld 14, which were obtained at a deeper depth of shoulder penetration than weld 9 and 12.

It can also be observed from Figure 4-7 and Figure 4-8 that the internal voids between the shoulder flow zone and nugget zone reduces as the depth of shoulder penetration increases. At 0.6mm depth of shoulder penetration, the internal voids in the welds have been eliminated (see weld 10, 11 and weld 14).

After examining the cross section of welds (weld 9 vs. 12 and weld 10 vs. 13) produced by the tool at the same depth of shoulder penetration, it can also be found that the internal voids between the shoulder flow zone and nugget zone increases as the tool travelling speed increases.

4.2.4 Summary

The results have been obtained through the investigation of the weld profiles, and the macro and microstructures of the weld cross sections. They include:

1. The weld surface quality improves as the depth of shoulder penetration increases, and at a depth of **0.6mm** shoulder penetration surface defects have disappeared. In addition, the weld surface quality worsens as the tool travelling speed increases.

2. In a transverse cross section of weld, the weld internal voids size reduces as the depth of shoulder penetration (H) increases up to $H \leq$ **0.5mm**. The internal voids size increases as the tool travelling speed increases.

3. There is a quarter or half onion rings pattern appears in the shoulder flow zone on the advancing side of the weld transverse cross section.

4. In a transverse cross section of weld, the weld zone is not symmetric versus the welding centre line.

5. There is a simple banded structure appearing in the longitudinal cross section of weld. The spacing (λ) of these bands is equal to the tool advance per revolution, and hence to V/ω. These bands in the centre are curved away from the tool travelling direction.

6. The thickness of the shoulder flow zone increases as the depth of shoulder penetration increases, and it also increases as the tool travelling speed increases.

7. The shallowest shoulder flow zone thicknesses (in weld longitudinal cross section, sectioning through welding centre line) for each of the two groups of post-welds are equal to **2.0mm** and **2.6mm**. These two values were measured from weld 9 and 12.

8. In a longitudinal cross section of weld, the internal voids between the shoulder flow zone and nugget zone decreases as the depth of shoulder penetration increases. However, the internal voids increases as the tool travelling speed increases.

9. Using more than **0.6mm** depth of shoulder penetration, the internal voids in all longitudinal cross sections of welds has been eliminated.

4.3 Flow Interface and Patterns in Shoulder Flow Zone

As shown previously in Figure 4-8 and indicated in weld 12 and 13, the thickness of the shoulder flow zone (sectioning through the welding centre line) increases as the depth of shoulder penetration increases. Hence, it is reasonable to use the thickness of the shoulder flow zone obtained at a shallow tool shoulder penetration (defect weld), to determine the flow interface between the shoulder flow zone and nugget zone in a weld cross section produced by the same tool using similar FSW conditions, but at deeper shoulder penetration (no-defect weld). Therefore, as presented in section 4.2, the shallowest thicknesses of 2.0mm and 2.6mm in the shoulder flow zone will be used as an approximation of the flow interface between the shoulder flow zone and nugget zone

in weld 11 and weld 14, which were obtained at a deeper depth of shoulder penetration than weld 9 and 12 respectively.

Figure 4-9 shows the microstructure of a longitudinal cross section of weld 11, the flow interface between the shoulder flow zone and nugget zone was determined by drawing a line parallel to the workpiece top surface and at a depth of 2.0mm. It can also be observed from the figure that there is a simple banded structure appearing in the bottom portion of shoulder flow zone and nugget zone. However, the top portion of shoulder flow zone is featureless.
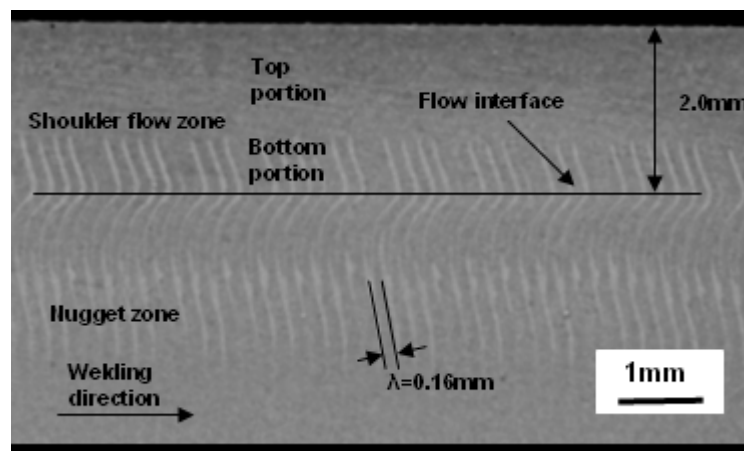
Figure 4-9 Microstructure of weld 11 longitudinal cross section (sectioning through welding centre line, on X-Z plane), indicating the shoulder flow zone and nugget zone, and the spacing of banded lines (λ), using scroll shoulder and tapered thread pin tool FSW at ω=250rpm, H=0.6mm and V=40mm/min

Figure 4-10 shows the microstructure of area 'A' in the weld 11 transverse cross section indicated in Figure 4-5. It can be observed from the figure that there is a half onion rings pattern appearing on the advancing side of the shoulder flow zone and nugget zone. Additionally, it was also found that the top portion of the half onion rings pattern is cut off, and that the cutting interface of the remaining flow pattern seems to fall into a line in the shoulder flow zone as indicated in Figure 4-10. The other observation is that the majority of flow patterns are located in the advancing side of weld transverse cross section.
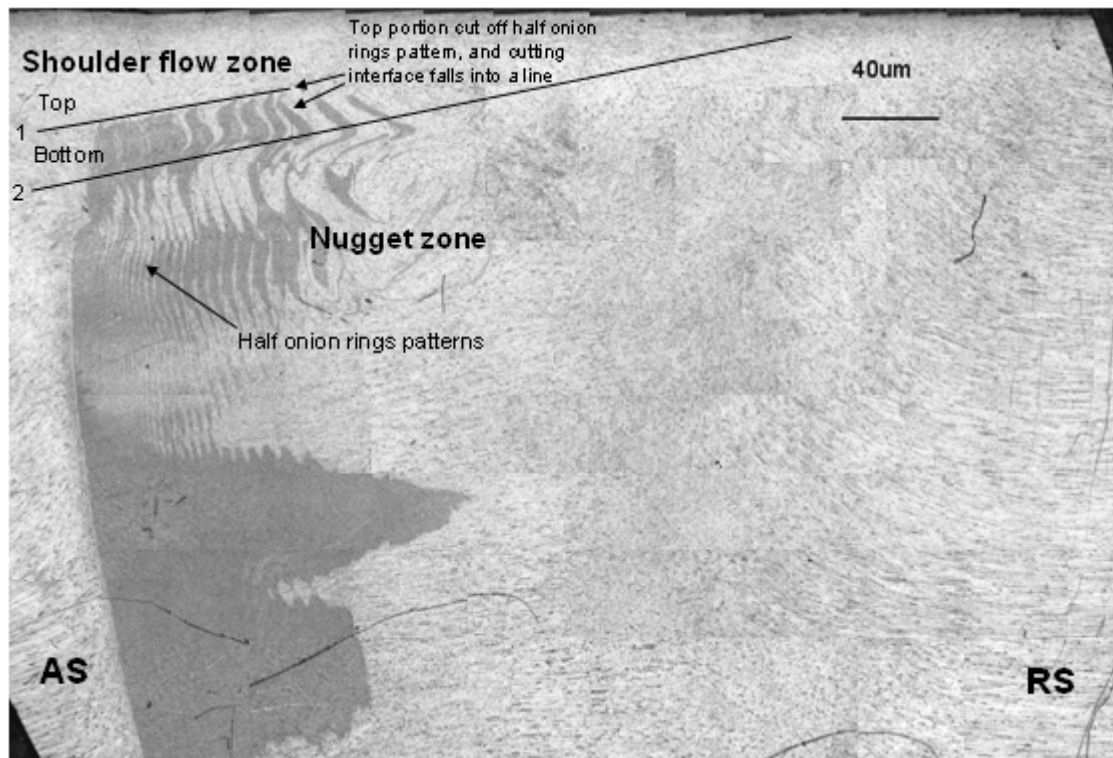
Figure 4-10 Microstructure of area 'A' in the weld 11 transverse cross section as indicated in Figure 4-5, showing a half onion rings patterns appearing on advancing side of the weld zone, indicating the shoulder flow zone and nugget zone, using scroll shoulder and tapered thread pin tool FSW at ω=250rpm, H=0.6mm and V=40mm/min

The microstructure of weld 14 transverse cross section is demonstrated in Figure 4-11 shown below. The welding centre line and tool pin profile were constructed based on the geometry of the tool shoulder and pin used to make weld 14. There is an internal void appearing within the area 'B' of Figure 4-11 as indicated in the enlarged image. This internal void, combined with the thickness of 2.6mm in shoulder flow zone, were used to determine the interface between the shoulder flow zone and nugget zone in the transverse cross section of the weld 14. As shown in Figure 4-11, the interface between the shoulder flow zone and nugget zone was determined by the joining line, through the internal void and the point along the welding centre at the depth of 2.6mm from the weld top surface.
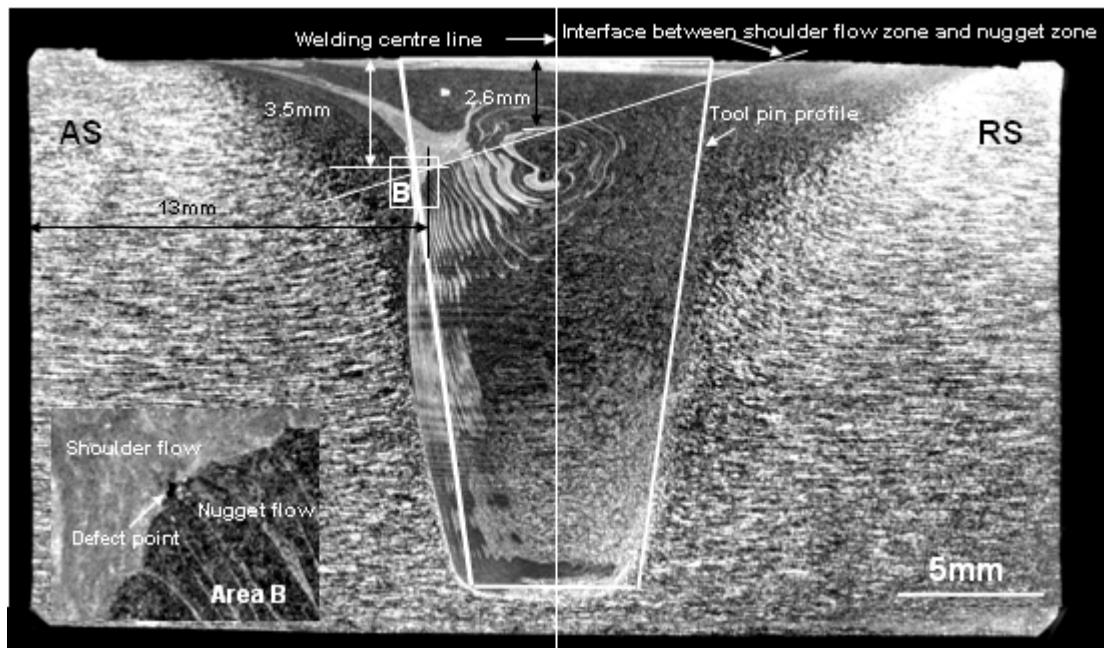
Figure 4-11 Microstructure of weld 14 transverse cross section (sectioning on Z-Y plane) and area 'B', showing tool pin profile, welding centre line, interface between shoulder flow zone and nugget zone, and defect (internal void) point, obtained by FSW at ω=250rpm, H=0.6mm and V=56mm/min

It can be observed from Figure 4-11 that the weld zone is not symmetric versus the welding centre line, and the majority of flow patterns appear on the advancing side of weld zone. It can also be noticed from Figure 4-11 that the flow interface crosses through the weld top surface outside the retreating side of tool pin profile. This result indicates that the thickness of the shoulder flow zone varies based on the position of the weld zone, with a thicker shoulder flow zone on the advancing side than on the retreating side. The variation of the shoulder flow zone thickness is not necessarily linear.

In summary, the results have been acquired through the examination of micrographic cross sections of weld 11 and 14. They contain:

1. There are simple banded structures appearing in the bottom portion of shoulder flow zone and nugget zone. However, the top portion of shoulder flow zone is featureless.

2. There is a half onion rings patterns appearing on the advancing side of shoulder flow zone and nugget zone. In the shoulder flow zone, the top portion of half onion rings pattern is cut off, and the cutting interface of the remaining flow pattern seems to fall into a line.

87

3. The thickness of shoulder flow zone varies, with a thicker shoulder flow zone on the advancing side than on the retreating side.
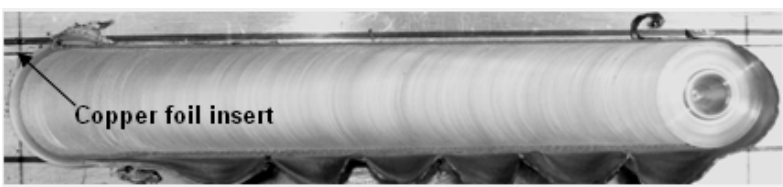
4.4 Identification of Flow Pattern in Shoulder Flow Zone by Markers

The results of 'marker insert' experiments will be presented in this section. Results show the variation of the shoulder flow zone thickness in the longitudinal cross section of weld. Additionally, the flow patterns documented by copper foil fragments in the shoulder flow zone will also be demonstrated.

4.4.1 Shoulder Flow Zone Weld Structure with Marker Insert
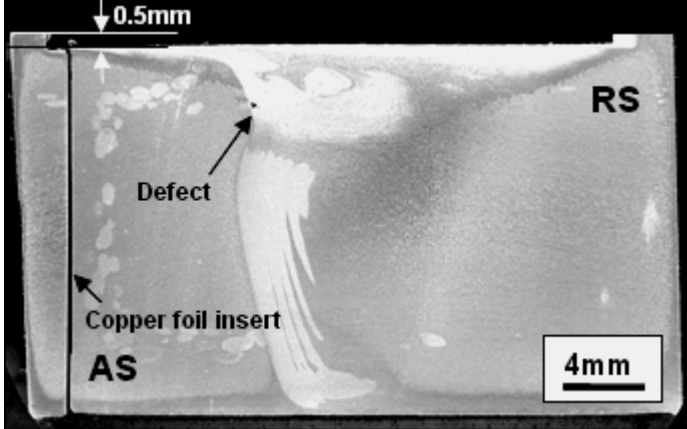
As described in section 3.3.1 and shown in Figure 3-17, the shoulder flow zone flow movement was studied by means of the 'marker insert' technique using a copper foil as a tracer. FSW parameters used in this experiment were shown in Table 5. The study was carried out by directly observing the weld top surface profile, weld transverse cross section (Z-Y plane see Figure 1-3 for coordinate) and three longitudinal cross sections of welds (sectioning on Z-X planes, through the mid retreating side, welding centre line and mid advancing side).

Figure 4-12 shows the experimental result of the post-weld profile. It can be observed that there is no weld surface defect occurring on the weld profile. Additionally, it can also be found that a copper foil was embedded within the post-weld profile along the advancing side of the weld.

Weld No.	Weld profile	Conditions
15	Copper foil insert	ω=250rpm H=**0.5**mm V=**40**mm/min

40mm

Figure 4-12 Post-weld profile, showing a defect-free weld, indicating the copper foil insert, using scroll shoulder and tapered thread pin tool; welding parameters as indicated
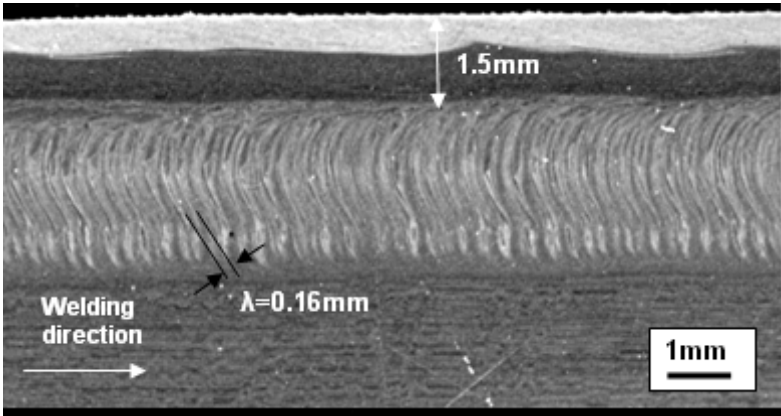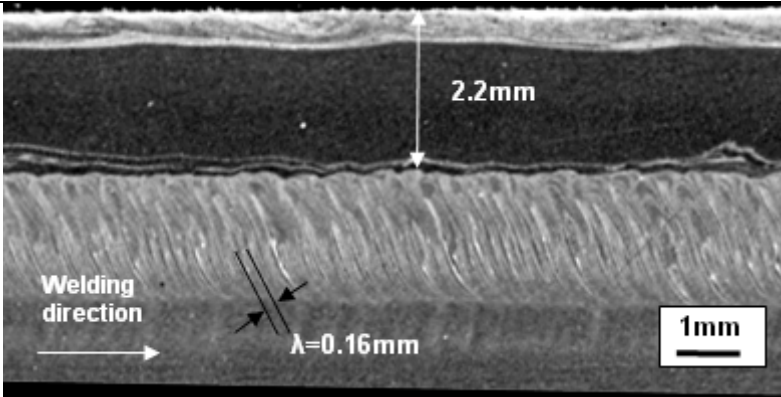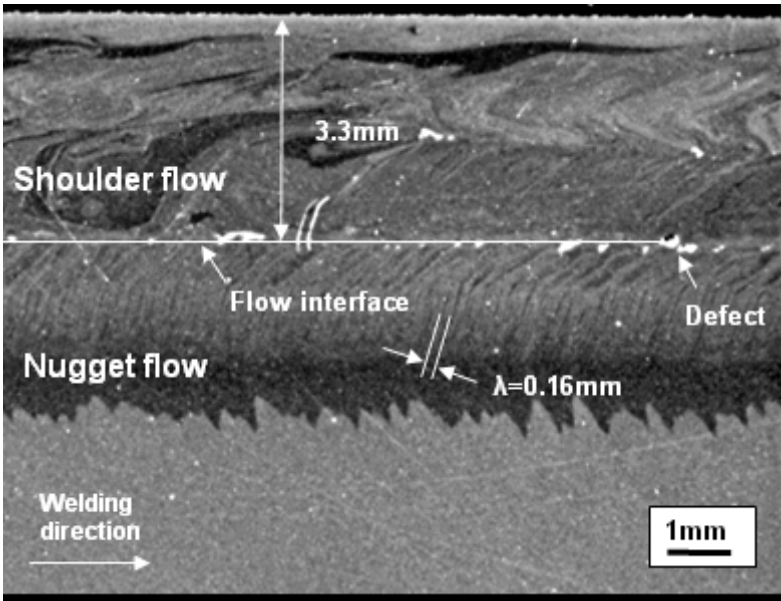
Figure 4-13 shows the macrostructure of the transverse cross section of weld 15. It can be observed that there is an internal void appearing on the advancing side of weld as indicated. It was found that this internal void is similar in size to the one appearing in the macrostructure of the transverse cross section of weld 10 as shown in Figure 4-5, because these two welds were produced by the same tool using the same welding parameters. Additionally, it was also found that the weld zone in the transverse cross section of weld 15 is not symmetric about the welding centre line.

Weld No.	Macrostructure of weld transverse cross section	Conditions
15		ω=250rpm H=**0.5**mm V=**40**mm/min

Figure 4-13 Macrostructure of transverse cross section of weld 15 (sectioning on Z-Y plane), indicating the copper foil insert and an weld defect (internal voids), using scroll shoulder and tapered thread pin tool; welding parameters as indicated

Figure 4-14 shows three microstructures of the longitudinal cross sections of weld 15. These samples were obtained by sectioning weld 15 at three different positions as indicated in the figures. It can be observed from the figure that a simple banded structure occurs in these three cross sections of weld 15.

Further, it was found from Figure 4-14 that the distance between the weld top surface and the interface between the banded structures and the upper featureless region increases from 1.5mm to 3.3mm, as the sectioning position in weld transverse cross section moves from the retreating side to the advancing side.

Weld No.	Microstructure of weld longitudinal cross sections, sectioning in three different positions, with λ=V/ω=40/250=0.16mm	Sectioning position
15		**(a)** Mid retreating side (7.5mm away from welding centre line)
		(b) Welding centre line
		(c) Mid advancing side (7.5mm away from welding centre line)

Figure 4-14 Microstructure of longitudinal cross sections of weld 15 (sectioning on X-Z plane), showing defect and no-defect weld structures, indicating interface between shoulder flow zone and nugget zone, also showing the thickness of shoulder flow zone increase from figure (a) to (c)

The other observation is that the distance between the weld top surface and the interface between the banded structures and the upper featureless region is equal to 2.2mm in Figure 4-14 (b). This distance is similar to the one indicating in the microstructure of the longitudinal cross section of weld 10 shown in Figure 4-7, because these two welds were produced by the same tool using the same welding parameters. In addition, it can also be observed from Figure 4-14 (c) that a defect (internal voids) appears on the longitudinal cross section of weld. It indicated the interface between the shoulder flow zone and nugget zone.

4.4.2 Shoulder Flow Zone Flow Pattern Confirmed by Marker

Figure 4-15 shows the microstructure of the longitudinal cross section of weld obtained by sectioning weld 15 through the mid advancing side. The cross section was taken from a position 7.5mm away from the welding centre line which is the same sectioning position as Figure 4-14 (c) but further along the weld path.
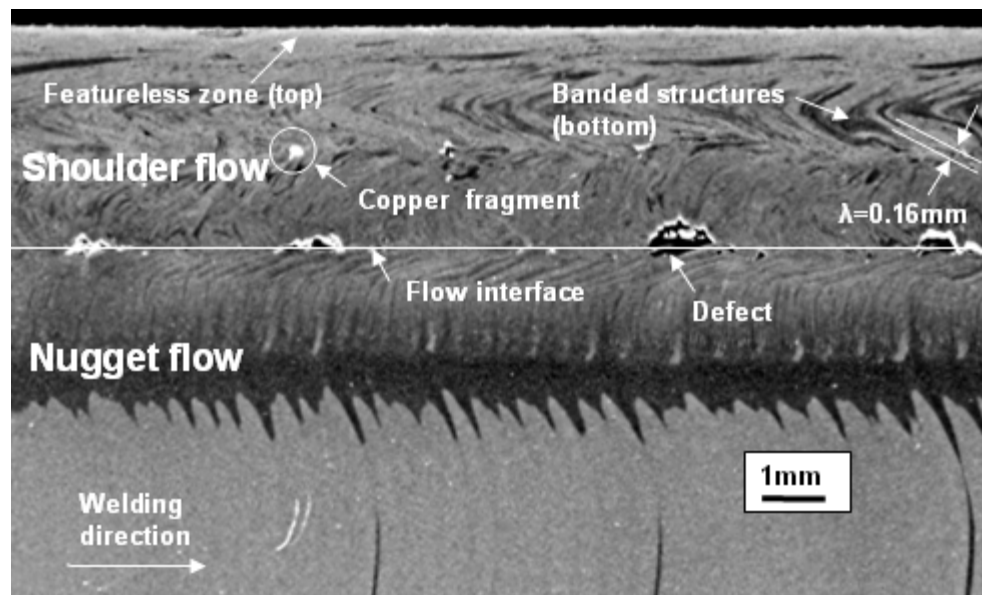
Figure 4-15 Microstructure of longitudinal cross section of weld 15, sectioning through mid advancing side (7.5mm away from welding centre line), indicating the interface between shoulder flow zone and nugget zone, and a copper fragment distributed in the shoulder flow zone, using scroll shoulder and tapered thread pin tool FSW at ω=250rpm, H=0.5mm and V=40mm/min

It can be observed from Figure 4-15 that there are two internal voids that occur in the weld zone. Accordingly, the flow interface between the shoulder flow zone and nugget zone was determined by linking these two internal voids. The other observation is that a

copper fragment was found in the shoulder flow zone as indicated by a circle and shown in the figure.

It can also be observed from Figure 4-15 that there is a simple banded structure in a layer to layer manner appearing in the shoulder flow zone as indicated. However, the simple banded structure disappears in the top portion of shoulder flow zone, and is replaced by the featureless zone as indicated.

4.4.3   Summary

The 'marker insert' experimental results are given in the figures as shown above. It can be concluded that the shoulder flow zone flow pattern induced by the scroll shoulder tool has been confirmed using a copper foil as tracer. This flow pattern has a simple banded structure and in a layer to layer manner. In addition, the relationship between the thickness of the shoulder flow zone and the position of the weld zone has been revealed, with a thicker shoulder flow zone on the advancing side than on the retreating side.

5 Discussion

This chapter presents discussion on the quantitative results of the mass of induced PUM, and the effect of welding parameters on the shoulder flow zone formation. In addition, the 'marker insert' technique, the identification of the shoulder flow zone flow patterns using a 'marker insert' technique, and the forming mechanism of the shoulder flow zone will also be discussed in this section. The discussion of these aspects during scroll shoulder tool FSW will be compared with the suggestions made by the researchers as reviewed in the chapter two.

5.1 Quantification of Induced PUM

This section discusses the quantitative results of the effect of various welding parameters on the net mass of PUM induced by the tool during tool pin plunging, tool shoulder plunging and tool travelling. Quantitative results indicated that in order to obtain a defect-free FSW weld produced by scroll shoulder tool, the scroll groove needs to be fully filled up with PUM before the tool begins travel. The mass of induced PUM accumulated within the scroll groove before tool travelling is the sum of the mass of PUM induced by the tool during tool pin plunging and tool shoulder plunging. In this study, the maximum mass of displaced workpiece material (WPM) that could theoretically accumulate within the tool scroll groove was **1.29g** (*tool 1* and *tool 2* have same spacing of scroll groove beneath the shoulder, see Appendix 2). Additionally, these results will also be compared with the findings of other researchers.

5.1.1 Mass of Induced PUM during Tool Pin Plunging

Trial 'A' as described in section 3.1.2, was conducted to evaluate the effect of tool plunging speed on the mass of induced PUM during tool pin plunging. It was found that the average net mass of induced PUM decreases from **0.79g** to **0.52g**, and the percentage of displaced WPM converted into PUM decreases from **43.4%** to **28.6%**, at tool plunging speeds of **3mm/min** and **6mm/min** respectively. It was also found that the faster the tool pin is plunged, the less net mass of PUM is induced, and the lower percentage of displaced WPM is converted into PUM during tool pin plunging. The shoulder scroll groove has not been fully filled up with PUM in trial 'A', in weld 1

(**0.79g**) and weld 2 (**0.52g**), after the tool pin was plunged with zero depth of shoulder penetration at two different speeds.

The 'mass of induced PUM during tool pin plunging' results indicate that in order to obtain a defect-free FSW weld, the shoulder of the scroll shoulder tool has to be plunged into the workpiece at a certain depth to ensure sufficient PUM is supplied and the scroll spacing is fully filled up with PUM before tool travelling. This is because the results shown in Figure 4-1 and Table 6 demonstrate that the shoulder scroll groove could not be fully filled up with PUM in weld 1 (**0.79g**) and weld 2 (**0.52g**) after the tool pin was plunged with zero depth of shoulder penetration at two different plunging speeds, as the maximum mass of displaced WPM that could theoretically accumulate within the tool scroll groove is **1.29g**. Therefore, it is impossible to have a sustainable defect-free FSW weld by setting the tool shoulder such that it just touches the workpiece (zero depth of shoulder penetration). This finding is in contrast to the suggestion of Dawes and Thomas [8], as they suggested that a near zero depth of shoulder penetration could lead to the elimination of the weld flash and any additional workpiece contact would produce significant amounts of weld flash, resulting in a risk of voids occurring in the weld reviewed in section 2.5.1. Additionally, this finding also strongly supports the suggestion of Fuller [22] that plunging the tool shoulder into workpiece at a depth of 0.1mm to 0.5mm is an optimal depth of shoulder penetration for scroll shoulder tool FSW reviewed in section 2.1.2.

Furthermore, these results also show that at a faster tool pin plunging speed, a lower quantity of induced PUM remains beneath the scroll groove due to a greater amount of displaced WPM being pushed out of the shoulder face as the percentage of the displaced WPM converted into PUM is lower (see Table 6). These results also indicated the percentage of the shoulder scroll groove that is filled up by the induced PUM and its relationship to the tool pin plunging speed. A total of 61% (0.79g/1.29g) of the scroll spacing was filled up at a 3mm/min tool plunging speed and 40% (0.52g/1.29g) of it was filled up at a 6mm/min tool plunging speed.

5.1.2   Mass of Induced PUM during Tool Shoulder Plunging

As described in section 3.1.2, trial 'B' was implemented to study the effect of depth of shoulder penetration on the mass of induced PUM during tool shoulder plunging. It was

found that the average net mass of induced PUM increases from **0.15g** to **1.25g**, and the percentage of displaced WPM converted into PUM increases from **22%** to **73.1%**, at depths of shoulder penetration from **0.40mm** to **1.0mm** respectively. It was also found that the deeper the scroll shoulder is penetrated into the workpiece, the more net mass of PUM is induced, and the higher percentage of displaced WPM is converted into PUM during tool shoulder plunging. The shoulder scroll groove seems to have been fully filled up with PUM in trial 'B'-weld 6 (**1.25**g), after the tool shoulder was plunged into the workpiece at a 1.0mm of depth of shoulder penetration.

The 'mass of induced PUM during tool shoulder plunging' results show that the mass of induced PUM is a vital factor in forming a non-defective weld in the scroll shoulder tool FSW. It also indicates that a defect-free FSW weld can be achieved by fully filling up the shoulder scroll groove with PUM before tool travelling. As can be observed from Figure 4-7 and Figure 4-8, there is no defect appearance on weld 11 and 14. Those welds were obtained at a 3mm/min tool plunging speed and 0.6mm depth of shoulder penetration, where the mass of induced PUM in weld 11 and 14 are **1.4g** (0.79g + 0.61g, see Table 6 and 7), and the shoulder scroll groove was fully filled up with PUM before tool travelling, as the maximum mass of displaced WPM that could theoretically accumulate within the tool scroll groove is **1.29g** only. This finding is important in the design of the scroll shoulder tool and the selection of welding parameters to ensure FSW weld quality. Additionally, these results also support the hypothesis of the preliminary investigation of the present study that 'a deeper shoulder penetration may result in an increase of the accumulated workpiece material within the scroll groove beneath the shoulder, which would improve the shoulder flow zone formation'.

Further, the finding, 'a defect-free FSW weld can be achieved by fully filling up the scroll groove with PUM before tool travelling' could also be used to explain why both lower and higher tool travelling speeds result in defect formation obtained by Colligan et al [15] during FSW thick 5083-H131 Al plate. The formation of these two defect welds presented by Colligan et al may be due to the scroll groove of the tool used to produce these welds having not been fully filled up with PUM before tool travelling. They neither recorded any control of the depth of shoulder penetration during these FSW experiments nor reported the depth of shoulder penetration they used in their publication. Insufficient depth of shoulder penetration could result in a small amount of PUM being induced, leading to inadequate induced PUM filling into the scroll groove.

In this case, the issue of the scroll groove has not been fully filled up with PUM may dominate the defect weld formation more than the tool travelling speed.

Furthermore, these results also show that at a shallower shoulder penetration, a lower quantity of induced PUM remains beneath the scroll groove due to a greater amount of displaced WPM being pushed out of the shoulder face as the percentage of the displaced WPM converted into PUM is lower (see Table 7). These results also show the percentage of the shoulder scroll groove that is filled up by the induced PUM and its relationship to the depth of shoulder penetration. A total of 11.6% (0.15g/1.29g) of the scroll spacing was filled up at a 0.4mm depth of penetration, 31.8% (0.41g/1.29g) at 0.5mm, 47.3% (0.61g/1.29g) at 0.6mm and 96.9% (1.25g/1.29g) at 1.0mm.

5.1.3   Mass of PUM Induced during Tool Travelling

Trial 'C' as described in section 3.1.2, was performed to investigate the effect of tool travelling speed on the mass of induced PUM during tool travelling. It was found that the average net mass of induced PUM decreases from **1.11g** to **0.6g**, and the percentage of displaced WPM converted into PUM decreases from **85.4%** to **46.2%**, at tool travelling speeds of **40mm/min** and **56mm/min** respectively. It was also found that the faster the tool travels, the less net mass of PUM is induced, and the lower percentage of displaced WPM is converted into PUM during tool travelling at these two different speeds.

The 'mass of induced PUM during tool travelling' results could be used to explain why faster travelling speeds lead to the appearance of the internal voids in the upper advancing side of the weld obtained by Colligan et al [15] during FSW thick 2195-T8P4 Al plate. This is because the faster the tool travels, the less mass of PUM is induced after the tool travels a certain distance. The insufficient amount of PUM induced during tool travelling leads to the formation of a defect weld. Additionally, these results also support that two scroll grooves cut on the shoulder face is the minimum number of scrolls required for effective scroll shoulder tool design. This is because the entrance of the shoulder scroll groove is only open to the workpiece, to induce the workpiece material into the scroll groove, during the each half of tool revolution. The scroll grooves should be equally spaced, and the entrances are positioned 180 degrees

opposite to each other as measured along the rotating axis, to ensure there is an available entrance at every half of tool rotational positions.

Figure 5-1 shows the different positions of the shoulder scroll groove entrance versus tool travelling and rotating direction. It can be observed that firstly, the entrance of scroll groove starts to open to the workpiece (see illustration (1) in Figure 5-1) at the beginning of tool rotating and travelling; secondly, the entrance is increased until it is fully opened to the workpiece (see illustration (2) in Figure 5-1), after the first quarter of tool revolution is complete and the entrance direction is parallel to the tool travelling direction; thirdly, the entrance is reduced until it is fully blocked to the workpiece (see illustration (3) in Figure 5-1), after the second quarter of tool revolution is complete and the entrance direction is normal to the tool travelling direction; finally, the entrance is also fully blocked (see illustration (4) in Figure 5-1) during the rest of third and fourth quarters of tool revolution due to its entrance direction being opposite to the tool travelling direction. Therefore, a minimum two opposite spaced scroll grooves cut on the shoulder face will ensure that the entrance of the scroll groove is open to the workpiece to induce workpiece material in at any angular position. This will provide more opportunity to induce sufficient PUM.
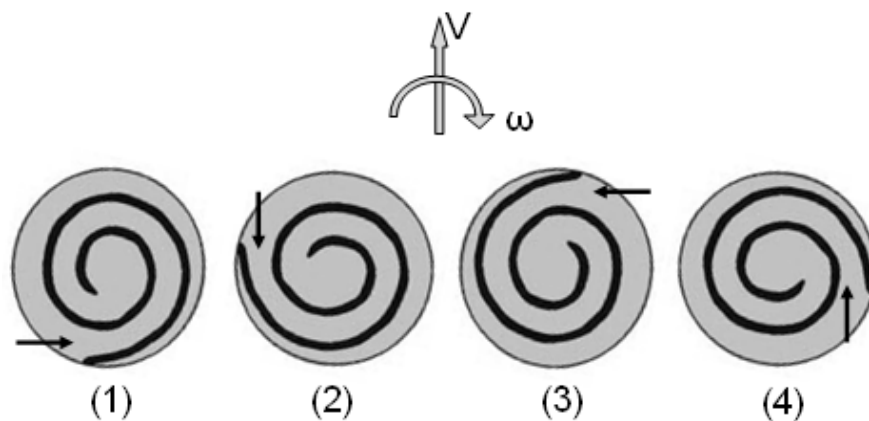
Figure 5-1 Schematic illustration of tool travelling and rotating direction vs. entrance position of the shoulder scroll groove after each quarter of tool revolution; (1) entrance starts to open, (2) entrance is fully opened after the first quarter of tool revolution, (3) entrance is reduced until it is blocked after the second quarter of tool revolution, and (4) entrance is also fully blocked during the rest of the third and fourth of tool revolution

These results also show the effect of tool travelling speed on the average net mass of induced PUM during each tool revolution. Using the distance travelled and the travelling speed, the tool travelling time can be calculated; using the rotational speed

97

and the travelling time, the total number of tool revolutions can also be calculated; and finally, the average net mass of PUM induced per revolution can be determined by dividing the average net mass of PUM by the number of revolutions.

For a tool travelling 40mm, it will take 1 minute and 0.714 minute at travelling speeds of 40 mm/min and 56mm/min respectively. Therefore, the total numbers of tool revolutions at a 250rpm rotational speed are 250rev. (1x250) and 178.5 rev. (0.714x250) respectively. Hence, the average net mass of induced PUM per tool revolution at 40mm/min and 56mm/min travelling speeds are 4.44 mg/rev (1.11/250) and 3.36 mg/rev (0.6/178.5) respectively. It is believed that there is a relationship between the average net mass of PUM induced per revolution and the weld quality that will need to be further investigated.

5.2 Effect of Welding Parameters on Shoulder Flow Zone Formation

Trial 'D' was conducted to evaluate the effect of depth of shoulder penetration and tool travelling speed on the shoulder flow zone formation. The 'effect of welding parameters on the shoulder flow zone formation' results indicated that there is a positive linear relationship between the mass of PUM and the weld quality in the shoulder flow zone. In addition, it was also found that in order to obtain a defect-free FSW weld produced by scroll shoulder tool, the scroll groove not only needs to be fully filled up with PUM before the tool starts to travel, but also needs to be filled in with a sufficient amount of PUM per tool revolution during tool travelling. These results will be discussed and compared with the suggestions of other researchers from the reviewed literature.

5.2.1 Effect of Depth of Shoulder Penetration on Shoulder Flow Zone Formation

The first part of trial 'D' was conducted to evaluate the effect of depth of shoulder penetration on the shoulder flow zone formation. Figure 4-4 to Figure 4-8 show post-weld profiles, weld transverse cross sections and weld longitudinal cross sections. It was found that the weld surface defects, weld transverse cross section internal voids and weld longitudinal cross section internal voids reduce as the depth of shoulder penetration increases. Weld defects in the surface profile, transverse cross sections and longitudinal cross sections have disappeared at 0.6mm depths of shoulder penetration which was the maximum value used in this study.

The 'effect of depth of shoulder penetration on the shoulder flow zone formation' results strongly support that there is a positive linear relationship between the mass of PUM and the weld quality in the shoulder flow zone. This is because the 'mass of induced PUM during tool shoulder plunging' indicated that the deeper the scroll shoulder is penetrated into the workpiece, the more net mass of PUM is induced. While the 'effect of depth of shoulder penetration on the shoulder flow zone formation' results demonstrated that the weld surface defects, weld transverse cross section internal voids, and weld longitudinal cross section internal voids reduce as the depth of shoulder penetration increases. The weld defect reductions (including weld surface defects, weld transverse cross section internal voids and weld longitudinal cross section internal voids) were due to a greater amount of PUM supplied which filled into the shoulder flow zone at deeper depths of tool shoulder penetration.

Furthermore, the 'effect of depth of shoulder penetration on the shoulder flow zone formation' results also support the findings of Kumar and Kailas [55], who stated that an adequate depth of shoulder penetration could generate sufficient hydrostatic pressure in the weld zone, to produce a defect-free weld. This is because the deeper tool shoulder penetration leads to a reduction of the size of weld defects in the shoulder flow zone. Additionally, both experimental results obtained in the present study and the findings of Kumar and Kailas [55] all showed that the weld defects have disappeared after a certain depth of shoulder penetration.

5.2.2   Effect of Tool Travelling Speed on Shoulder Flow Zone Formation

The second part of trial 'D' was conducted to evaluate the effect of tool travelling speed on the shoulder flow zone formation. Figure 4-4 to Figure 4-8 show post-weld profiles, weld transverse cross sections and weld longitudinal cross sections. It was found that the weld surface defects, weld transverse cross section internal voids and weld longitudinal cross section internal voids increase as tool travelling speed increases.

The 'effect of tool travelling speed on the shoulder flow zone formation' results also support that there is a positive linear relationship between the mass of PUM and the weld quality in the shoulder flow zone. This is because the 'mass of induced PUM during tool travelling' indicated that the faster the tool travels, the less net mass of PUM is induced. While the 'effect of tool travelling speed on the shoulder flow zone

formation' results demonstrated that the weld surface defects, weld transverse cross section internal voids, and weld longitudinal cross section internal voids increase as tool travelling speed increases.

The weld defect increases (including weld surface defects, weld transverse cross section internal voids and weld longitudinal cross section internal voids) were due to a smaller amount of PUM induced and filled into the shoulder flow zone per tool revolution at faster tool travelling speeds. The quantification results of the 'mass of induced PUM during tool travelling' also indicated that the faster the tool travels, the less net mass of PUM is induced per tool revolution. It is believed that during tool travelling, there is still a minimum amount of PUM that is required to be induced per tool revolution to ensure a defect-free weld, although the scroll groove having been fully filled up with PUM before the tool starts to travel. It is also speculated that there is an optimal combination among the tool geometry, welding parameters and mass of PUM to ensure FSW weld quality that will need to be further investigated.

Furthermore, the 'effect of tool travelling speed on the shoulder flow zone formation' results correlate well with a previous study conducted by Colligan et al [15] whom demonstrated that the internal voids occur in the upper advancing side of the weld zone at a faster scroll shoulder tool travelling speed during FSW thick 2195-T8P4 Al plate. In addition, these results also correlate well with the finding of Fujii et al [57] that a defect appearing in the weld produced by tool at a faster tool travelling speed during FSW 6061 Al alloy.

5.3   Flow Interface and Patterns in Shoulder Flow Zone

As described in chapter three, trail 'D' was conducted to evaluate the effect of depth of shoulder penetration and tool travelling speed on the shoulder flow zone formation. The experimental results of the microstructures of weld 11 and 14 have been presented in chapter four. The weld zone flow interface and patterns will be discussed by combining the observations of these cross sections of weld shown in Figure 4-9, Figure 4-10 and Figure 4-11. Additionally, these results will also be compared with the findings of other researchers from the reviewed literature.

Figure 4-9 shows the microstructure of a longitudinal cross section of weld 11, where the weld cross section was divided into the shoulder flow zone and nugget zone. It can be observed from the figure that there is a simple banded structure (a layer to layer) appearing in the bottom portion of the shoulder flow zone, but the banded structure disappeared in the top portion of shoulder flow zone. The top portion of the shoulder flow zone is featureless, which implies that there is a flow interaction occurring within this region. The flow interaction details will be explained later in the revelation of the shoulder flow zone forming mechanism section. Furthermore, the appearance of simple banded structures in the longitudinal cross section of welds obtained from the present study are similar to the findings of Zettler et al [19], who presented a banded structure in the transverse cross section of the weld shown in Figure 2-38.

Figure 4-10 shows a higher magnification view of the area 'A' of Figure 4-5, where a small portion of microstructure of transverse cross section of weld 11 was demonstrated. It can be observed from the figure that the advancing side of the transverse cross section of weld is separated by line '1' and '2', and that there is a featureless zone which appears upon the line '1'. The occurrence of this featureless zone correlates well with the appearance of a featureless pattern in the top portion of the shoulder flow zone shown in Figure 4-9. Additionally, the flow pattern shown in Figure 4-10 strongly supports the finding of the present study that there is a flow interaction occurring within this region (top portion of shoulder flow zone). This is because there is an obvious flow interface (present as dark and light coloured bands) appearing in Figure 4-10 as separated by line '1' and '2'. The appearance of these two different coloured bands is due to the different microstructures of the bands within the cross section of weld.

The other observation of Figure 4-10 is a quarter onion ring pattern (a layer to layer) that appears on the advancing side of shoulder flow zone. This is because the top portion of the half onion ring pattern is cut off, to leave a quarter onion ring pattern. As can be observed form Figure 4-10, the cutting interface aligns with a line in the top portion of this remaining quarter section of the onion ring pattern as indicated by line '1'. This observed result suggests that the flow interaction in the shoulder flow zone has a shear interface. This result also implies that the top portion of annular ring material (ARM) shears with the bottom portion of having been driven downward ARM, causing the flow interface to 'fall into a line'. The reason why flow interaction forms in such

101

manner will be explained more details in the later section. Additionally, the appearance of a quarter of onion ring pattern (with a layer to layer sheared manner) in the transverse cross section of welds obtained in the present study are well correlated with a similar finding of Colligan et al [15] whom exhibited a layer to layer flow pattern in the upper advancing side of a transverse cross section of weld during FSW 2195-T8P4 Al plate and demonstrated in Figure 2-36.

In summary, in longitudinal and transverse cross sections of welds, a simple banded structure and onion ring pattern have been found in the shoulder flow zone using an approximation of the thickness of the shoulder flow zone. These suggested flow patterns will be confirmed by the marker insert technique presented in the next section and the confirmed flow patterns will be used to reveal the forming mechanism of the shoulder flow zone later.

5.4 Identification of Flow Pattern in Shoulder Flow Zone by Markers

This section discusses the 'marker insert' technique, variation of weld structure in the shoulder flow zone and the confirmation of the flow pattern in shoulder flow zone using a 'marker insert' technique. Additionally, these results will also be compared with the suggestions of other researchers from the literature.

5.4.1 'Marker Insert' Technique

The marker (same as PUM) movement expected in trial 'E' was described in section 3.3.1. It was hypothesised that the marker is cut by the edge of the scroll groove and pushed into the scroll groove by the incoming workpiece material, and then driven downward by the tip-off pin (root portion of tool pin) subsequently distributing it within the weld zone. If the marker fragments are found in the weld zone, it can be concluded that the zone upon the marker fragment is shoulder flow zone, and the flow patterns in this zone is shoulder flow zone flow pattern.

In the present study, copper foil was positioned with a distance (13mm) offset from the welding centre line as shown in Figure 3-17. This positioning is different compared with the experiments conducted by Guerra et al [50] and Reynolds et al [52], where the marker was set along the welding centre line, reviewed in section 2.3.2 and 2.3.3. As

shown in Figure 2-18 , positioning a marker along the welding centre line results in a difficulty to distinguish the shoulder flow zone flow and nugget zone flow, as marker materials are mixed within the weld zone.

Furthermore, a copper foil fragment was found in a longitudinal cross section of weld obtained by the present study and demonstrated in Figure 4-15. Copper foil fragments not only identified the location of the shoulder flow zone but also supported the hypothesis of the marker (or PUM) movement in the present study.

5.4.2   Weld Structure in Shoulder Flow Zone

As presented in chapter four, Figure 4-14 shows three microstructures of longitudinal cross sections of weld obtained by sectioning weld 15 at three different positions. It can be observed from the figure that the distance from the weld top surface to the interface between the banded structures and the upper featureless region increases. This distance increase from 1.5mm to 3.3mm as the sectioning position in the transverse cross section of weld moves from the retreating side to the advancing side. These results proved the finding of the present study shown in Figure 4-11 that the thickness of the shoulder flow zone varies based on the position of the weld zone, with a thicker shoulder flow zone on the advancing side than on the retreating side. Additionally, these results also correlated well with the experimental result obtained during the preliminary investigation of the present study shown in Figure 1-14. As can be observed from Figure 1-14, a cavity is along the advancing side of the weld and has a deeper downward distance from the workpiece top surface on the advancing side than on the retreating side. This cavity needs to be fully filled up by the shoulder flow zone material to form a defect-free weld during FSW.

5.4.3   Confirmation of Shoulder Flow Zone Flow Pattern

Figure 4-15 shows the microstructure of a longitudinal cross section of weld obtained by sectioning weld 15 through the mid advancing side. It can be observed from the figure that there is a simple banded structure in a layer to layer manner occurring in the shoulder flow zone. It can also be noticed from the figure that a featureless zone appears in the top portion of shoulder flow zone. Additionally, a copper fragment was found in the shoulder flow zone as indicated by a circle in the figure.

Figure 4-15 documented the results of the shoulder flow zone flow movement and the flow movement was described such that; firstly, the copper foil and workpiece material are cut by the edge of the scroll groove, pushed by the incoming workpiece material and then driven into the shoulder scroll groove to form the PUM beneath the shoulder; secondly, the central portion of PUM (denoted as ARM) is driven downward by the root portion of tool pin and then detaches from the pin (tip portion) in a layer to layer manner to form the shoulder flow zone; finally, top portion of ARM, which has been driven downward by the root portion of pin, shears with remaining ARM beneath the shoulder groove resulting in a featureless zone appears in the top portion of shoulder flow zone.

Furthermore, the flow pattern documented by markers shown in Figure 4-15 also confirmed the flow patterns suggested by the present study, that there is a simple banded structure (a layer to layer) appearing in the bottom portion of shoulder flow zone as shown in Figure 4-9. This is because a simple banded structure (layer to layer) occurred upon a copper fragment in the weld zone, and a copper fragment was found above the two internal voids that distinguish the shoulder flow zone and nugget zone as shown in Figure 4-15. Additionally, these results correlate well with the previous finding of the present study that a featureless zone appears in the top portion of the shoulder flow zone shown in Figure 4-9. These results also support the hypothesis of the marker (or PUM) movement in the present study as presented in section 3.3.1. This is because the results shown in Figure 4-15 provide evidence to the movement of the marker after a copper fragment has been identified in the weld zone. The confirmation of the simple banded structure in the shoulder flow zone will strongly support the revelation of the shoulder flow zone forming mechanism.

5.5 Revelation of Shoulder Flow Zone Forming Mechanism

The work presented in chapter two has identified that the nugget zone is formed by the shear layer detachment from the pin in a layer to layer manner, and the banded structures can be identified in the nugget zone within the longitudinal cross section of weld. The work also showed there is a strong correlation between the flow pattern and the flow forming mechanism. Therefore, it is possible to reveal the shoulder flow zone forming mechanism based on the shoulder flow zone flow pattern indentified in the present study to achieve the research goal.

As discussed in the last section, a simple banded structure (in a layer to layer manner) has been confirmed in the shoulder flow zone within the longitudinal cross section of the weld shown in Figure 4-15. In addition, Figure 4-9 demonstrated a simple banded structure (layer to layer) in the bottom portion of shoulder flow zone and a featureless zone in the top portion of shoulder flow zone. This flow pattern indicates that the shoulder flow zone is formed by ARM (annular ring material is central portion of PUM as defined in chapter one) that is driven downward by the tip-off pin (root portion) and detached from the pin (tip portion) in a layer to layer manner. The forming mechanism of the shoulder flow zone using a scroll shoulder tool is explained and discussed as follows. Firstly, after the tool pin and shoulder have been plunged into the workpiece to a certain depth, workpiece material is plasticized and driven into the shoulder scroll groove to form PUM (green, shown in Figure 5-2). The PUM accumulates around the tip-off pin (root portion) and the central portion of PUM forms ARM (red) as indicated in Figure 5-2. As introduced in chapter one and illustrated in Figure 1-9, the ARM rotates in the opposite direction to the tool pin beneath the shoulder face. The movement of ARM during tool pin plunging has also been described by Dawes and Thomas [8] previously.
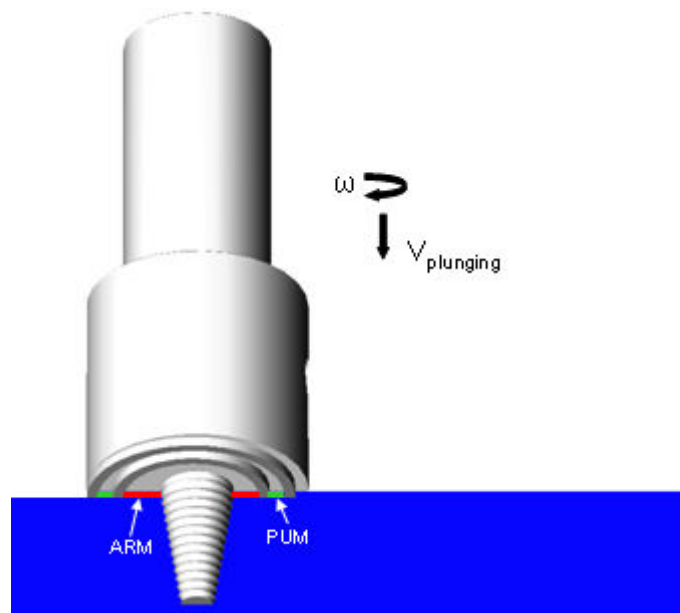
Figure 5-2 Schematic 3D illustration of PUM and ARM formation after tool shoulder has plunged into workpiece at a certain depth, and tool rotates and plunges at ω and V$_{plunging}$ respectively (size of ARM is enlarged and is not real proportion of PUM)

Secondly, when the tool is moving forward, a cavity (yellow, shown in Figure 5-3, and similar to the cavity as indicated in Figure 1-14) is formed due to the nugget zone shear

layers being driven downward by the threaded pin (tip portion) and then detaching from the trailing-retreating location of pin (tip portion) leaving little material to rotate with the pin. The explanation of the formation of this cavity is supported by the direct observation of the surface defect weld obtained in the preliminary investigation of the present study shown in Figure 1-14. This explanation is also similar to the suggestion provided by Chen et al [43] for nugget zone formation shown in Figure 2-22. The cavity shown in Figure 5-3 that needs to be filled up by the ARM is formed in a layer to layer manner and along the advancing side of the weld. This cavity also has a deeper downward distance from the workpiece top surface on the advancing side than on the retreating side shown in Figure 1-14.
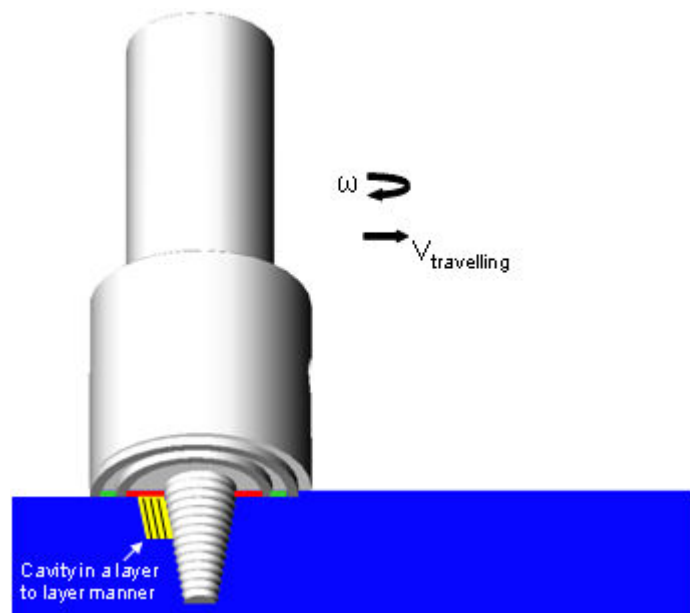
Figure 5-3 Schematic 3D illustration of a cavity formed after tool moving forward, tool rotates and travels at ω and V$_{travelling}$ respectively (cavity is similar to the cavity as indicated in Figure 1-14, size of cavity is enlarged and not real proportion)

Simultaneously, the ARM is pushed by the incoming PUM due to the forward movement of the tool. The ARM is then driven downward by the rotating tip-off pin (root portion), and detaches at the trailing-retreating location of the pin (tip portion) to fill up the cavity created by the forward moving pin (tip portion). The accumulation of the detached ARM forms the shoulder flow zone with a layer by layer manner as shown in Figure 5-4. The suggestion of, the shoulder flow zone is formed by a layer to layer detachment of the ARM, is supported by the findings of the present study, that a simple banded structure in a layer to layer manner occurs in the shoulder flow zone shown in

Figure 4-15. In addition, ARM rotates in the opposite direction to the tool pin which enhances the ability of the tip-off pin to drive the ARM downward significantly.
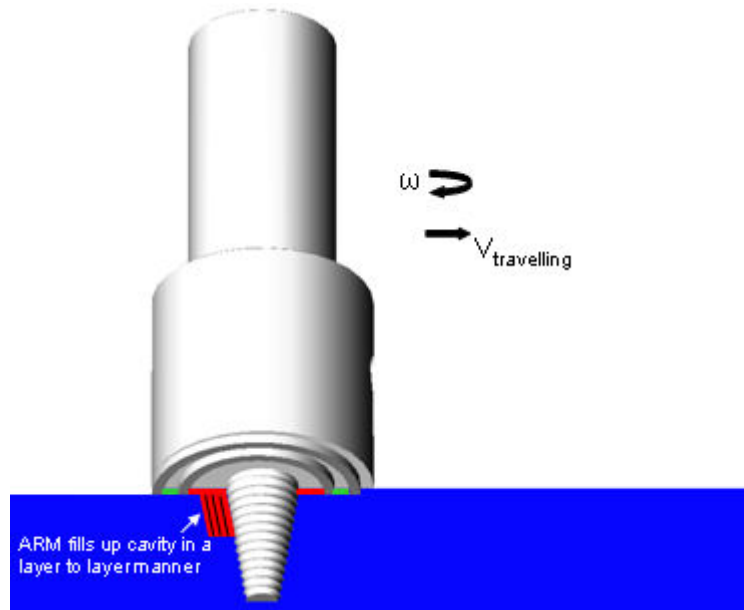
Figure 5-4 Schematic 3D illustration of ARM filling up the cavity simultaneously, forming a shoulder flow zone with a layer to layer manner, tool rotates and travels at ω and V$_{travelling}$ respectively (cavity is not to scale and similar to the cavity as indicated in Figure 1-14)

The top portion of ARM, which has been driven downward by the tip-off pin (root portion), shears with the remaining ARM beneath the shoulder groove. Specifically, this shear occurs at the interface between the top surface of the detached ARM (having been driven downward) and the bottom face of the remaining ARM (retained within the scroll groove beneath the shoulder). A layer to layer pattern at the top portion of shoulder flow zone is interrupted by the wiping motion of the bottom face of the remaining ARM. This interruption leads to the formation of a distinct top portion of shoulder flow zone without a layer by layer attribute as illustrated in Figure 5-5. The suggestion of, a layer to layer pattern at the top portion of shoulder flow zone is interrupted by the wiping motion of the bottom face of the remaining ARM, is supported by the finding of the present study shown in Figure 4-9 that a simple banded structure in a layer to layer manner is not found in the top portion of shoulder flow zone. Additionally, due to the opposite rotation of ARM in relation to the tool pin, the interruption wiping motion is enhanced, this then results in a significant disappearance of the layer by layer flow pattern in the top portion of shoulder flow zone.
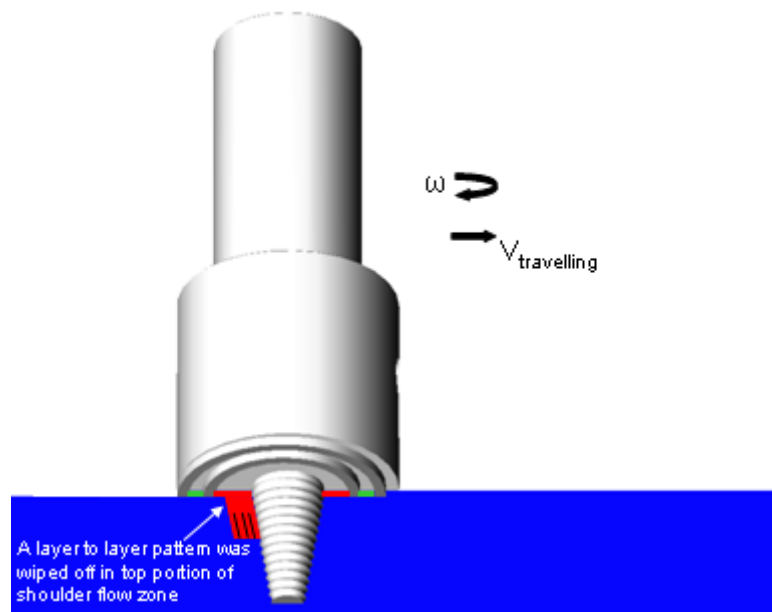
Figure 5-5 Schematic 3D illustration of a layer to layer pattern within the shoulder flow zone, where the top portion of the pattern has been wiped off, tool rotates and travels at ω and V_travelling respectively (cavity is not to scale and similar to the cavity as indicated in Figure 1-14)

The other analysis is that during scroll shoulder tool advancement, if the shoulder scroll geometry and welding parameters are designed and used improperly, the spacing of the ARM may be smaller than the size of cavity shown in Figure 5-6. Under this improper welding condition, as illustrated in Figure 5-7, the cavity may be partially filled up by the PUM. This may result in an ARM supply discontinuity, and consequently may lead to the formation of the defect weld during FSW.
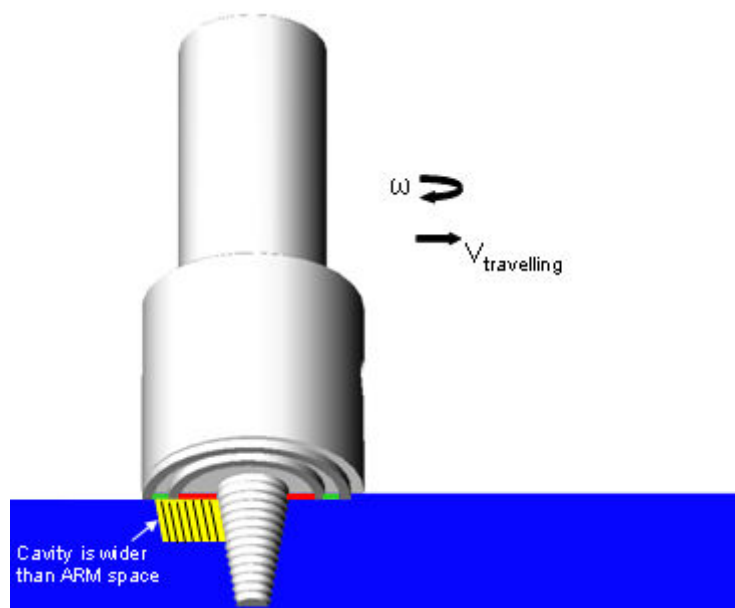
Figure 5-6 Schematic 3D illustration of a shoulder flow zone cavity that is wider than ARM space (cavity is not to scale)
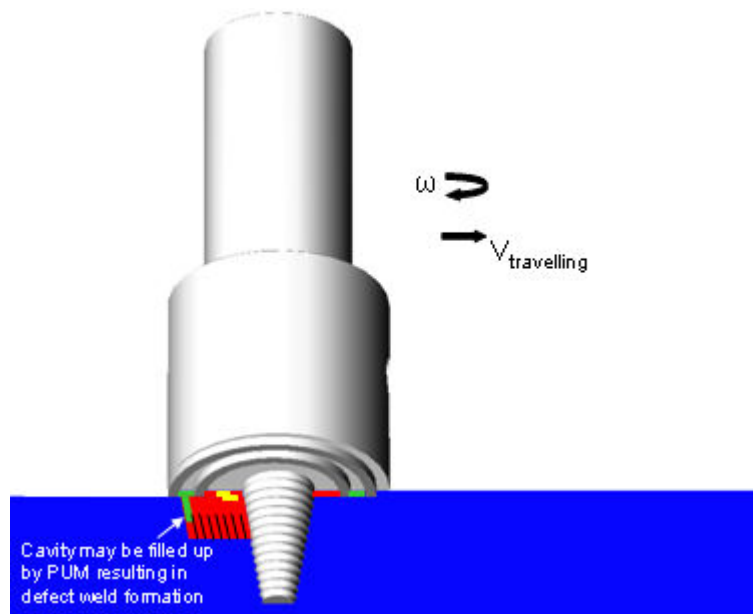
Figure 5-7 Schematic 3D illustration of a shoulder flow zone cavity that is filled by PUM resulting insufficient ARM supply, and leading to defect weld formation (cavity is not to scale)

As explained and discussed above, the shoulder flow zone forming mechanism using a scroll shoulder tool has been revealed. Additionally, the factors that may affect the shoulder flow zone formation have been evaluated. Based on the experimental results shown in those figures, and the explanation of the formation of the banded structures and the half onion ring discussed above, the shoulder flow zone forming mechanism will be summarized and concluded in the next chapter.

6 Concluding Results and Furtherwork

6.1 Concluding Results

FSW experiments have been conducted successfully and the proposed research objectives as stated in chapter one have been achieved with the following conclusions:

1. Quantify the mass of PUM induced by tool during FSW

Quantitative results of the mass of induced PUM are well correlated with the results of the effect of welding parameters on the shoulder flow zone formation. There is a positive linear relationship between the mass of induced PUM and the weld quality in the shoulder flow zone.

2. Evaluate the effect of welding parameters on the shoulder flow zone formation

Weld surface defects (surface quality); weld transverse cross section internal voids; and weld longitudinal cross section internal voids reduce as the depth of shoulder penetration increases.

Weld surface defects (surface quality); weld transverse cross section internal voids; and weld longitudinal cross section internal voids increase as the tool travelling speed increases.

3. Identify the weld structure and flow pattern in the shoulder flow zone

The thickness of the shoulder flow zone varies based on the position of the weld zone, with a thicker shoulder flow zone on the advancing side than on the retreating side.

There is a simple banded structure in a layer to layer manner appearing in the bottom portion of the shoulder flow zone, but the top portion of shoulder flow zone is featureless.

4. Suggest the forming mechanism of shoulder flow zone

Based on the experimental results demonstrated in Figure 4-9 and Figure 4-15, and the explanation of the banded structures and onion rings formation discussed earlier, the overall shoulder flow zone formation is summarized schematically in Figure 6-1. The shoulder flow zone forming mechanism is proposed as follows.
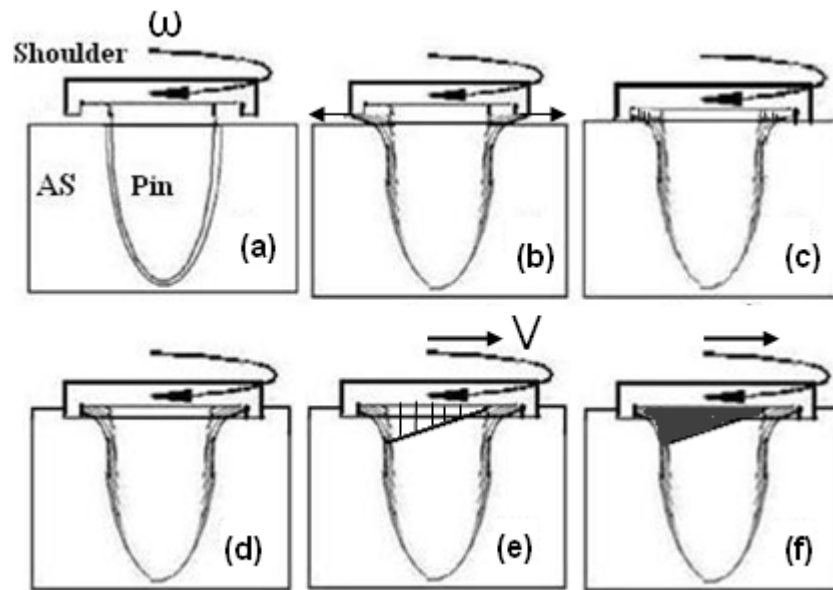
Figure 6-1 Schematic illustration of the shoulder flow zone formation at different shoulder and pin interaction (different stages of FSW process), viewed in transverse cross section, tool rotating and travelling direction as indicated, and the advancing side on left in all sections

(1) When the tool pin is plunged into the workpiece, the workpiece material is extruded by the pin and pushed up into the shoulder scroll groove forming the PUM, or is pushed out of the shoulder face forming the weld flash as illustrated in Figure 6-1 (a) and (b).

(2) During the tool pin (tip portion) plunging, as can be observed from Figure 6-1 (c), the scroll groove is not fully filled up with PUM, where the tool shoulder is brought to just touch the workpiece surface (zero depth of shoulder penetration).

(3) After the tool shoulder penetrates into the workpiece to a certain depth, as illustrated in Figure 6-1 (d), the spacing of the scroll groove has been fully filled up with PUM, and an adequate quantity of ARM is accumulated within this spacing.

(4) During the tool pin travelling, the thread of the pin (tip portion) drives the nugget zone material (shear layers) helically downward from the retreating side to the advancing side, the material then detaches from the pin, forming a cavity that has a layer by layer feature as shown in Figure 6-1 (e).

(5) Simultaneously, as soon as the cavity is formed, the ARM is pushed by the incoming PUM and driven downward by the threaded pin (root portion), it then detaches from the pin (tip portion) to fill up the cavity forming the shoulder flow zone as shown in Figure 6-1 (f).

6.2 Furtherwork

Based on the results discussed in chapter five, the following further works are recommended:

1. Preheat the workpiece material to improve the accuracy of the mass of PUM induced during tool shoulder plunging and tool travelling.

2. Develop a 'shoulder-breaking' technique to break the rotating shoulder suddenly and hence embed it into the workpiece during FSW, in which a real-time shoulder-workpiece couple could be produced for a better three-dimensional examination of the shoulder-workpiece interaction region (shoulder flow zone).

3. Design a tool with a different number of scroll grooves, or a different size of ARM spacing beneath the shoulder to evaluate the induction of the shoulder flow zone material flow during FSW.

7 Reference

1. Robert, W. and J. Messler, *Principles of welding: processes, physics, chemistry*, and metallurgy. 1st ed. 1999, New York: John Wiley. 3.

2. Kalpakjian, S., *Manufacturing engineering and technology*. 4th ed. 1999, Harlow: Addison-Wesley.

3. Mathers, G., *The welding of aluminium and its alloys*. 2002, Boca Raton, FL: CRC Press/Woodhead Publishing.

4. Vill, V.I., *Friction welding of metals*. 1962, New Yark: American Welding Society

5. Thomas, W.M., E.D. Nicholas, and S.W. Kallee, *Friction based technologies for joining and processing,* in *Friction stir welding and processing*, K.V. Jata, et al., Editors. 2001, TMS: Warrendale, Pennsylvania. p. 3-13.

6. Mishra, R.S. and Z.Y. Ma, *Friction stir welding and processing*. Materials Science and Engineering: R: Reports, 2005. 50(1-2): p. 1-78.

7. Schneider, J., R. Beshears, and J.A.C. Nunes, *Interfacial sticking and slipping in the friction stir welding process*. Materials Science and Engineering: A, 2006. 435-436: p. 297-304.

8. Dawes, C.J. and W.M. Thomas, *Development of improved tool design for FSW of aluminium,* in *1st International FSW Symposium*. 1999: Thousand Oaks, California, USA.

9. Chen, Z.W., R. Peris, and R. Maginness, *Material flow in the upper weld zone during friction stir welding*. International Journal of Modern Physics B, 2006: p. 1-5.

10. Nelson, T.W., *FSW-a brief review and perspective for the future,* in *Friction stir welding and processing III* K.V. Jata, et al., Editors. 2005, TMS: Warrendale, Pennsylvania. p. 149-159.

11. Mishra, R.S. and M.W. Mahoney, *Introduction,* in *Friction stir welding and processing,* R.S. Mishra and M.W. Mahoney, Editors. 2007, ASM International: Materials Park, OH. p. 1-5.

12. Schneider, J.A., *Temperature distribution and resulting metal flow*, in *Friction stir welding and processing,* R.S. Mishra and M.W. Mahoney, Editors. 2007, ASM International: Materials Park, OH. p. 37-49.

13. Toskey, A., et al., *Fabrication of Al box beams using self-reacting and standard fixed pin FSW*, in *Friction stir welding and processing III*, K.V. Jata, et al., Editors. 2005. p. 171-178.

14. Burford, D.A., B. Tweedy, and C.A. Widener, *Influence of shoulder configuration and geometric features on FSW track properties*, in *6th International FSW Symposium*. 2006: Montreal, Canada.

15. Colligan, K.J., et al., *Friction stir welding of thick section 5083-H131 and 2195-T8P4 aluminum plates*, in *3rd International FSW Symposium*. 2001: Kobe, Japan.

16. Nandan, R., T. DebRoy, and H.K.D.H. Bhadeshia, *Recent advances in friction-stir welding - Process, weldment structure and properties*. Materials Science, 2008. 53(6): p. 980-1023.

17. Reynolds, A.P. and W.D. Lockwood, *Digital image correlation for determination of weld and base metal constitutive behavior,* in *1st International FSW Symposium*. 1999: Thousand Oaks, California, USA.

18. Nelson, T.W., H. Zhang, and T. Haynes, *Friction stir welding of aluminium MMC 6061-boron carbide* in *2nd International FSW Symposium*. 2000: Quality Hotel 11, Gothenburg, Sweden.

19. Zettlerl, R., et al., *A Study on Material Flow in FSW of AA 2024-T351 and AA 6056-T4 Alloys,* in *5th International FSW Symposium*. 2004: Metz, France.

20. Colligan, K.J. and J.R. Pickens, *FSW of Al using a tapered shoulder tool*, in *Friction stir welding and processing III* K.V. Jata, et al., Editors. 2005, TMS: Warrendale, Pennsylvania. p. 161-170.

21. Hishihara, T. and Y. Nagasaka, *Development of Micro-FSW,* in *5th International FSW Symposium.* 2004: Metz, France.

22. Fuller, C.B., *Friction stir tooling: tool materials and designs,* in *Friction stir welding and processing,* R.S. Mishra and M.W. Mahoney, Editors. 2007, ASM International: Materials Park, OH. p. 14-15.

23. Nishihara, T., *Development of simplified FSW tool* in *6th International FSW Symposium.* 2006: Montreal, Canada.

24. Dubourg, L. and P. Dacheux, *Design and properties of FSW tools: a literature review*, in *6th International FSW Symposium*. 2006: Montreal, Canada.

25. Dawes, C.J., E.J.R. Spurgin, and D.G. Staines, *Development of the new FSW technique for welding aluminium - Phase 2,* in *Member report 5651/35/95.* 1995, TWI Ltd Cambridge United Kingdom.

26. Colligan, K.J. and S.K. Chopra, *Examination of material flow in thick section FSW of Al using a stop-action technique*, in *5th International FSW Symposium*. 2004: Metz, France.

27. Colegrove, P.A., H.R. Shercliff, and P.L. Threadgill, *Modelling and development of the Trivex friction stir welding tool*, in *4th International FSW Symposium*. 2003: Park City, Utah, USA.

28. Colligan, K.J., J. Xu, and J.R. Pickens, *Welding tool and process parameter effects in FSW of Al alloys,* in *Friction stir welding and processing II*, K.V. Jata, et al., Editors. 2003, TMS: Warrendale, Pennsylvania. p. 181-190.

29. Arbegast, W.J., *Application of friction stir welding and related technologies*, in *Friction stir welding and processing*, R.S. Mishra and M.W. Mahoney, Editors. 2007, ASM International: Materials Park, OH. p. 276-277.

30. Ding, R.J., *Force characterization on the welding pin of a friction stir welding retractable pin-tool using aluminium-lithium 2195,* in *2nd International FSW Symposium.* 2000: Quality Hotel 11, Gothenburg, Sweden.

31. Smith, C.B., *Robots and machines for FSW/FSP*, in *Friction stir welding and processing*, R.S. Mishra and M.W. Mahoney, Editors. 2007, ASM International: Materials Park, OH. p. 230-231.

32. Thomas, W.M., A.B.M. Braithwaite, and R. John, *Skew-stir technology*, in *3rd International FSW Symposium*. 2001: Kobe, Japan.

33. *TWI, Com-stir - compound motion for friction stir welding and machining.* 2003 [cited 2007 October, 24]; Available from: http://www.twi.co.uk/j32k/unprotected/band_1/c1248.html.

34. Thomas, W.M., *FSW of ferrous materials; a feasibility study,* in *1st International FSW Symposium.* 1999: Thousand Oaks, California, USA.

35. Thomas, W.M., et al., *The simultaneous use of two or more friction stir welding tools,* in *Member report.* 2005, TWI Ltd Cambridge United Kingdom.

36. Loftus, Z., R. Venable, and G. Adams, *Development and implementation of a load controlled friction stir welder,* in *1st International FSW Symposium.* 1999: Thousand Oaks, California, USA.

37. McLane, M.W. and P.W. Carter, *Free-form friction stir welding,* in *4th International FSW Symposium*. 2003: Park City, Utah, USA.

38. Zettler, R., et al., *Material flow in friction stir butt welded aluminium alloys*, in *6th International FSW Symposium*. 2006: Montreal, Canada.

39. London, B., et al., *Material flow in FSW monitored with Al-SiC and Al-W composite markers,* in *Friction stir welding and processing II,* K.V. Jata, et al., Editors. 2003, TMS: Warrendale, Pennsylvania. p. 3-12.

40. London, B., et al., *Experimental methods for determining material flow in FSW* in *3rd International FSW Symposium*. 2001: Kobe, Japan.

41. Ouyang, J.H., R. Kovacevic, and J. Mater, *Material flow behavior in butt FSW 2024Al and 6061Al plate*s. Engineering Perform, 2002. 11: p. 51-58.

42. Colligan, K.J., *Dynamic material deformation during FSW of aluminium*, in *1st International FSW Symposium.* 1999: Thousand Oaks, California, USA.

43. Chen, Z.W., T. Pasang, and Y. Qi, *Shear flow and formation of Nugget zone during friction stir welding of aluminium alloy 5083-O.* Materials Science and Engineering: A, 2007.

44. Chen, Z.W. and R. Maginness, *Formation of weld zones during friction stir welding of aluminium alloys,* in *5th International FSW Symposium*. 2004: Metz, France.

45. Arbegast, W.J., *Using process forces as a statistical process control tool for FSW,* in *Friction stir welding and processing III K.V*. Jata, et al., Editors. 2005, TMS: Warrendale, Pennsylvania. p. 193-195.

46. Chen, Z.W. and S. Cui, *On the forming mechanism of banded structures in aluminium alloy friction stir welds*. Scripta Materialia, 2007.

47. Krishnan, K.N., *On the formation of onion rings in friction stir welds*. Materials Science and Engineering A, 2002. 327(2): p. 246-251.

48. Prado, R.A., et al., *Self-optimization in tool wear for friction-stir welding of Al 6061+20% Al2O3 MMC*. Materials Science and Engineering A, 2003. 349(1-2): p. 156-165.

49. Colegrove, P.A. and H.R. Shercliff, *3-Dimensional CFD modelling of flow round a threaded friction stir welding tool profile*. Journal of Materials Processing Technology, 2005. 169(2): p. 320-327.

50. Guerra, M., et al., *Flow patterns during friction stir welding*. Materials Characterization, 2002. 49(2): p. 95-101.

51. Ke, L., L. Xing, and J.E. Indacochea, *The materials flow pattern and model in the FSW of Al alloy,* in *Joining of advanced and specialty materials IV,* J.E. Indacochea, et al., Editors. 2002, A S M International: Materials Park, Ohio. p. 125-134.

52. Reynolds, A.P. and W.D. Lockwood, *Visualisation of material flow in an autogenous friction stir weld,* in *1st International FSW Symposium*. 1999: Thousand Oaks, California, USA.

53. Arbegast, W.J., *Modeling friction stir joining as a metal work process*, in *Hot Deformation of Aluminum Alloys III,* Z. Jin, et al., Editors. 2003, TMS: Warrendale, PA, USA. p. 313-316.

54. Bendzsak, G.J., T.H. North, and C.B. Smith, *An experimentally validated 3D model for FSW,* in *2nd International FSW Symposium*. 2000: Quality Hotel 11, Gothenburg, Sweden.

55. Kumar, K. and S.V. Kailas, *The role of friction stir welding tool on material flow and weld formation*. Materials Science and Engineering: A, 2007.

56. Elangovan, K. and V. Balasubramanian, *Influences of tool pin profile and tool shoulder diameter on the formation of friction stir processing zone in AA6061 aluminium alloy*. Materials & Design, 2008. 29(2): p. 362-373.

57. Fujii, H., et al., *Effect of tool shape on mechanical properties and microstructure of friction stir welded aluminum alloys*. Materials Science and Engineering: A, 2006. 419(1-2): p. 25-31.

58. Elangovan, K. and V. Balasubramanian, *Influences of pin profile and rotational speed of the tool on the formation of friction stir processing zone in AA2219 aluminium alloy*. Materials Science and Engineering: A, 2007. 459(1-2): p. 7-18.

59. Kim, Y.G., et al., *Three defect types in friction stir welding of aluminum die casting alloy*. Materials Science and Engineering: A, 2006. 415(1-2): p. 250-254.

60. Dubourg, L., et al., *Process window optimization for FSW of thin and thick sheet Al alloys using statistical methods,* in *6th International FSW Symposium*. 2006: Montreal, Canada.

61. Chen, Z.W., et al., *Material flow and shear layer in the upper weld zone during FSW of aluminium alloys*. International Journal of the Society of Materials Engineering for Resources, 2006. 14: p. 78-81.

62. Chen, Z.W. and S. Cui, *Tool-workpiece interaction and shear layer flow during friction stir welding of aluminium alloy*, in Transactions of Nonferrous Metals Society of China. 2007: China.

63. Leonard, A.J. and S.A. Lockyer, *Flaws in FSW,* in *4th International FSW Symposium*. 2003: Park City, Utah, USA.

64. Arbegast, W.J., *Application of friction stir welding and related technologies,* in *Friction stir welding and processing*, R.S. Mishra and M.W. Mahoney, Editors. 2007, ASM International: Materials Park, OH. p. 289-294.

65. Perrett, J.G., et al. *Recent developments in friction stir welding of thick section aluminium alloys.* 2007 [cited 2007 December, 24]; Available from: http://www.twi.co.uk/j32k/unprotected/band_1/c1248.html.

66. Scialpi, A., L.A.C. De Filippis, and P. Cavaliere, *Influence of shoulder geometry on microstructure and mechanical properties of friction stir welded 6082 aluminium alloy*. Materials & Design, 2007. 28(4): p. 1124-1129.

67. Davis, J.R., *Tool materials*. 1995, Materials Park, Ohio ASM International.

68.   *Mettler Toledo product details-PB602-S/FACT Precision Balance* 2008 [cited 2008 May, 24]; Available from: http://nz.mt.com/mt/products/products/PB602-S_053221330710252411.jsp?v=V0bmVjX3Ryb3BwdXMicm.

69.   Chen, C.M. and R. Kovacevic, *Joining of Al 6061 alloy to AISI 1018 steel by combined effects of fusion and solid state welding.* International Journal of Machine Tools and Manufacture, 2004. 44(11): p. 1205-1214.

70.   Davis, J.R., *Aluminium and aluminium alloys.* 1993, Materials Park, Ohio ASM International.

71.   *Alfa Aesar product details-copper foil.* 2008 [cited 2008 May, 24]; Available from: http://www.alfa.com/alf/index.htm.

72.   Callister, W.D., *Materials science and engineering: an introduction.* 6th ed. 2003, New York; Chichester: Wiley.

8   Appendices

8.1   Appendix 1

8.1.1   Drawing of Scroll Shoulder Tool Assembly
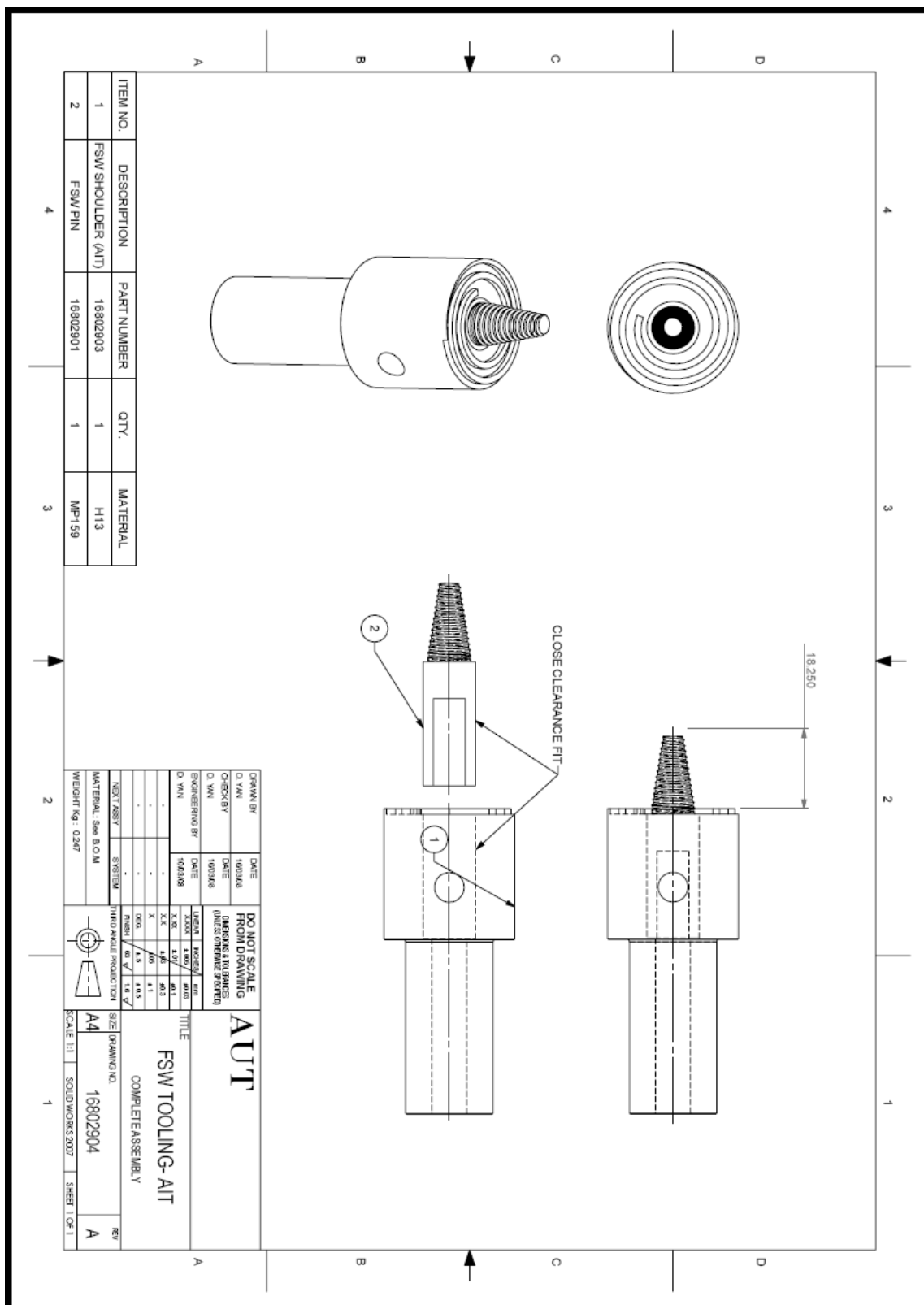
8.1.2   Drawing of Scroll Shoulder Tool Pin

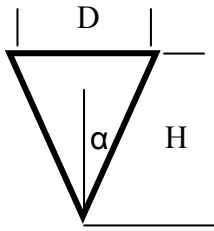### 8.1.3 Drawing of Scroll Shoulder Tool Shoulder

8.2 Appendix 2

8.2.1 Raw Data for Mass of Theoretical Displaced WPM and Experimental Induced PUM during Tool Pin Plunging

Mass of Theoretical Displaced Workpiece Material (WPM):

Mass of 6061 Al WPM displaced by tool during tool pin plunging:

Tool 1 pin (tip portion)
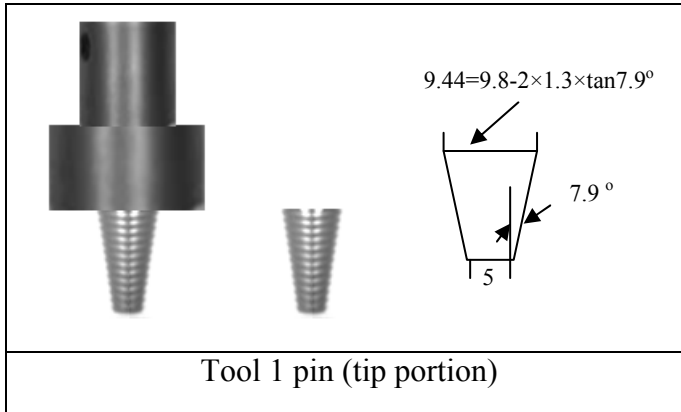
$$V_{\text{Cone volume}} = \frac{1}{12} \times \pi \times D^2 \times H , \ H = \frac{D}{2 \times \tan \alpha}$$

$D_1 = 9.44$ mm, $H_1 = \dfrac{9.44}{2 \times \tan 7.9^0} = 34.02$ mm.

$V_1 = \dfrac{1}{12} \times \pi \times 9.44^2 \times 34.02 = 793.28$ mm^3.

$D_2 = 5$ mm, $H_2 = \dfrac{5}{2 \times \tan 7.9^0} = 18.02$ mm.

$V_1 = \dfrac{1}{12} \times \pi \times 5^2 \times 18.02 = 117.88$ mm^3.

Therefore, Volume of tool pin (tip portion), $V_{\text{pin}} = V_1 - V_2$

$$= 793.28 - 117.88$$
$$= 675.4 \text{ mm}^3$$

Density of 6061 Al = 2.7mg/ mm^3 [70, 72], Therefore,
Mass of 6061 Al WPM displaced by too pin = $675.4 \times 2.7 = 1823$mg=**1.82g**

Mass of Experimental Induced PUM:

Mass of induced PUM= Mass of tool **1** (after tool plunging - before tool plunging)

Average (Avg.) of induced PUM= Mass of induced PUM in (run **1**+ run **2** + run **3**)/3

Table 9 Raw data for mass of induced PUM during tool pin plunging

Weld No.	Tool plunging speed	Mass (g) of tool **1** before / after run **1**	Mass (g) of tool **1** before / after run **2**	Mass (g) of tool **1** before / after run **3**	Avg. net mass of PUM
1	3mm/min	242.77/243.65	242.79/243.50	242.78/243.56	(0.88+0.71+0.78)/3=**0.79g**
2	6mm/min	242.78/243.28	242.79/243.39	242.80/243.26	(0.50+0.60+0.46)/3=**0.52g**

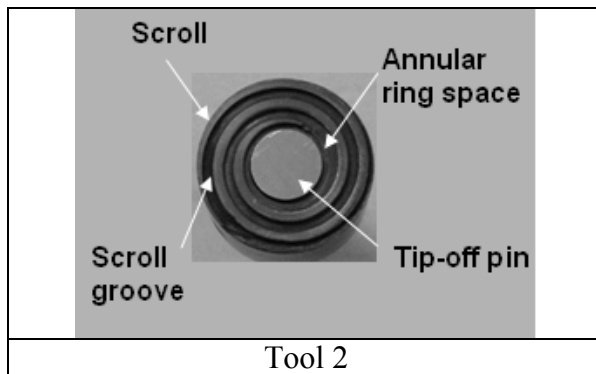## 8.2.2 Raw Data for Mass of Theoretical Displaced WPM and Experimental Induced PUM during Tool Shoulder Plunging

Mass of Theoretical Displaced Workpiece Material:

Mass of 6061 Al WPM fully filling up scroll groove:

Tool 2

Mass of 6061 Al WPM filling up scroll groove
= Volume of spacing beneath shoulder × Density of 6061 Al

Volume of spacing beneath shoulder
= Volume of scroll groove + Volume of annular ring

Volume of scroll groove
= Length of scroll groove × Width of scroll groove × Depth of scroll groove penetration

Volume of annular ring

$= \dfrac{\pi}{4} \times [(\text{Diameter of larger ring})^2 - (\text{Diameter of smaller ring})^2] \times \text{Depth of scroll groove penetration}$

Based on tool design:

Length of scroll groove (measured) = 146mm, Width of scroll groove = 2mm and
Depth of scroll groove penetration =1.3mm (maximum). Hence,
Volume of scroll groove = 146 × 2 × 1.3 = 379.6mm^3

125

Diameter of larger ring = 13.8mm, Diameter of smaller ring = 9.8mm, Hence,

Volume of annular ring = $\frac{\pi}{4} \times [(13.8)^2 - (9.8)^2] \times 1.3 = 96.3$ mm^3, Hence,

Volume of spacing beneath shoulder = 379.6 + 96.3 = 475.9 mm^3,
Density of 6061 Al = 2.7mg/ mm^3, Therefore,

Mass of 6061 Al WPM fully filling up scroll groove = 475.9 × 2.7 = 1285mg=**1.29g**

Mass of 6061 Al WPM displaced by tool 2 at various depth of shoulder penetration:

Mass of 6061 Al WPM displaced by tool 2
= (Volume of penetrated shoulder – Volume of penetrated annular ring) × Density of 6061 Al

(The volume of scroll groove is ignored due to the rotating movement of the scroll)

Volume of penetrated shoulder

$= \frac{\pi}{4} \times$ Diameter of shoulder $^2 \times$ Depth of shoulder penetration

Volume of penetrated annular ring

$= \frac{\pi}{4} \times [(\text{Diameter of larger ring})^2 - (\text{Diameter of smaller ring})^2] \times$ Depth of shoulder penetration

Based on tool design:

Diameter of shoulder = 30mm, Depth of shoulder penetration = 0.4mm, 0.5mm, 0.6mm and 1.0mm, therefore,

Volume of penetrated shoulder = $\frac{\pi}{4} \times 30^2 \times (0.4, \text{ or } 0.5, \text{ or } 0.6, \text{ or } 1.0)$
$= 282.6, \text{ or } 353.25, \text{ or } 423.9, \text{ or } 706.5 \text{mm}^3$

Diameter of larger ring = 13.8mm, Diameter of smaller ring = 9.8mm, Hence,

Volume of penetrated annular ring = $\frac{\pi}{4} \times [(13.8)^2 - (9.8)^2] \times (0.4, \text{ or } 0.5, \text{ or } 0.6, \text{ or } 1.0)$
$= 29.63, \text{ or } 37.04, \text{ or } 44.45, \text{ or } 74.08 \text{mm}^3$, Therefore,

Volume of penetrated shoulder – Volume of penetrated annular ring =252.97, or 316.21, or 379.45, or 632.42mm^3,

Density of 6061 Al = 2.7mg/ mm^3, Therefore,

Mass of 6061 Al WPM displaced by tool 2 at various depth of penetration
= (252.97, or 316.21, or 379.45, or 632.42) × 2.7
=683.02, or 853.77, or 1024.52, or 1707.53mg
=**0.68g**, or **0.85g**, or **1.03g**, or **1.71g**

Mass of Experimental Induced PUM:

Mass of induced PUM= Mass of tool **2** after tool plunging - Mass of tool **2** before tool plunging

Average (Avg.) of induced PUM= Mass of induced PUM in (run **1**+ run **2** + run **3**)/3

Table 10 Raw data for mass of induced PUM during tool shoulder plunging

Weld No.	Depth of shoulder plunging	Mass (g) of tool **2** before / after run **1**	Mass (g) of tool **2** before / after run **2**	Mass (g) of tool **2** before / after run **3**	Avg. net mass of PUM
3	0.4 mm	234.02/234.17	234.04/234.20	234.03/234.17	(0.15+0.16+ 0.14)/3=**0.15**g
4	0.5 mm	234.03/234.43	234.05/234.53	234.06/234.41	(0.40+0.48+ 0.35)/3=**0.41**g
5	0.6 mm	234.05/234.68	234.07/234.73	234.05/234.59	(0.63+0.66+ 0.54)/3=**0.61**g
6	1.0 mm	234.04/235.22	234.06/235.40	234.06/235.29	(1.18+1.34+ 1.23)/3=**1.25**g

8.2.3 Raw Data for Mass of Theoretical Displaced WPM and Experimental Induced PUM during Tool Travelling

Mass of Theoretical Displaced Workpiece Material:

Mass of 6061 Al WPM displaced by tool 2 after tool travelling 40mm:
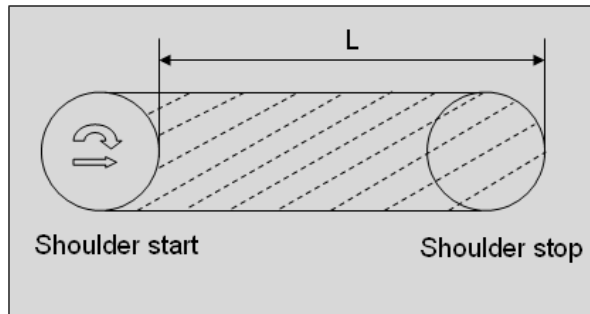
Mass of 6061 Al WPM displaced by tool 2
= Volume of displaced WPM × Density of 6061 Al

Volume of displaced WPM = Area of dash line × Depth of tool penetration

Area of dash line = Diameter of shoulder × L

Based on tool design:
Diameter of shoulder = 30mm, L = 40mm, Depth of tool penetration = 0.4mm Hence,

127

Volume of displaced WPM = $30 \times 40 \times 0.4 = 480$ mm^3

Density of 6061 Al = 2.7mg/ mm, Therefore,

Mass of 6061 Al WPM displaced by tool 2 after tool travelling 40mm:
= 480×2.7
= 1296mg=**1.3g**

Mass of Experimental Induced PUM:

Mass of induced PUM= Mass of tool **2** after tool travelling - Mass of tool **2** before tool

plunging − Average mass of induced PUM after 0.4mm depth of tool **2** plunging

Average of induced PUM= Mass of induced PUM in (run **1**+ run **2** + run **3**)/3

Table 11 Raw data for mass of induced PUM during tool travelling

Average (Avg.) mass of induced PUM =**0.15**g (after 0.4mm depth of tool **2** plunging, before tool **2** travelling)					
Weld No.	Tool travelling speed	Mass (g) of tool **2** before / after run **1**	Mass (g) of tool **2** before / after run **2**	Mass (g) of tool **2** before / after run **3**	Avg. net mass of PUM
7	40mm/min	234.05/235.28	234.04/235.39	234.07/235.27	(1.23+1.35+ 1.20)/3- 0.15=**1.11**g
8	56mm/min	234.07/234.78	234.06/234.76	234.06/234.92	(0.68+0.71+ 0.86)/3- 0.15=**0.60**g